MODELING AND MULTI-OBJECTIVE OPTIMIZATION OF AN

INDUSTRIAL HIGH DENSITY POLYETHYLENE SLURRY REACTOR

A thesis submitted to the
University of Petroleum and Energy Studies

For the Award of
Doctor of Philosophy
in
Chemical Engineering

By
Amit Kumar Thakur

March 2021

Supervisor(s)

Dr. Pranava Chaudhari
&
Dr. Santosh Kumar Gupta

UPES
UNIVERSITY WITH A PURPOSE

Department of Chemical Engineering
School of Engineering
University of Petroleum and Energy Studies
Dehradun – 248007; Uttarakhand

MODELING AND MULTI-OBJECTIVE OPTIMIZATION
OF AN
INDUSTRIAL HIGH DENSITY POLYETHYLENE SLURRY
REACTOR

A thesis submitted to the
University of Petroleum and Energy Studies

For the Award of
Doctor of Philosophy
in
Chemical Engineering

By
Amit Kumar Thakur
(SAP ID: 500042449)

March 2021
Supervisor

Dr. Pranava Chaudhari
Asst. Professor
Department of Chemical Engineering
University of Petroleum and Energy Studies

Co-Supervisor

Dr. Santosh Kumar Gupta
Distinguished Professor
Department of Chemical Engineering
University of Petroleum and Energy Studies

UPES
UNIVERSITY WITH A PURPOSE

Department of Chemical Engineering
School of Engineering
University of Petroleum and Energy Studies
Dehradun – 248007; Uttarakhand

DECLARATION

I declare that the thesis entitled "Modeling and multi-objective optimization of an industrial high density polyethylene slurry reactor", has been prepared by me under the guidance of Dr. Santosh Kumar Gupta, Distinguished Professor and Dr. Pranava Chaudhari, Assistant Professor of Chemical Engineering Department, University of Petroleum & Energy Studies. No part of this thesis has formed the basis for the award of any degree or fellowship previously.

Amit Kumar Thakur

Department of Chemical Engineering,
School of Engineering,
University of Petroleum and Energy Studies,
Dehradun – 248007, Uttarakhand.

Date: 24/05/2021

THESIS COMPLETION CERTIFICATE

This is to certify that the thesis on *"Modeling and multi-objective optimization of an industrial high density polyethylene slurry reactor"* by **Amit Kumar Thakur** in partial completion of the requirements for the award of the degree of doctor of philosophy (in Chemical Engineering) is an original work carried out by him under our joint supervision and guidance.

It is certified that the work has not been submitted anywhere else for the award of any other diploma or degree of this or any other university.

Supervisor

Pranava Chaudhari 24-05-2021

Dr. Pranava Chaudhari
Asst. Professor
Department of Chemical Engineering,
School of Engineering,
University of Petroleum and Energy Studies,
Dehradun – 248007, Uttarakhand
Email- pchaudhari@ddn.upes.ac.in

Co-Supervisor

Dr. Santosh Kumar Gupta
Distinguished Professor
Department of Chemical Engineering,
School of Engineering,
University of Petroleum and Energy Studies,
Dehradun – 248007, Uttarakhand
Email-skgupta@iitk.ac.in

Energy Acres: Bidholi Via Prem Nagar, Dehradun - 248 007 (Uttarakhand), India T: +91 135 2770137, 2776053/54/91, 2776201,9997799474 F: +91 135 2776090/95
Knowledge Acres: Kandoli Via Prem Nagar, Dehradun - 248 007 (Uttarakhand), India T: +91 8171979021/2/3, 7060111775

ENGINEERING | COMPUTER SCIENCE | DESIGN | BUSINESS | LAW | HEALTH SCIENCES | MODERN MEDIA | SMART AGRICULTURE

ABSTRACT

Slurry polymerization processes using Zeigler-Natta catalysts are most widely used for the production of polyethylene due to their several advantages over other processes. Significant advancements have been made in the modeling of these processes to obtain high-quality final products. The modeling work in this field has a very wide scope due to the great diversity of the catalyst types, polymerization processes, polymerization conditions, product qualities, and micro-structures that exist at the commercial scale.

This study is on the multi-scale modeling, simulation and multiobjective optimization in an *industrial* high density polyethylene (HDPE) continuous stirred tank slurry reactor. The multi-scale modeling framework mainly comprises of the kinetic model, single-particle diffusion models, multiphase hydrodynamics, phase equilibria, reactor residence time distribution and the overall mass and heat balances. Guidelines to implement the multi-scale mathematical modeling and simulation in slurry phase olefin polymerization processes are proposed. Special focus is given on the need to reduce the computational time for the simulation of industrial reactors so that the models can be used as an effective tool-kit for optimization studies using state-of-art algorithms.

A hierarchical and computationally-efficient multiscale mathematical model is developed to explain the polymerization of HDPE in an isothermal, industrial, continuous stirred tank reactor (CSTR). A modified polymeric multigrain model (PMGM) is used. Steady-state macroscopic mass balance equations are derived for all the species (namely, monomer, solvent, catalyst and polymer) to obtain the final

particle size and the required monomer and solvent input rates for a given catalyst input and the reactor residence time. The interphase mass transfer coefficients are calculated for the *industrial* CSTR using operating data on a reactor. The present model is tuned with some data on an isothermal *industrial* reactor and the simulation results are compared with data on another set of the industrial reactor. The comparison reveals that the present tuned model is capable of predicting the productivity and the polymer yield at various catalyst feed rates and mean residence times. The effects of the variation of two operating variables (catalyst feed rate and the mean residence time) on the productivity, the polymer yield, the polydispersity index (PDI) and the operational safety, are analyzed. The present study indicates that an optimal value of the reactor residence time (for maximum productivity per catalyst particle) exists at any catalyst feed rate.

Optimal operating conditions are required to obtain the maximum productivity of the polymer at minimal cost while ensuring operational safety. The main focus of the optimization study is to obtain the optimal operating conditions corresponding to the maximization of the productivity and yield at a minimal operating cost. The single objective optimization (SOO) and multiobjective optimization problems are solved using genetic algorithm (GA). The Pareto optimal solution is obtained using the NSGA-II algorithm. The solution of SOO problems gives only one set of optimal solutions, whereas, the solution of MOO problems gives a whole range of optimal solutions.

ACKNOWLEDGEMENT

I take this opportunity to express my sincere thanks to my Ph. D thesis co-supervisor Dr. Santosh Kumar Gupta, Distinguished Professor, Department of Chemical Engineering, UPES, Dehradun for the precious guidance, continuous encouragement, and affectionate treatment. His down-to-earth nature makes him the most admirable person in my life. I would like to express my sincere gratitude to my supervisor, Dr. Pranava Chaudhari, Asst. Professor, Department of Chemical Engineering, UPES, Dehradun. He is the person who acted as a friend, philosopher, and guide. The interactive sessions with him have helped me to learn the technical and soft skills that are much needed while pursuing the Ph. D thesis. I will always be indebted to both of them throughout my life.

I wish to express my profound gratitude to Dr. S. J. Chopra (Chancellor), Dr. Sunil Rai (Vice-Chancellor), Dr. Kamal Bansal (Senior Director Academic Development) and Dr. Gurvinder Singh Virk (Dean-SoE) UPES, Dehradun for providing the necessary infrastructure and resources to accomplish my research work. I am also grateful to the faculty members of my department who have supported and encouraged me during this tenure.

I should not forget to express my heartfelt thanks to Dr. Rahul Kumar, Dr. Nilanjana Banerjee, and my other colleagues for their continuous motivation and support.

I am especially thankful to Mrs. Sudha (wife), Priyanshi (Daughter), Yash Thakur (Son), Shri Baleshwar Thakur (Father), Mrs. Sunaina Devi (Mother), and other family members for supporting me spiritually during the thesis work and my life in general. I should not forget the help of my friends who are always with me. I thank the faculty and staff at UPES, Dehradun who have directly and indirectly helped me in completing this thesis successfully.

Last but not the least, I will be grateful to "Almighty God" forever for giving me this opportunity to complete my Ph. D thesis.

Date: 24 May 2021   **AMIT KUMAR THAKUR**
Place: Dehradun

TABLE OF CONTENTS

LIST OF SYMBOLS

a_{gl}	Interfacial area of the gas-liquid interface (m^2/m^3)
a_{ls}	Interfacial area of the liquid-solid interface (m^2/m^3)
B	Concentration of by-product
[cocat]	Co-catalyst concentration (mol/m^3)
C_d	Concentration of deactivated catalyst sites (mol/m^3)
C_P	Concentration of potential active sites not yet activated (mol/m^3)
$C_{P,mp}$	Heat capacity of the macroparticle
$C_{P,\mu p}$	Heat capacity of the microparticle
C^*	Concentration of catalyst active site (kmol site/m^3 of catalyst)
d_a	Diameter of the impeller (m)
d_b	Average diameter of the gas bubbles (m)
d_{mp}	Diameter of macroparticle (m)
D_{amp}	Diffusivity of monomer in amorphous phase (m^2/s)
D_{cat}	Diameter of original catalyst particle (m)
D_{ef}	Effective diffusivity of monomer inside the macroparticle (m^2/s)
$D_{ef,PMGM}$	Effective diffusivity of monomer inside the macroparticle in PMGM model (m^2/s)
$D_{ef,RPPFM}$	Effective diffusivity of monomer inside the macroparticle in RPPFM model (m^2/s)

D_i^P	Diffusivity of component i in amorphous phase (m²/s)
D_{ij}^o	Diffusivity of component i in presence of component j (m²/s)
D_L	Diffusivity of monomer in the bulk liquid (m²/s)
D_{mp}	Diffusivity of monomer in the macroparticle (m²/s)
$D_{\mu p}$	Diffusivity of monomer in the microparticle (m²/s)
D_n	Concentration of dead polymer chains of n monomeric units (kmol/m³ catalyst)
D_{Poly}	Diffusivity of monomer in the pure polymer (m²/s)
F	Volumetric fraction of solids in the slurry (m³ of solid/m³ of slurry)
f_c	Mass fraction of catalyst present in the solid (kg cat/kg solid)
h	Heat transfer coefficient
H_2	Hydrogen concentration (kmol/m³)
$H_{in,i}$	Enthalpy of component i in feed stream (kJ/s)
$H_{out,i}$	Enthalpy of component i in product stream (kJ/s)
ΔH_P	Heat of polymerization
I_C	Catalyst mass flow rate (kg/s)
I_M	Monomer mass flow rate (kg/s)
I_P	Polymer mass flow rate (kg/s)
I_S	Solvent mass flow rate (kg/s)
k_a	Rate constant for activation (m³ kmol⁻¹ s⁻¹)

k_d Rate constant for deactivation (m^3 kmol^{-1} s^{-1})

k_{in} Rate constant for initiation (m^3 kmol^{-1} s^{-1})

k_{gl} Mass transfer coefficient at the gas liquid interface (m/s)

k_{in} Rate constant for initiation (m^3 kmol^{-1} s^{-1})

k_{ls} Mass transfer coefficient at the liquid solid interface (m/s)

k_{mp} Thermal conductivity of the macroparticle

k_P Rate constant for propagation (m^3 kmol^{-1} s^{-1})

k_s Sorption parameter (s^{-1})

k_t Rate constant for chain transformation (m^3 kmol^{-1} s^{-1})

k_{tr} Rate constant for chain transfer (m^3 kmol^{-1} s^{-1})

$k_{\mu p}$ Thermal conductivity of the microparticle

M^* Equilibrium monomer concentration (kmol/m^3)

M_0 Initial molar concentration (kmol/m^3)

M_b Molar concentration of monomer in the bulk of the reacting liquid (kmol/m^3)

M_{eq} Equilibrium molar concentration of the monomer at the surface of the polymeric shell (kmol/m^3)

M_{mp} Molar concentration of monomer in the macroparticle (kmol/m^3)

$M_{mp,in}$ Molar concentration of monomer at the liquid solid interface (kmol/m^3)

M_n Number average molecular weight (kg/kmol)

$M_{\mu p}$	Monomer concentration in the microparticle (kmol/m^3)
M_w	Weight average molecular weight (kg/kmol)
MW	Molecular weight of the monomer (kg/kmole)
N	Number of ideal CSTR in series
N_e	Total number of catalyst particles entering the reactor per second (s^{-1})
N_F	Dimensionless flow number
N_P	Dimensionless power number
N_S	Speed of impeller (rps)
P_0	Concentration of empty sites (kmol/m^3 catalyst)
P_d	Power delivered to liquid (W)
P_n	Concentration of live polymer chain with n monomer (mol/m^3)
P_S	Power delivered to the impeller shaft (W)
P_t	Total pressure inside the reactor (Pa)
PDI	Polydispersity index
Q_{ext}	Heat transfer by external cooler (kJ/s)
Q_{imp}	Heat transfer by impeller (kJ/s)
Q_{jacket}	Heat transfer through reactor jacket (kJ/s)
Q_T	Rate of withdrawal of product (slurry) (m^3/s)
r_{cf}	Radius of the catalyst after fragmentation (m)
$r_{i,0}$	Radius of catalyst particle in the feed (m)
r_{mp}	Radial position in the macroparticle

$r_{\mu p}$	Radial position in the microparticle
$R_{c,i}$	Radius of catalyst sub-particle in the i-th shell (m)
$R_{h,i}$	Radius of macroparticle at the hypothetical grid point i (m)
Re	Reynolds number
R_{gl}	Rate of monomer transfer from the gas phase to the liquid phase (kmol/s)
R_{ls}	Rate of monomer transfer from the liquid phase to the solid phase (kmol/s)
R_{mp}	Radius of the macroparticle (m)
R_{poly}	Rate of formation of polymer inside the reactor (kg/s)
R_{μ}	Radius of the polymeric shell around the microparticle (m)
$R_{\mu p}$	Rate of polymerization in the microparticle
R_v	Rate of reaction per unit volume (kmol/m^3-s)
S	Solvent concentration (mol/m^3)
Sc	Schmidt number
S_{He-PE}	Solubility of hexane in polyethylene (gm of hexane/gm of PE)
Sh	Sherwood number
T_0	Initial temperature (K)
T_b	Temperature of the bulk liquid (K)
T_{mp}	Temperature inside the macroparticle (K)
$T_{\mu p}$	Temperature inside the microparticle (K)
u_s	Velocity of gas bubble (m/s)
v_G	Total volume of gas dissolved in the n-hexane (m^3)

v_L Total volume of liquid in the slurry (m^3)

v_s Total volume of solid in the slurry (m^3)

V   Volume of the reactor (m^3)

Superscripts and Subscripts

cocat	co-catalyst
G	Gas phase
gl	Gas liquid interface
i	Refer to molar species *i*
in	input
k	Catalyst active site type
L	liquid
ls	Liquid solid interface
mp	macroparticle
N	Number
out	output
S	Solid
μp	microparticles

Greek letters

α   Correction factor for diffusivity

β	Correction factor for diffusivity
ε	porosity
ζ	Catalyst tortuosity
τ	Mean residence time of the reactor (s)
θ	Dimensionless time
λ	Moment of the live polymer chains (kg/kmol)
Λ	Moment of the dead polymer chains (kg/kmol)
μ_G	Viscosity of the gas (Pa s)
μ_L	Viscosity of the liquid (Pa s)
ρ_C	Density of the catalyst (kg/m^3)
ρ_L	Density of the liquid (kg/m^3)
ρ_M	Density of the monomer (kg/m^3)
ρ_P	Density of the polymer (kg/m^3)
ρ_S	Density of the solvent (kg/m^3)
$\rho_{S,avg}$	Average density of the macroparticle [kg (catalyst + polymer)/m^3 macroparticle]
σ_L	Surface tension of liquid (N/m)

LIST OF FIGURES

LIST OF TABLES

CHAPTER 1

INTRODUCTION

Polyolefins (POs), including polyethylene (PE) and polypropylene (PP), make a very significant contribution to the global petrochemical economy. As per recent data [1], nearly 185 million metric tons per annum of polyolefins (PE and PP) are manufactured globally. The global PO market is expected to expand at a rate exceeding about 6.2% from 2019 to 2025 [2]. PE accounts for a major portion of about 58% of the total global production of POs. The production of such large volumes of PE is due to its versatile physical and mechanical properties, high resistance towards chemicals, non-toxicity, low cost and non-polluting production. The physical and mechanical properties of PE can be varied by controlling the reactor operating conditions, thus producing a wide variety of PE for various applications, e.g., films, injection molding, blow molding, extrusion molding, pipes, etc. [3], [4]. PE can be classified as low-density PE (LDPE) with densities around 910-930 kg/m^3 and high-density PE (HDPE) with densities around 930-970 kg/m^3. LDPE can further be classified as low-density polyethylene (LDPE) and *linear* low-density polyethylene (LLDPE), based on the amount of chain branching of the molecules and the process of their synthesis.

Commercially, low pressure continuous catalytic processes are employed for the production of PE. These processes are categorized based on the flow regime as slurry-phase, gas-phase and solution processes. The slurry processes produce about 57% of the total PE [5]. Some of the advantages of slurry processes include their simple design, mild operating conditions, easier temperature control, well-defined mixing, high (as high as 99 %) monomer conversion and relative ease of processing [6], [7]. The gas-phase processes face the challenge of poor heat removal due to a relatively lower heat transfer coefficient compared to the slurry phase. The average

catalyst particle size is much bigger in the gas phase (50-300 micron) compared to the slurry phase (5-20 micron) and this results in a relatively higher intraparticle heat transfer resistance in the gas phase ethylene polymerization processes. In addition to poor heat removal, gas phase processes produce more off-spec (off-specification) of the polymer during grade change-over. The generation of excessive fines in the product and relatively low-profit margins. This makes the gas phase processes less competitive compared to the slurry phase processes. Solution processes operate at relatively high temperatures (140 – 250℃) and pressures (3,500 – 10,500 kPa) and are mainly used for the production of LLDPE. With the growing commercial demand for the slurry processes, especially due to their advantages, a comprehensive understanding of slurry phase polymerization processes is vital for academia as well as the industrial community.

The most widely used catalyst for ethylene polymerization is *heterogeneous* Zeigler-Natta (Z-N) catalysts [8]. Metallocenes catalysts and chromium oxide-based Phillips catalysts are versatile for ethylene polymerization but their market share is quite low compared to the heterogeneous Z-N catalysts. The Z-N catalysts are typically supported on high specific surface crystalline magnesium dichloride and amorphous silica. A high specific surface provides several highly accessible active sites. These active sites maximize catalyst productivity. The metallocenes and Phillips catalysts are typically supported on silica or alumina/silica.

The objective of this work is not the catalyst synthesis and its characterization, but equally important research aspects in this area. This work is focused on the development of a mathematical model to understand the polymerization of high-density polyethylene (HDPE) in an isothermal, industrial, continuous stirred tank slurry reactor (CSTR). In recent years, considerable effort has been made by several workers to develop the mathematical model of ethylene polymerization in various reactor systems. These modeling studies are primarily focused on the prediction of the molecular weight distributions (MWDs), chemical composition distributions (CCDs) and the particle size distribution (PSD) of the final product. A multi-scale

computationally-efficient mathematical model is developed in this work to explain the polymerization of high-density polyethylene (HDPE) in an isothermal, industrial, continuous stirred tank slurry reactor (CSTR). This model is not only for the prediction of the behavior of an industrial slurry reactor for the ethylene polymerization process but also can be used as an effective tool for process optimization studies. To develop a mathematical model for the ethylene polymerization process, a clear understanding of the process is vital. The following section discusses the slurry phase ethylene polymerization processes and highlights their advantages and limitations.

1.1 SLURRY PHASE ETHYLENE POLYMERIZATION PROCESSES

The slurry processes employ either continuous stirred tank reactors (CSTRs) or loop reactors. Some major licensors of the CSTRs based slurry processes are Mitsui (CX® process) and LyondellBasell (Hostalen® process). Whereas, major licensors of the loop reactors-based slurry processes are Chevron-Phillips (MarTECH®) and BP Solvay. CSTRs based slurry processes are mainly used for the production of HDPE. Loop reactors are used for the production of both HDPE and LDPE.

1.1.1 SLURRY POLYMERIZATION IN CSTRs

The slurry polymerization of ethylene in CSTRs involves a suspension of catalyst, co-catalyst and solvent. These are injected into the reactor along with the gaseous monomer, comonomer, hydrogen and the liquid solvent. A typical flowchart of slurry polymerization in CSTR slurry processes is shown in Fig. 1.1. The monomer, comonomer and hydrogen *partially* dissolve in the liquid solvent (medium) and diffuse from the gaseous bubble to the suspended solid catalyst particles (through the liquid medium). The polymerization occurs at the active sites on the inside of the catalyst and the polymer builds upon these catalyst particles. Thus, the (initially) smaller *catalyst particles* grow to larger *polymer particles* as the reaction progresses. The reaction mass, thus, comprises the gas bubble phase, the liquid phase and the solid polymer particles, a three-phase region. The unreacted

3

gases accumulate in the vapor space at the top of the reactor. The vapor space, thus, consists of vapors of monomer, solvent, comonomer and hydrogen. The reactor, therefore, consists of two gaseous regimes, one at the top of the reactor in the continuous vapor space and the other in the form of gas bubbles in the three-phase region of the reaction mass [9].
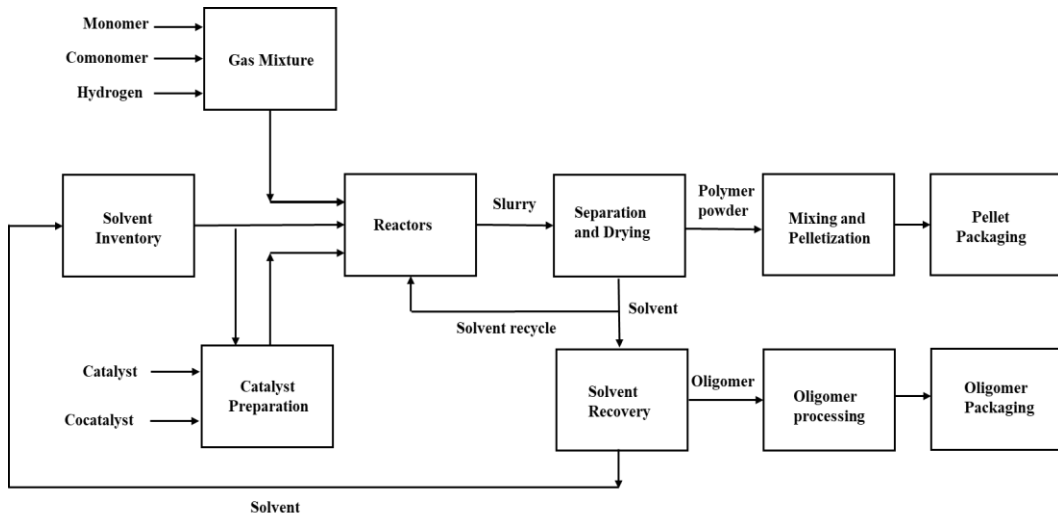
Fig. 1. 1 A typical flowchart of slurry polyethylene polymerization is CSTR

The amount of solids present in the slurry is a very important factor in these processes. A higher solids concentration corresponds to a higher throughput per reactor volume. A typical solid concentration in the slurry varies from 15 - 45% [7]. Slurry from the reactor outlet enters the separation and drying sections. Here, the polymer slurry is separated from the solvent, unreacted monomer and low molecular weight polymer (oligomer or wax). A part of the solvent may be recycled to the reactor and the rest goes to the solvent recovery section. Here, the oligomer (by-product) is recovered and the separated solvent is returned to the solvent recovery section. Meanwhile, the polymer powder from the drying section undergoes mixing and pelletizing, followed by the packaging of the pellets.

Slurry polymerization in CSTRs provides a wide range of multi-modal HDPE. The operating conditions (temperature, pressure, ethylene partial pressure and the molar

4

ratio of hydrogen to ethylene) of all the reactors can be controlled *independently* to obtain the final product with different specifications. Depending on the product requirement, CSTRs can be operated using different cascade arrangements. Reactors can be operated in a parallel mode using identical operating conditions giving fairly narrow MWDs (almost a *unimodal* product, for injection-molding). Reactors operating in series-cascades and operating under different conditions with a low hydrogen content in the second reactor give broad MWD (*bimodal*) HDPE [10].

The polymerization of olefins is highly exothermic, with the heat of reaction of the order of 10^5 kJ/kmol [11]. Therefore, efficient heat removal and temperature control in the reactor is very important to ensure product quality and specifications. Hence, the reactors are equipped with different heat removal mechanisms for efficient heat removal and good temperature control. The main difference between the Mitsui (CX) process and the LyondellBasell Hostalen process lies in the mode of heat removal. In the Hostalen process, the heat of polymerization is removed by cooling water in a jacket whereas, in the CX process, jacket cooling water can remove only about 10% of the total heat, the remaining 90% of the heat is removed in an overhead condenser (by condensing the solvent vapor) and external slurry coolers.

Hostalen Process:

The *Hostalen* process is a very popular technology for the production of bimodal HDPE. This process uses cascades of slurry CSTRs for producing high-quality HDPE products having a range of MWDs (from narrow to broad). The rate of polymerization, polymer yield and MWDs are controlled using the concentrations of monomer, comonomer and hydrogen and the type and concentration of the catalyst [12].

Depending on the requirement of the final product, the reactors in this process can be operated in three different modes, namely, the BM process mode, the K1 process mode and the K2 process mode. A typical flowchart of the BM process mode for Hostalen process is shown in Fig. 1.2. In the BM process mode, three reactors are

arranged in series in a cascade with different operating conditions. The catalyst and cocatalyst are injected *only* into the first reactor whereas, the monomer, solvent and hydrogen are independently fed to each of the reactors. A higher concentration of hydrogen is maintained in the first reactor while the second reactor uses a lower hydrogen concentration to produce bimodal and multimodal HDPE grades. A small amount of comonomer is fed to the second reactor to control the density of the final product. The slurry from the second reactor enters a *post* reactor to reduce the unreacted monomer, hence eliminating its recovery using separation and drying sections. In the K1 process mode, reactors are operated in parallel and use identical operating conditions to give a narrow MWD product. The K2 process mode is also a parallel mode of operation with different operating conditions in each of the reactors. This mode produces a bimodal MWD product.

The main advantages of the Hostalen processes are the self-stabilization of the process, accurate reproducibility of polymerization, easy scale-up and low operating costs [10], [12].

Fig. 1. 2 A typical flowchart of the BM process mode for Hostalen process (adapted from reference, [10])

CX Process:

This process consists of two CSTRs of equal capacity arranged in series or parallel. The solvent is hexane, while the comonomers are propylene and butene-1. Hydrogen is used as the chain transfer agent. There are three ways of heat removal in this process, overhead condenser, cooling water in the reactor jacket and external slurry coolers. A major portion (nearly 60%) of heat is removed using an overhead condenser in which the vapor from the top of the reactor is condensed and recycled to the reactor. The remaining heat is removed *via* cooling water in a jacket and external cooling of the slurry. The reactor is continuously fed with the catalyst ($MgCl_2$ supported Zeigler-Natta), cocatalyst (triethyl aluminium) suspended in hexane and fresh hexane.

The slurry from the reactors enters a centrifuge which separates the polymer from the mother liquor. A part of the mother liquor (which contains a small amount of unreacted monomer and catalyst) is recycled to the reactor without any purification and the rest goes to the solvent recovery section where the oligomers are separated from the hexane.

A typical flow chart for the series and parallel modes of CSTRs in the CX process is illustrated in Fig. 1.3. In the series mode, the slurry from the first reactor enters the second reactor along with fresh ethylene, comonomer and hydrogen [13]. In this mode, a high molar ratio of hydrogen to ethylene concentration is maintained in the first reactor and a small molar ratio of hydrogen to ethylene concentration is maintained in the second reactor. The yield of the polymer on the catalyst is usually very high and, therefore, the separation of catalyst from the polymer is unnecessary. A comparison between the Hostalen process and the CX process is given in Table 1.1. In the parallel mode, catalyst and cocatalyst are fed to both the reactors. The slurry from both the reactors enters a flash vessel where the unreacted hydrocarbons

7

are removed and recycled to the reactor. The slurry from the flash vessel enters the centrifuge followed by the drying, mixing, pelletizing and packaging sections.

Table 1. 1 A comparison between the Hostalen process and CX process

	Hostalen process	CX process
Reactor type	2-3 CSTRs	2 CSTRs
Reactor configuration	BM (series) K1 (parallel) K2 (parallel)	Series and parallel
Pressure, kPa	200-800	300-1000
Temperature, $^\circ$C	76-85	75-85
Solvent	hexane	hexane
Residence time per reactor	1-5 hr	45 min-2 hr
Heat removal	reactor jacket cooling	overhead condenser reactor jacket cooling and external slurry cooling
Ethylene conversion (%)	up to 99.5 %	up to 99%
Polymer grades	bimodal and trimodal	bimodal
Wax generation	< 0.5 %	~ 1%

The advantages of the CSTRs-based slurry processes are unmatched product quality, low-cost production, excellent process stability, safe behavior of the process, environment-friendly operation and a wide range of product-producing capability. The main disadvantages of CSTR slurry phase processes are wax generation and relatively poor mixing and temperature control with high slurry concentration.

1.1.2 SLURRY POLYMERIZATION IN LOOP REACTORS

Loop reactors are jacketed tubular reactors with recycle. The Chevron-Phillips slurry loop reactors use the reactor temperature and other operating conditions to

control the MWD, whereas the BP Solvay slurry loop reactors use hydrogen for molecular weight control. The Chevron-Phillips process uses all three major families of catalysts. A high-yield supported chromium-based catalyst is used to produce medium to broad MWD PE, a supported ZN catalyst produces narrow MWD PE and metallocene catalysts are used to produce a very narrow MWD PE [10]. In contrast, the BP Solvay process uses supported ZN catalysts [14].

The slurry loop reactor operates at pressures of 3,000-9,000 kPa, and temperatures of 70-120 $^{\circ}$C [6]. The mean residence time of the loop reactor is 1.5-2 hrs. The solid concentration in the slurry varies from 18-50%. The heat of polymerization is removed by the countercurrent flow of cooling water in a jacket. The operating temperature range inside the reactor does not allow the polymer to melt and, therefore, form a slurry of discrete particles in the liquid diluent.

A typical industrial slurry cascade-loop reactor in a series arrangement is shown in Fig. 1.4. In loop reactors, the catalyst suspension, monomer, comonomer, solvent and the anti-fouling agent are continuously fed using an axial pump placed near the bottom of the reactor. This axial pump is designed to maintain a high fluid velocity (5-7 m/s) ensuring adequate mixing and turbulence inside the reactor to facilitate sufficient heat removal from the reactor mixture [6], [15]. Moreover, high fluid velocity prevents solid deposition on the inner tube-wall even at high slurry concentrations. However, a higher velocity also increases the pumping cost and the pressure drop.

The main advantage of the slurry loop reactor over the CSTRs is the efficient mixing and heat removal even at higher solid concentrations. Other advantages of the slurry loop reactors are high monomer conversion, uniform reactor content, quick grade transition, low power consumption, no wax generation and higher profit margins. Some major limitations of the slurry loop reactors include unstable start-up, fouling, concentration gradient at low slurry velocities and inability to produce some of the LLDPE grades. A brief comparison between the CSTR slurry

polymerization and the loop reactor slurry polymerization is summarized in Table 1.2.
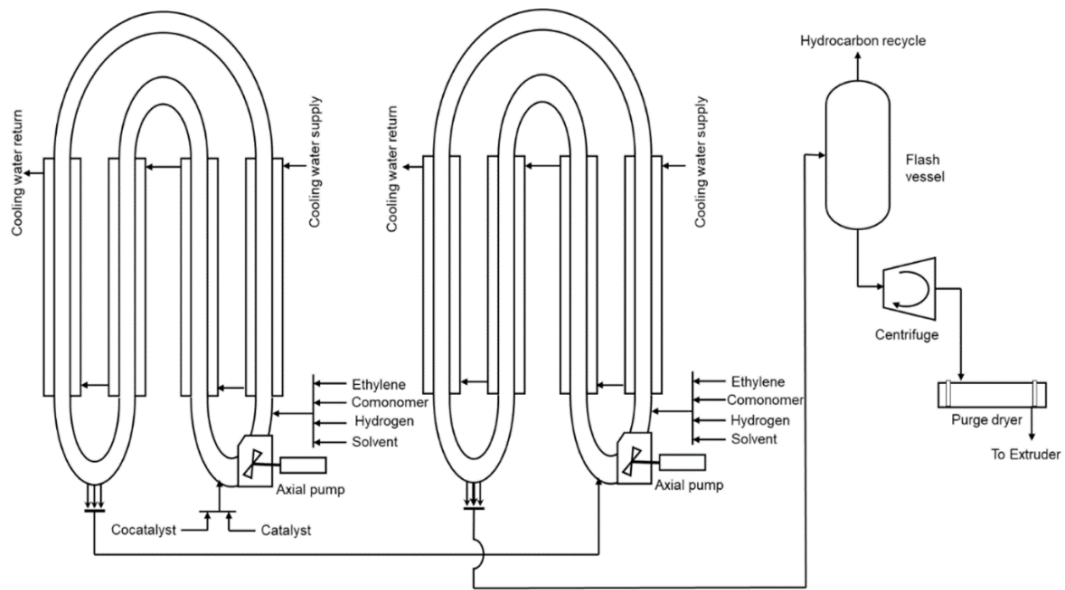
Fig. 1. 3 Schematic of an industrial slurry-phase loop reactor series

Table 1. 2 A comparison between the CSTR slurry polymerization and the loop
reactor slurry polymerization of ethylene

Reactor type	Slurry phase ethylene polymerization in CSTRs	Slurry phase ethylene polymerization in loop reactors
Solvent	n-hexane	iso-butane, iso-pentane, n-pentane, propane, neopentane and n-hexane
Co-monomer	Propylene and 1-butene	1-hexene and 1-butene
Catalyst	Supported Z-N	Supported Z-N, supported chromium based, metallocenes
Cocatalyst	Triethyl aluminium	Triethyl aluminium
Reactor temperature, ºC	75-85	70-120
Reactor pressure, kPa	300-1000	3,000-9,000
Average residence time, hr	1.5-3	0.5-1
Overall conversion, %	CX: 95-99 Hostalen: 95-99.5	upto 99.5 %
Product MWD	CX: freely controlled from narrow to very wide Hostalen: definite MWD from narrow to broad	Very narrow to wide MWD
Density, kg/m³	930-970	920-970
Melt index, g/10 min	0.01-80	0.01-100
Heat removal	CX: overhead condenser, reactor jacket and external slurry cooling Hostalen: jacket cooling	jacket cooling
Product	HDPE	HDPE and some of the LLDPE grades
solid concentration in the slurry	15-45 wt. %	up to 60 wt. %

1.2 MATHEMATICAL MODELING

 A mathematical model is the conceptualization of the real process. The process model is useful in performance improvement, process safety, process optimization and process control [16], [17]. In recent years, considerable effort has been made by several workers to develop the mathematical model of olefin polymerization in various reactor systems. These modeling studies are primarily focused on the prediction of the MWDs, CCDs and the particle size distribution (PSD) of the final product. To develop a model that can predict the physical and chemical properties of the final product, a clear understanding of the physics and chemistry of the relevant phenomena is required at multiple length scales namely, microscale, mesoscale and macroscale [18], [19].

1.3 MOTIVATION FOR THE PRESENT WORK

The work reported [20]–[25] on the modeling of ethylene polymerization is limited to the micro and meso levels. Only a few studies [6], [26], [27] developed a *complete* model for olefin polymerization. Sarkar and Gupta [27] developed a model for polypropylene polymerization in CSTRs. However, their simulation was not validated against any experimental/industrial data. The model of Touloupides et al. [6] for a loop olefin reactor was also not validated against any experimental data. The model of Casalini et al. [26] for polyethylene polymerization in a series of CSTRs, indeed, was validated against a set of experimental data. This study used the MGM with multisite catalysts along with a segregated residence time distribution (RTD) model to describe the effect of RTD on the polymer properties. The MGM itself requires significantly high computational times than the PMGM for the simulation of an industrial reactor [24]. Considering the reactor residence time distribution in a model will significantly increase the simulation time. The computational time will further increase by incorporating a family of sites. The high

computational times of such a model limits its use for optimization studies. Thus, there is a need to develop a computationally efficient reactor model that requires lower computational times for the simulation of *industrial* reactors, without losing much in terms of the accuracy in its prediction capability. The investigation of reactor operating variables requires a model that is tuned and validated against *several* sets of experimental or industrial data. The multi-objective optimization study on a computationally efficient reactor model is required to obtain the optimal operating conditions.

1.4   OBJECTIVES

The objectives of this work are as follows

1) To develop a computationally-efficient multi-scale mathematical model for an industrial high-density polyethylene (HDPE) slurry phase continuous stirred tank slurry reactor (CSTR).
2) To develop a MATLAB^{TM} code for the simulation of the developed model.
3) Tuning of the model using the industrial data.
4) Validation of tuned model with the industrial data.
5) The investigation of reactor operating variables on the productivity, polymer yield, plant safety and the product polydispersity index.
6) The multi-objective optimization study of the industrial HDPE continuous CSTR using the tuned model

1.5   ORGANISATION OF THE THESIS

This thesis is divided into six chapters. Chapter 1 presents an overview of the slurry phase ethylene polymerization processes, underlines the motivation of the present work and sets the objective of this work. In chapter 2, a detailed literature review is presented on the multi-scale mathematical modeling and simulation approach of the ethylene polymerization in slurry reactors. Guidelines to implement the multi-

scale mathematical modeling and simulation in slurry phase olefin polymerization processes are also proposed. Special focus is given on the need to reduce the computational effort for the simulation of industrial reactors so that the models can be used as an effective tool-kit for optimization studies using state-of-art algorithms. Chapter 3 is focused on the development of a computationally efficient multi-scale mathematical for an industrial slurry phase high-density polyethylene reactor. This chapter also covers the computational procedure for the simulation of the reactor model followed by the tuning of the developed model with the available industrial data. Chapter 4 deals with the optimization aspects and formulation of the optimization problems. In chapter 5, the key results are discussed which comprises the validation of the reactor model with the available industrial data on an industrial reactor, the sensitivity analysis of the tuned model concerning the tuning parameters and the multi-objective optimization study. Special focus is given on the study of the effects of the variation of operating variables on productivity, the polymer yield, the polydispersity index (PDI), and operational safety. Chapter 6 discusses the conclusions of the thesis followed by the opportunities for future work.

CHAPTER 2

MULTI-SCALE MODELING AND SIMULATION APPROACH

Mathematical modeling of a polymerization process requires a complete understanding of the various physical and chemical phenomena at various scales. The model equations for a polymerization process are used to describe the phenomena of mass and heat transport, the reaction kinetics, phase equilibria and reactor hydrodynamics. The process model is useful in performance improvement, process safety, process optimization and process control [16], [17].

The polymerization reaction begins when the monomer reaches an active site through pores of the catalyst. As soon as the polymer accumulates at the active sites, the local stress build-up at different points. This leads to the fragmentation of the original catalyst into microparticles. The process continues until the entire catalyst particle disintegrates into several fragments. These fragments are also referred to as microparticles, catalyst sub-particles, micro-grains, or primary particles. The microparticles remain in-tact with the polymer which is already formed due to the polymerization reaction. As the reaction proceeds, a layer of polymer grows around *every* microparticle and, consequently, these microparticles with the surrounding polymers undergo radial expansion [28], [29]. This process continues as long as the particles remain inside the reactor or until the catalyst is completely deactivated. The mechanism of catalyst fragmentation is well documented for the heterogeneous Z-N catalysts [30]–[34] and the Phillips catalysts [35], [36]. The ideal fragmentation phenomenon is called *replication*. The particle size distribution of the final product after the polymerization in a batch or semi-batch reactor replicates the particle size distribution of the original catalyst particle entering the reactor. Ideal replication is supposed to be achieved when there

is an appropriate balance between the mechanical properties of the particle and catalyst activity [11].

In recent years, considerable effort has been made by several workers to develop the mathematical model of olefin polymerization in various reactor systems. These modeling studies are primarily focused on the prediction of the MWDs, CCDs and the particle size distribution (PSD) of the final product. To develop a model that can predict the physical and chemical properties of the final product, a clear understanding of the physics and chemistry of the relevant phenomena is required at multiple length scales. The ethylene polymerization processes can be modeled at three different length scales [18], [19], namely, microscale, mesoscale and macroscale. Modeling at a microscale level includes the chemical kinetics, chain growth and its composition, molecular weights and its distribution, etc. Modeling at a mesoscale mainly comprises of intra-particle mass and energy transport and phase equilibria. Modeling at macroscale levels mainly consists of component balances, overall material and energy balances and the reactor residence time distribution (RTD). Each length scale emphasizes the phenomena at specific levels. However, there is no dividing line between these levels of modeling A complete model for a polymerization process includes modeling at *all* three scales. The following sections discuss the multi-scale modeling and simulation approach for the slurry phase ethylene polymerization processes.

2.1 KINETIC MODEL (MICRO-SCALE MODEL)

A general kinetic model of heterogeneous Z-N polymerization may include a series of elementary steps. A general kinetic model may include the following elementary steps:

- Site activation

- Chain initiation

- Chain propagation

- Chain transfer

- Chain transformation

- Site deactivation and

- Reversible catalytic inhibition

Different workers have proposed different elementary reactions to model these elementary steps. Table 2.1 gives a brief review of the different elementary reactions proposed by different workers for each of the elementary steps. A generalized kinetic model of olefin polymerization processes is given in Table 2.2. This table consists of all the proposed elementary reactions by different workers (Table 2.1) for each of the elementary steps in the polymerization process. Every elementary reaction has a distinct kinetic rate constant.

 It is observed in Table 2.1 that some workers [37] [5] proposed the comprehensive kinetic model which comprises almost all possible elementary reactions of the generalized kinetic model (Table 2.2). Zacca and Ray [15] proposed a simplified kinetic model. This simplified kinetic model includes site activation by co-catalyst, chain propagation, chain transfer to monomer and hydrogen, spontaneous site deactivation and site transformation by a co-catalyst. This model has been used by several workers [6], [38], [39] in this field. A comprehensive kinetic model proposed by Kissin and co-workers [40], [41] was used by Pladis et al. [42] to study catalytic olefin copolymerization in a series of CSTRs. Several workers simplified the kinetic model by eliminating site activation [17], [22], [43]–[45] or chain transfer [22], [44], [46]. Some workers also eliminated the site deactivation step [23], [47] in their kinetic model.

Table 2. 1 A brief review of the kinetic model used in olefin polymerization processes

Elementary step	Elementary reaction	References*													
		[48]	[24]	[15]	[37]	[41]	[5]	[46]	[17]	[49]	[6]	[45]	[50]	[51]	[20]
Site activation	by co-catalyst	✓		✓	✓	✓	✓			✓	✓		✓	✓	
	by hydrogen				✓	✓	✓								
	by monomer				✓		✓	✓							
	spontaneous				✓		✓								✓
Chain Initiation	monomer	✓	✓		✓	✓	✓			✓	✓	✓		✓	
Chain propagation	monomer	✓	✓	✓	✓	✓	✓	✓	✓	✓	✓	✓	✓	✓	✓
Chain transfer	to co-catalyst				✓	✓			✓						
	to hydrogen	✓	✓	✓	✓	✓	✓			✓	✓	✓	✓		✓
	to monomer	✓		✓	✓	✓	✓			✓			✓	✓	✓
	β-hydride					✓									
	spontaneous	✓		✓	✓		✓		✓		✓	✓			
Chain transformation	to co-catalyst			✓	✓										
	to hydrogen				✓		✓								
	to monomer				✓										
	spontaneous				✓		✓								
Site deactivation	by co-catalyst						✓								
	by hydrogen				✓		✓								
	by monomer				✓										
	by poison	✓				✓	✓								
	spontaneous	✓		✓	✓	✓	✓	✓	✓	✓	✓	✓	✓	✓	✓
Reversible catalyst inhibition	By hydrogen													✓	

18

Table 2. 2 A generalized kinetic model of olefin polymerization

Site activation

By co-catalyst: $C_P^k + [\text{cocat}] \xrightarrow{k_{act}^k} P_o^k$

By hydrogen: $C_P^k + H_2 \xrightarrow{k_{aH_2}^k} P_o^k$

By monomer: $C_P^k + M_i \xrightarrow{k_{aM_i}^k} P_o^k + M_i$

Spontaneous: $C_P^k \xrightarrow{k_{aSP}^k} P_o^k$

Site transformation

To hydrogen: $P_{n,i}^k + H_2 \xrightarrow{k_{tH}^k} P_0^m + D_n^k$

To co-catalyst: $P_{n,i}^k + [\text{cocat}] \xrightarrow{k_{tcocat}^k} P_0^m + D_n^k$

To solvent: $P_{n,i}^k + S \xrightarrow{k_{tS}^k} P_0^m + D_n^k$

Spontaneous: $P_{n,i}^k \xrightarrow{k_{tSP}^k} P_0^m + D_n^k$

Chain initiation by monomer *i*:

$P_o^k + M_i \xrightarrow{k_{\text{in},i}^k} P_{1,i}^k$

Chain Propagation

By monomer $i = 1$:
$P_{n,1}^k + M_1 \xrightarrow{k_{p,11}^k} P_{n+1,1}^k$

$P_{n,2}^k + M_1 \xrightarrow{k_{p,21}^k} P_{n+1,1}^k$

By monomer $i = 2$:
$P_{n,1}^k + M_2 \xrightarrow{k_{p,12}^k} P_{n+1,2}^k$

$P_{n,2}^k + M_2 \xrightarrow{k_{p,22}^k} P_{n+1,2}^k$

Reversible catalyst inhibition by hydrogen

$C_P^k + H_2 \leftrightarrow C_{PH_2}^k$

Chain Transfer

To hydrogen: $P_{n,i}^k + H_2 \xrightarrow{k_{trH}^k} P_0^k + D_n^k$

To monomer: $P_{n,i}^k + M_i \xrightarrow{k_{trM,i}^k} P_{1,i}^k + D_n^k$

Spontaneous: $P_{n,i}^k \xrightarrow{k_{trSP,i}^k} P_0^k + D_n^k$

To co-catalyst: $P_{n,i}^k + [\text{cocat}] \xrightarrow{k_{trcocat}^k} P_0^k + D_n^k$

To solvent: $P_{n,i}^k + S \xrightarrow{k_{trS}^k} P_0^k + D_n^k$

β- hydride elimination: $P_{n,i}^k \xrightarrow{k_{tr\beta}^k} P_0^k + D_n^{=k}$

Site deactivation

By hydrogen: $P_{n,i}^k + H_2 \xrightarrow{k_{dH}^k} C_d^k + D_n^k$

By co-catalyst: $P_{n,i}^k + [\text{cocat}] \xrightarrow{k_{dH}^k} C_d^k + D_n^k$

By monomer: $P_{n,i}^k + M_j \xrightarrow{k_{dM,ij}^k} C_d^k + D_n^k$

By by-product: $P_{n,i}^k + B \xrightarrow{k_{dB}^k} C_d^k + D_n^k$

Spontaneous: $P_{n,i}^k \xrightarrow{k_{dSP,i}^k} C_d^k + D_n^k$

Based on the literature review (Table 2.1), it is observed that a majority of workers employed chain initiation, chain propagation, chain transfer and site deactivation as elementary steps in their kinetic model. Chain propagation is an essential elementary reaction employed in all kinetic models. Chain transfer to monomer and hydrogen and spontaneous site deactivation are commonly used in the kinetic model. In recent studies, site activation by co-catalyst [26], [50], [51] and reversible

catalytic inhibition by hydrogen [26], [50], [51] are also employed as elementary reactions.

2.1.1 MULTIPLE ACTIVE SITES vs. SINGLE SITE IN A KINETIC MODEL

The kinetic model using a heterogeneous Z-N catalyst often uses multiple active sites, each with a distinct kinetic rate constant. The use of multiple sites in the kinetic model leads to a broad MWD in the predictions. The experimental evidence [32], [52] also supports the presence of multiple active sites in the Z-N catalyst. The kinetic behavior of Z-N catalytic olefin polymerization using multiple sites is described by several workers [6], [44], [47], [53][37]. Touloupides et al. [6] suggested that five to six active sites may be required to describe the breadth in the MWD in olefin polymerizations using heterogeneous Z-N catalysts. However, a kinetic model using multiple active sites significantly increases the number of kinetic parameters involved in the model. The computational time for the simulation of an industrial reactor is significantly increased by increasing the number of active sites in the kinetic model. Modeling the actual behavior of Z-N catalysts in terms of the rate of polymerization and the PDIs of the final product using a small number of kinetic parameters is also a big challenge. One way to reduce the number of kinetic parameters in a model is to lump the active sites [54]. In the lumped active site model, each site can be assumed to be activated using different mechanisms (e.g., by co-catalyst, hydrogen, etc.) to give distinct active centers. In this way, even a single site or a two-site kinetic model with multiple active centers can provide a satisfactory prediction of the MWDs and PDIs [54]. This will significantly reduce the number of kinetic parameters.

In contrast, the use of a single-site catalyst in a kinetic model [24][22][55] kinetic model can be used for the accurate prediction of the rate of polymerization and polymer yield, multiple sites are generally incorporated in the kinetic model to

predict broadness in the MWD. The lumped active site model [54]using a single catalytic site can also predict some broadness in the MWD. A single site kinetic model also results in a decrease in the number of kinetic parameters to be estimated. This leads to a drastic reduction in the computational time for the simulation of the industrial reactor. Small computational time is vital for a model to be useful for optimization studies. The multi-objective optimization (MOO) [56], [57] study is a computationally rigorous activity. In reality, the MOO problem has to be solved several times with different combinations of algorithmic parameters to confirm the convergence of the results. Thus, the time consumed in a single simulation is crucial for solving MOO problems. Therefore, a balance between accuracy and simplicity is required for kinetic models to be used for optimization studies. A simplified lumped site model using a single catalytic active site and a smaller number of kinetic parameters can make a reasonable balance between accuracy and simplicity.

2.1.2 ESTIMATION OF KINETIC PARAMETERS

As discussed earlier, a kinetic model using multiple active sites significantly increases the number of kinetic parameters involved in the model. Employing a generalized kinetic model (e.g., Table 2.2), also requires the estimation of several kinetic parameters. Generally, the values of the kinetic parameters are not disclosed in the literature. Although some of the values of the kinetic parameters may be available in the literature, wide ranges of their values are reported. Besides, the parameters not only depend on the kinetic mechanism but also the specific catalysts and co-catalysts. A small difference in catalyst composition may result in significant variations in the values of the kinetic parameters and consequently, the polymer properties. The olefin polymerization processes use a large number of high activity catalysts with different compositions and morphology for the production of polymer with various specifications. With the continuous evolution in catalyst technology, the reported values cannot be directly used with much confidence. An

accurate estimation of kinetic parameters is a challenging and computationally expensive task. A computationally efficient parameter estimation technique is vital to develop a kinetic model that is to be used for the prediction of product specifications with high accuracy at the industrial scale.

In the past, considerable effort has been made by several workers to estimate the kinetic parameters for olefin polymerization processes. The reported procedures involve the estimation of kinetic parameters using experimental/industrial data on a batch, semi-batch and continuous reactors. The experimental data related to polymer microstructure and MWDs are obtained using gel permeation chromatography (GPC), Fourier-transform infrared spectroscopy (FTIR) and nuclear magnetic resonance (NMR) spectroscopy [58]. The experimental/industrial data obtained from these techniques are used to estimate the best-fit values of the kinetic parameters. The best-fit values are generally obtained by *tuning* using a trial and error technique [59] or using error minimization *via* evolutionary algorithms [56], [57] so that the model predictions match with the experimental data-sets. Another approach to estimate the kinetic data may include the least-squares technique [60], nonlinear programming (NLP) techniques [61] and multi-response linear regression using the maximum likelihood estimation approach [60], [62], etc. These approaches are also used for parameter estimation, data reduction and optimization studies [63]. Table 2.3 presents a brief overview of the techniques used for the estimation of a large number of kinetic parameters in olefin polymerization processes.

Table 2. 3 A brief overview of the techniques used for the estimation of kinetic parameters

Source of data	Catalyst	Parameter estimation procedures/techniques	Ref.
Gas-phase olefin copolymerization in batch, semi-batch and continuous reactor data	Transition metal catalyst	Analytical equations are derived to estimate the kinetic parameters and reactivity ratio of the active sites	[64]
Computational experiment data	Transition metal catalyst	Two online estimation techniques are used namely, extended Kalman filter (EKF) and a non-linear programming technique (nonlinear dynamic parameter estimator) to estimate the kinetic parameters	[61]
Cascade stirred reactors for ethylene-propylene copolymerization	Z-N catalyst	The least-square technique is used to estimate kinetic parameters	[65]
Commercial slurry phase, CSTRs for HDPE	Z-N catalyst	A two-step manual iterative algorithm is developed to estimate a large number of kinetic parameters	[38]
Gas-phase PP polymerization in a stirred-bed reactor	Z-N catalyst	A two-step manual iterative algorithm is used to estimate a large number of kinetic parameters	[66]
Industrial slurry phase ethylene polymerization in reactor trains	Z-N catalyst	A non-linear optimization procedure subjected to hard and soft constraints is used to estimate a large number of kinetic parameters	[67]
Experimental data on ethylene/1-olefin copolymerization process	Z-N catalyst	Simultaneous deconvolution of MWD and the CCD and minimization of the sum of the square of error using the genetic algorithm is used	[68]
Industrial slurry phase series CSTRs for HDPE	Z-N catalyst	A multistep method by formulating three non-linear programmings is developed to estimate the kinetic parameters using the MWDs deconvolution	[13]
Co-polymerization of ethylene and 1,9-decadiene in a semi-batch reactor	Metallocene catalyst	An online data-driven strategy using retrospective cost model refinement algorithm is used for estimation of kinetic parameters	[69]

Some workers [38], [45] have used a two-step iterative technique to estimate the kinetic rate constants. In the first step, a single site catalyst was used to model all

the reactions except the MWDs and the PDI of the polymer so that the model predictions match with plant data. In the second step, multi-site modeling is incorporated to match the model-predicted MWDs and PDI with the plant data. The rate constant for chain transfer to hydrogen and monomer were adjusted to match the molecular weights at each active site. This approach is useful to handle the large number of kinetic parameters resulting from the consideration of multiple active site catalysts. A recent study [70] developed a technique for deconvolution and the estimation of the kinetic parameters based on the MWD, CCD and characterization techniques (GPC-IR, C-13 NMR spectroscopy, fractionation). In this study, the technique used was validated using a Monte Carlo simulation-based case study.

Kinetic modeling is a theoretical conceptualization of the real polymerization process. Estimation of kinetic parameters using the approach described above may lead to impractical outcomes [59]. Therefore, the parameters estimation approaches are not universal but process-dependent and may be unsuitable under particular conditions. Thus, further study is required in this field to develop a methodology that is suitable for most of the catalysts and processes for the accurate and efficient estimation of kinetic parameters.

2.1.3 A SIMPLIFIED KINETIC MODEL

A simplified kinetic model comprises only important kinetic parameters. Based on the literature review, a simplified kinetic model is proposed (see Table 2.4) for the olefin polymerization processes. The corresponding moment equations are also given in Table 2.4. A similar (or slightly modified) kinetic model with two active sites can be used to predict the actual behavior of ZN catalysts in most olefin polymerization processes. The number of kinetic parameters is significantly reduced using such simplified kinetic models. Some workers [24], [27] [9], [21], [22], [55] also used single active sites to model olefin polymerization processes.

2.1.4 METHOD OF MOMENTS

The (kinetic) model equations can be solved using the method of moments. This is a deterministic modeling technique to obtain the various moments of the live polymer chains and the dead chains produced at the catalyst sites. This method reduces a large number of mass balance equations into a much smaller and manageable number (using a fewer number of moments). This is a simple and computationally inexpensive method to determine the average MWD and the PDI. This method has been employed by several research groups [9], [24], [25], [71], [72] due to its simplicity and easy implementation.

Table 2. 4 A simplified kinetic model and the corresponding moment equations

Kinetic Scheme	Moment Equations
Site activation by co-catalyst $$C_P^k + [cocat] \xrightarrow{k_{act}^k} P_o^k$$	$$\frac{\partial \lambda_0^k}{\partial t} = \left(k_{in}^k P_0^k + k_{trM}^k P_0^k \right)M - \lambda_0^k \left(k_{dsP}^k + k_{trM}^k M + k_{trH}^k H_2 + k_P^k M \right) + k_P^k M \lambda_0^k$$
Chain initiation $$P_o^k + M \xrightarrow{k_{in}^k} P_1^k$$	$$\frac{\partial \lambda_1^k}{\partial t} = \left(k_{in}^k P_0^k + k_{trM}^k P_0^k \right)M - \lambda_1^k \left(k_{dsP}^k + k_{trM}^k M + k_{trH}^k H_2 + k_P^k M \right) + k_P^k M (\lambda_0^k + \lambda_1^k)$$
Chain propagation $$P_n^k + M \xrightarrow{k_p^k} P_{n+1}^k$$	$$\frac{\partial \lambda_2^k}{\partial t} = \left(k_{in}^k P_0^k + k_{trM}^k P_0^k \right)M - \lambda_2^k \left(k_{dsP}^k + k_{trM}^k M + k_{trH}^k H_2 + k_P^k M \right) + k_P^k M (\lambda_0^k + 2\lambda_1^k + \lambda_2^k)$$
Chain Transfer To hydrogen: $$P_n^k + H_2 \xrightarrow{k_{trH}^k} P_0^k + D_n^k$$	$$\frac{\partial \Lambda_0^k}{\partial t} = \lambda_0^k \left(k_{dsP}^k + k_{trM}^k M + k_{trH}^k H_2 \right)$$ $$\frac{\partial \Lambda_1^k}{\partial t} = \lambda_1^k \left(k_{dsP}^k + k_{trM}^k M + k_{trH}^k H_2 \right)$$
To monomer: $$P_n^k + M \xrightarrow{k_{trM}^k} P_0^k + D_n^k$$	$$\frac{\partial \Lambda_2^k}{\partial t} = \lambda_2^k \left(k_{dsP}^k + k_{trM}^k M + k_{trH}^k H_2 \right) , k = 1, 2, .. \text{ (depending on the number of site type)}$$
Site deactivation Spontaneous: $$P_n^k \xrightarrow{k_{dSP}^k} C_d^k + D_n^k$$	

The moment equations in Table 2.4 are solved to obtain the values of the first three moments of the live chains, λ_l^k, and of the dead chains, Λ_l^k (l = 0, 1, 2). The

average molecular properties such as the number average molecular weight, M_n, the weight average molecular weight, M_w, and the polydispersity index, PDI, can be obtained as,

$$M_n = \left(\frac{\sum_{k=1}^{N_s}(\lambda_1^k + \Lambda_1^k)}{\sum_{k=1}^{N_s}(\lambda_0^k + \Lambda_0^k)} \right) MW \tag{2.1}$$

$$M_w = \left(\frac{\sum_{k=1}^{N_s}(\lambda_2^k + \Lambda_2^k)}{\sum_{k=1}^{N_s}(\lambda_1^k + \Lambda_1^k)} \right) MW \tag{2.2}$$

$$PDI = \frac{M_w}{M_n} \tag{2.3}$$

Another method to obtain the MWD and PDI of the polymer is by using population balances (Dubé et al. 1997, Mantzaris et al. 2002) and the method of instantaneous distribution [75] using Flory's [76] most probable distribution. The interested reader is referred to a review article [75] for these methods.

2.2 SINGLE PARTICLE MODELS (MESO-SCALE MODEL)

2.2.1 OVERVIEW OF SINGLE PARTICLE MODELS

Modeling at the mesoscale primarily deals with intraparticle monomer and thermal diffusion. This leads to the intraparticle monomer concentration gradient and temperature gradient. The state-of-the-art *single-particle models* for olefin polymerization are at the heart of this scale of modeling. The *single-particle models* are classified as particle morphology models and performance models [11]. The particle morphology models [77]–[86] are mainly focused on the phenomena of

catalyst fragmentation and morphology development. The performance models are used to predict the rate of polymerization and polymer properties such as the MWDs and PDI [24], [27], [87], [88]. This model considers the radial variation in the local monomer concentration, responsible for the broad MWD in the formation of the polymer. The radial thermal gradient inside the macroparticle also alters the rate of reaction by altering the kinetic rate constants and results in the formation of a polymer with a broad MWD. The particle morphology models have been recently reviewed by Alizadeh and McKenna [29] and will not be discussed in this review.

Table 2. 5 Salient features of single-particle models

MGM [26], [89]–[91]	**PFM** [20], [92]–[94]	**PMGM** [24], [27], [55]	**RPPFM** [6], [95]
Assumes fragmentation of the original catalyst into microparticles	Considers the dispersion of catalyst fragments in a polymer continuum	Combines the continuum theory of the PFM and microstructural feature of the MGM	Combines the features of the PFM and the concept of random pore diffusion through the porous catalyst
Considers two levels of diffusion coefficients, microparticle diffusion and macroparticle diffusion	Considers only macroparticle diffusion	Considers instantaneous catalyst fragmentation into microparticles and their expansion like MGM	Considers two levels of diffusion, diffusion through pores of the macroparticle and also through the amorphous phase of the semi-crystalline polymer
Considers the intraparticle monomer concentration gradient and temperature gradient in the radial direction	Considered as a simplified pseudo-homogeneous MGM	Considers only macroparticle diffusion	Considers the intraparticle monomer concentration gradient and temperature gradient in the radial direction
	Considers the intraparticle monomer concentration gradient and temperature gradient in the radial direction	Considers the intraparticle monomer concentration gradient and temperature gradient in the radial direction	Includes the effect of monomer transport by convection through the pores of the growing macroparticle

Several single-particle models have been proposed in the literature. These include the multigrain model, MGM, the polymeric flow model, PFM, the polymeric multigrain model, PMGM and the random pore polymeric flow model, RPPFM.

Table 2.5 summarizes the salient features of single-particle models. Out of these models, the MGM and PFM are the most employed models at single-particle levels. The PMGM and RPPFM have also evolved from these two models.

2.2.2 MATHEMATICAL MODELING AT SINGLE PARTICLE LEVEL

The MGM gives a detailed and realistic picture of the particle growth by expansion due to polymerization. This model can incorporate the heterogeneous nature of active sites and considers the fragmentation of the catalyst into microparticles and their expansion during polymerization. The original catalyst particles are assumed to be aggregates of a large number of smaller microparticles with the active sites present on their surface. The microparticles are assumed, for simplification, to be arranged in a spherical shell to form close-packed layers in the macroparticle (Figure 2.1).

As the polymerization proceeds, a layer of polymer grows around *every* microparticle and, consequently, these microparticles with the surrounding polymers undergo radial expansion [11], [29]. This process continues as long as the particles remain inside the reactor or until the catalyst is completely deactivated. The mechanism of catalyst fragmentation is well documented for the heterogeneous ZN catalysts [30], [32]–[34], [96] and the Phillips catalysts [35], [97]. The ideal fragmentation process is called *replication*. This states that the particle size distribution of the final product after the polymerization in a batch or semi-batch reactor replicates the particle size distribution of the original catalyst particle entering the reactor [11]. The MGM considers that the incoming monomer has to first diffuse through the pores of the macroparticles to reach the polymer surface surrounding the microparticle. Thereafter, the monomer has to diffuse through the polymer layer to the active sites present at the surface of the microparticles (Figure 2.1). Thus, the MGM considers two levels of diffusional resistance and particle

morphology. The newly formed polymer chains push the previous layer and consequently, the macroparticle grows as the reaction progresses.
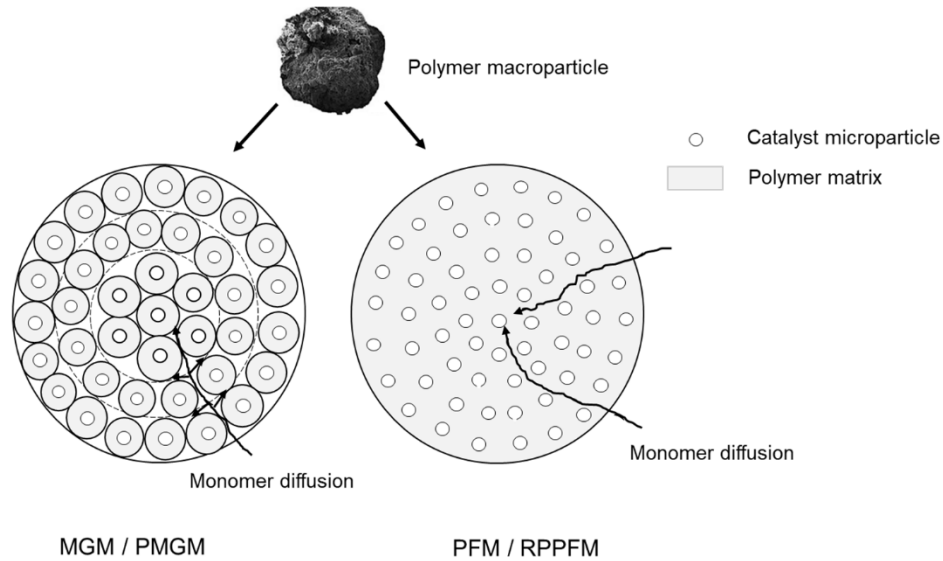

Fig. 2. 1 Schematic of the PFM and the MGM (adapted from references [11], [24], [95])

The PFM considers that the fragmented catalyst and the polymer chains form a continuum. Thus, the diffusion of monomer takes place through the pseudo-homogeneous polymer matrix (Figure 2.1). This model is considered as the simplified pseudo-homogeneous multigrain model. The major difference between the PFM and MGM is that the diffusivity at the microparticle level is neglected in the PFM whereas the MGM considers the different values of diffusion coefficients at both the macroparticle level and the microparticle level.

The mathematical modeling at the intraparticle level is a typical diffusion-reaction problem in which the monomer gradient exists only in the radial direction. Likewise, intraparticle thermal gradients also exist in only the radial direction but the direction of heat transport is opposite to that of the monomer transport.

The intraparticle mass balance equations for monomer for the diffusion inside a macroparticle can be given as follows

$$\frac{\partial M_{mp}}{\partial t} = \frac{1}{r_{mp}^2} \frac{\partial}{\partial r_{mp}} \left(D_{mp} r_{mp}^2 \frac{\partial M_{mp}}{\partial r_{mp}} \right) - R_v \tag{2.4}$$

IC : $t = 0$ $\qquad\qquad$ $M_{mp} = M_0$ $\tag{2.5}$

BC 1 : $r_{mp} = 0$ $\qquad$ $\dfrac{\partial M_{mp}}{\partial r_{mp}} = 0$ $\tag{2.6}$

BC 2 : $r_{mp} = R_{mp}$ $\qquad$ $-D_{mp} \dfrac{\partial M_{mp}}{\partial r_{mp}} = k_{1s}(M_{mp,in} - M_b)$ $\tag{2.7}$

where D_{mp} and M_{mp} are the diffusivity of monomer and monomer concentration in the macroparticle, R_v is the rate of monomer consumption per unit volume of the macroparticle, k_{1s} is the mass transfer coefficient, M_0, $M_{mp,in}$ and M_b are the initial monomer concentration in the macroparticle, monomer concentration at the liquid solid interface and monomer concentration in the bulk of the liquid, respectively. The diffusivity of the monomer in the macroparticle, D_{mp}, can be expressed in terms of the monomer diffusivity in the pure liquid, D_L, the catalyst porosity, ε and the catalyst tortuosity, ζ, as follows

$$D_{mp} = D_L \frac{\varepsilon}{\zeta} \tag{2.8}$$

The mass balance equation of monomer for the diffusion inside the polymers around the microparticle can be given as

$$\frac{\partial M_{\mu p}}{\partial t} = \frac{1}{r_{\mu p}^2} \frac{\partial}{\partial r_{\mu p}} \left(D_{\mu p} r_{\mu p}^2 \frac{\partial M_{\mu p}}{\partial r_{\mu p}} \right) \tag{2.9}$$

IC : $t = 0$ $\qquad\qquad$ $M_{\mu p} = M_0$ $\tag{2.10}$

BC 1 : $r_{\mu p} = r_{cf}$ $\qquad$ $4\pi r_{cf}^2 D_{\mu p} \left. \dfrac{\partial M_{\mu p}}{\partial r_{\mu p}} \right|_{r_{\mu p} = r_{cf}} = \dfrac{4}{3} \pi r_{cf}^3 R_{\mu P}$ $\tag{2.11}$

BC 2: $r_{\mu p} = R_\mu$ $M_{\mu p} = M_{eq}$ (2.12)

Here $D_{\mu p}, M_{\mu p}$ and $R_{\mu p}$ are the diffusivity of monomer, the concentration of monomer and rate of monomer consumption in the polymeric shell around a microparticle, respectively, r_{cf} is the radius of the catalyst after fragmentation and R_μ is the radius of polymeric shell around the microparticle. M_0 and M_{eq} are the initial monomer concentration and the equilibrium monomer concentration at the surface of the polymeric shell around the microparticle. The value of $D_{\mu p}$ is obtained in terms of the diffusivity of monomer in the amorphous phase, D_{amp}, and the correction factors, α and β, using the equation proposed in the literature [98]–[100],

$$D_{\mu P} = \frac{D_{amp}}{\alpha\beta}$$ (2.13)

The rate of polymerization at the microparticle, $R_{\mu p}$, can be obtained as

$$R_{\mu P} = k_P C^* M$$ (2.14)

where k_P is the propagation rate constant, C^* is the concentration of active sites at the surface of the microparticle and M is the monomer concentration at the active site.

The intraparticle heat balance equation at the macroparticle level is given as

$$\rho C_{P,mp} \frac{\partial T_{mp}}{\partial t} = \frac{1}{r_{mp}^2} \frac{\partial}{\partial r_{mp}} \left(k_{mp} r_{mp}^2 \frac{\partial T_{mp}}{\partial r_{mp}} \right) + (-\Delta H_P) R_v$$ (2.15)

IC : $t = 0$ $T_{mp} = T_0$ (2.16)

BC 1: $r_{mp} = 0$ $\frac{\partial T_{mp}}{\partial r_{mp}} = 0$ (2.17)

BC 2: $r_{mp} = R_{mp}$ $-k_{mp} \frac{\partial T_{mp}}{\partial r_{mp}} = h(T_{r_{mp}=R_{mp}} - T_b)$ (2.18)

31

where ρ and $C_{P,mp}$ are the density and specific heat capacity of the macroparticle, ΔH_P is the heat of polymerization, h and k_{mp} are the heat transfer coefficient and the thermal conductivity and T_0 and T_{mp} are the initial temperature and temperature of the macroparticle, respectively at any time, t.

Similarly, the heat balance equation at the microparticle level is given as

$$\rho C_{P,\mu p} \frac{\partial T_{\mu p}}{\partial t} = \frac{1}{r_{\mu p}^2} \frac{\partial}{\partial r_{\mu p}} \left(k_{\mu p} r_{\mu p}^2 \frac{\partial T_{\mu p}}{\partial r_{\mu p}} \right) \tag{2.19}$$

$$\text{IC}: \quad t = 0 \qquad\qquad T_{\mu p} = T_{\mu 0} \tag{2.20}$$

$$\text{BC 1}: \quad r_{\mu p} = r_{cf} \qquad 4\pi r_{cf}^2 k_{\mu p} \left. \frac{\partial T_{\mu p}}{\partial r_{\mu p}} \right|_{r_{\mu p} = r_{cf}} = \frac{4}{3} \pi r_{cf}^3 (-\Delta H_P) \tag{2.21}$$

$$\text{BC 2}: \quad r_{\mu p} = R_{\mu p} \qquad T_{\mu p} = T_{mp} \tag{2.22}$$

where $C_{P,\mu p}$ and $k_{\mu p}$ are the specific heat capacity and the thermal conductivity of the polymeric shell around the microparticle, respectively. $T_{\mu 0}$ and $T_{\mu P}$ are the initial temperature and the temperature of the polymeric shell around the microparticle at any time, t.

The PMGM [24], [25] combines the attributes of the PFM and the MGM. The effective diffusivity in the macroparticle in PMGM is obtained by multiplying the diffusivity in the pure polymer and the volume fraction of polymer in the macroparticle and can be given as

$$D_{eff,PMGM} = D_{Poly} \left(1 - \frac{V_c}{V_P} \right) \tag{2.23}$$

Kanellopoulos et al. [95] developed a modified PFM using the concept of random pore diffusion through the porous catalyst [101]. They referred to their model as

the random pore polymer flow model, RPPFM. This model also includes the intraparticle monomer transport through convection as suggested by Kittilsen et al. [102] . The intraparticle monomer balance using this model can be given as

$$\frac{\partial M}{\partial t} = D_{eff,RPPFM} \left(\frac{2}{r} \frac{\partial M}{\partial r} + \frac{\partial^2 M}{\partial r^2} \right) + \frac{\partial D_{eff,RPPFM}}{\partial r} \frac{\partial M}{\partial r} - R_v \qquad (2.24)$$

$$\text{IC}: \ t = 0 \qquad \qquad \text{M} = M_0 \qquad \qquad (2.25)$$

$$\text{BC 1}: \ r = 0 \qquad \frac{\partial M}{\partial r} = 0 \qquad \qquad (2.26)$$

$$\text{BC 2}: \ r = R \qquad \text{M} = M_e (1 - e^{-k_s t}) \qquad \qquad (2.27)$$

This model (RPPFM) also considers the dual diffusion of monomer through the pores of the macroparticle and also through the amorphous phase of the semi-crystalline polymer. At the beginning of the polymerization process, when the catalyst undergoes fragmentation, monomer transport takes place through the highly porous pseudo-homogeneous network of the catalysts and polymer. As the polymerization progresses, the particle morphology changes and the monomer has to diffuse through the permeable amorphous phase of the particle since the crystalline phase is (almost) impermeable to the monomer. The effective diffusivity for this model can be given as

$$D_{eff,RPPFM} = \frac{\varepsilon}{\zeta^2} D_{ij}^o + (1 - \varepsilon)(1 + 3\varepsilon) D_i^P \qquad (2.28)$$

Here, D_{ij}^o is the gas phase binary diffusion of component i in presence of component j using the Chapman and Enskog equation and D_i^P is the diffusivity of component, i, in the amorphous phase. Table 2.6 summarizes the mathematical model equations, prediction capabilities, advantages and limitations of the single-particle models.

Table 2. 6 A comparison between the various single-particle models (mesoscale)

	MGM	PFM	PMGM	RPPFM
Mass balance	Eq. 2.4-2.7 Eq. 2.9-2.12	Eq. 2.4-2.7	Eq. 2.4-2.7	Eq. 2.24-2.27
Heat balance	Eq. 2.15-2.18 Eq. 2.19-2.22	Eq.2.15-2.18	Eq. 2.15-2.18	Eq. 2.15-2.18
Effective diffusivity	Eq. 2.8 Eq. 2.13	Eq. 2.8	Eq. 2.23	Eq. 2.28
Prediction capabilities	predicts a high rate of polymerization	predicts a lower rate of polymerization compared to the MGM	predicts a lower rate of polymerization	predicts a high rate of polymerization
	predicts broad MWD	predicts less broad MWD	predicts narrow to broad MWD	predicts less broad MWD
	predicts PDI: up to 45	predicts PDI: 4-9	predicts PDI: 4- 10	PDI: not reported
Advantages	a most realistic and detailed description of the single-particle model	considered as the simplified version of MGM	incorporates the salient features of both PFM and MGM	this model links the rate of diffusion to the evolution of particle morphology
	predictions match well with the values at industrial scale both qualitative and quantitative	predictions match well with the values at the industrial scale qualitatively but not quantitatively	computationally efficient than MGM for the simulation of industrial reactors	
Limitations	the experimental evidence for most of the supported olefin catalysts do not support the phenomena of replication considered in the model	fails to describe the particle morphology for most of the polymerization processes using supported Z-N and Phillips catalyst	predicts the low rate of polymerization	the effective diffusivity is difficult to calculate as it depends on the porosity which varies with time, the composition of the continuous phase and the nature of the polymerization reaction. This limits the use of this model for several polymerization processes on an industrial scale
	two levels of structural organization (micro and macro) makes this model complex and computationally expensive			

2.2.3 THE COMPUTATIONAL FLUID DYNAMICS (CFD) MODELS

A fundamental understanding of reactor hydrodynamics is vital to ensure the maximum yield, productivity, product quality and smooth reactor operation. The non-ideal behavior of the slurry phase polyolefin reactors results in the heterogeneity in the flow field [103], non-uniform solid distribution (slug formation) [104], [105] and non-uniform temperature field [106]. These phenomena influence the polymer properties, yield and reactor safety. A fundamental understanding of these phenomena requires the modeling of solid-liquid hydrodynamics at the mesoscale. Modeling the hydrodynamics at the mesoscale requires solving the equations of momentum, mass and heat transport using extensive numerical techniques and large-scale computing capabilities. Computational fluid dynamics (CFD) is a promising tool for modeling the hydrodynamics of multiphase flow in olefin reactors at the mesoscale level. Hydrodynamic modeling using CFD has been extensively studied for the *gas-solid* flow in fluidized bed reactor [107]–[110]. Khan et al. [111] have reviewed the CFD modeling for the *gas-solid* flow in the fluidized bed reactor. Hydrodynamic modeling using CFD has also been studied for the *liquid-solid* flow in the slurry loop reactor in the recent past [105], [106], [112], [113]. However, an extensive review of the *liquid-solid* flow in the slurry reactor has not been published in the open literature to the best of our knowledge.

Hydrodynamic modeling of the two-phase flow using CFD is done using either the Eulerian-Lagrangian or Eulerian-Eulerian approach. The Eulerian-Lagrangian approach in polyolefin reactors considers the liquid or gas phase (continuous) in the Eulerian frame of reference and tracks the solid particles in the Lagrangian frame of reference. The Eulerian-Eulerian approach considers both phases (liquid/gas and solid) as a continuum (i.e., two-fluid model) and solves the momentum and mass balance equations for each phase. Most studies in the CFD modeling of polyolefin reactors have employed the Eulerian-Eulerian two-fluid model. These models involve the k-ε turbulence model, the kinetic theory of

granular flow (KTGF), and drag models [103], [105], [112], [114]. The k-ε turbulence model consists of two transport equations and is used to characterize the turbulent flow in slurry reactors. The KTGF is used to obtain the solid shear-strain tensor and considers the particle-particle collisions in the solid phase [104], [105]. The drag models [108], [114], [115] are used to describe the momentum exchange between the solid and the liquid phases. In addition, the particle swelling [105], [116] is modeled by incorporating the species transport in the two-fluid model. This accounts for the diffusion of liquid into the amorphous region of the semi-crystalline polymer particles [105]. In the recent past, the CFD models have been employed to understand the fluid dynamics, particle swelling and segregation, cohesive force-induced particle agglomeration, etc., in the slurry loop reactors. Table 2.7 presents a review of the CFD modeling approach applied to model the solid-liquid hydrodynamics at mesoscale in the slurry reactors.

Table 2. 7 Application of the CFD modeling approach for liquid-solid hydrodynamics

Research aspect	Reactor/ system	CFD approach	Main findings	Reference
Modeling of slugging regime	Solid-liquid fluidization experimental set-up	Eulerian- Eulerian KTGF, Gidaspow drag law	The pressure drop was found to be higher than the theoretical values for all fluid velocities. This was in agreement with the experimental values for the slugging regime.	[117]
Model prediction of bed voidage	Solid-liquid (glass-water) experimental fluidization set up	Eulerian-Eulerian two-fluid model, Wen and Yu drag law and Gidaspow drag law	CFD simulations were in reasonable agreement (within 5%) with the experimental results.	[118]
3D-modeling of solid-liquid flow hydrodynamics	Tubular loop reactor	Eulerian-Eulerian two-fluid model, KTGF, Gidaspow drag model	The solid hold-up was found to be uniform for small particles and high circulation fluid velocity. The model predicted data of pressure gradient were found to agree with the classical calculated data.	[103]

3D-modeling of temperature field	Tubular loop reactor (pilot-scale)	Eulerian-Eulerian two-fluid model, KTGF, Gidaspow drag model and heat balance equations	The temperature distribution was found uniform in the ascending straight pipe section and asymmetric in the upper curve section of the tubular reactor. The reactor temperature decreases with the increase in the circulation velocity and increases with the increase in the slurry concentration.	[106]
Effect of drag correlations and mass force on solid-liquid hydrodynamics	Solid-liquid experimental fluidization set-up	Two fluid-model, KTGF with added mass force in momentum equations, and drag models (Gidaspow, Wen and Yu (1966) and Beetstra et al. (2007))	The drag model by Beetstra et al. (2007) showed the best prediction of solid holdup with the experimental data. The mass force in momentum balance showed a significant effect on solid-liquid hydrodynamics and should not be ignored.	[119]
2D CFD-PBM coupled modeling for flow field and the PSD	Tubular loop reactor (pilot-scale)	PBM and quadrature method of moments, Algebraic slip mixture model, KTGF, Gidaspow drag model	The particle aggregation and breakage resulted in a broad PSD and a small volume average mean diameter of the particle. A larger average particle diameter and a broader PSD resulted in the non-uniform slurry velocity distribution.	[120]
Solid-phase dispersion, segregation and formation of polymer slugs	8-leg slurry loop reactor	Eulerian-Eulerian two-fluid model, KTGF, Gidaspow drag model	Large particles (2.5 mm in average diameter) tended to segregate and form large slugs and led to reactor blockage and operational instability.	[112]
Effect of slug dynamics on the reactor operation	8-leg slurry loop reactor	Eulerian-Eulerian two-fluid model, KTGF, Gidaspow drag model	The slug formation led to severe fluctuations in the average solid volume fractions, flow velocities and pump pressure. This led to operational instabilities. A mitigation method to ensure mixing in the transverse direction was proposed.	[113]
Modeling of particle swelling and aggregation	Slurry loop reactor and stirred tank reactor	Swelling-dependent two-fluid model, KTGF, k-ε turbulence model, Gidaspow drag model and population balance equation	This model was able to describe the swelling and aggregation of solid particles. The model predicted a gradual increase and a sharp increase in the power consumption in a stirred tank and a loop reactor, respectively.	[105]

Particle agglomeration due to cohesive forces between swollen PE particles	Slurry loop reactor	Eulerian-Lagrangian model (CFD-DEM), simplified Johnson-Kendall-Roberts model for cohesive forces	The surface cohesive energy density for the swollen PE particles was measured to be in between 4000 J/m^3 and 5000 J/m^3	[121]

The advancement in computational power and developments in computationally efficient CFD codes have motivated the research community to employ the CFD models in olefin polymerization reactors. A complete reactor model of the olefin polymerization reactor requires combining the kinetic model, intra-particle mass and heat diffusion with the CFD hydrodynamic model. A complex kinetic model is required to predict the molecular weight distribution and PDI. This requires large-scale computations. Thus, the simulation of a complete reactor model using CFD is a big challenge to be used for process optimization and control [122]. Most of the reported work on CFD analysis of a complete reactor is limited to the lab or pilot scale. It is also a major challenge to develop and validate a complete reactor model using CFD for a large-scale industrial reactor.

2.2.4 PHASE EQUILIBRIA AND THERMODYNAMIC PROPERTIES

The slurry reactors for the polymerization of olefin are multi-phase systems. These include solid macroparticles, the continuous liquid phase, the dispersed gas bubble phase and the vapor phase (in the case of CSTRs). At steady-state conditions, an equilibrium is established among these phases. The rate of polymerization and the polymer properties depend on the value of the equilibrium monomer concentrations in the different phases. These concentrations can be obtained using concepts of phase equilibria and the equation of state (EOS). Henry's law [123], [124], sorption data [46], [125] and equations of state (EOS) [9], [27], [42], [123] have been used to determine the equilibrium monomer concentration in slurry reactors. The Sanchez-Lacombe EOS (S-L EOS), Soave-Redlich-Kwong EOS (S-R-K EOS), Peng-Robinson EOS (P-R EOS) and Benedict-Webb-Rubin EOS (B-W-R EOS) are

commonly used to estimate the equilibrium monomer concentration in slurry reactors.

The S-L EOS is probably the most commonly used EOS for the calculation of thermodynamic properties and equilibrium concentrations of various species involved in olefin polymerization systems. This EOS has been used to predict the various thermodynamic properties of pure components and mixtures such as molar volumes, heat capacities, enthalpies, fugacity coefficients and various departure functions related to entropy, enthalpy and Gibbs free energy. The mixing rule can be used to predict mixture properties using the values of the pure components. The Chao-Seader and Scatchard-Hildebrand correlations have been used to obtain the activity coefficients for interphase equilibrium calculations [38].

2.3 MACRO SCALE MODEL

2.3.1 RESIDENCE TIME DISTRIBUTION

The residence times of different macroparticles are not the same in slurry CSTRs due to their non-ideal behavior. The different macroparticles stay for different times in the reactor and hence the macroparticles will have a residence time distribution (RTD). The macroparticles will have different sizes and molecular weights. The intraparticle monomer concentration gradients are also different for microparticles with different residence times. The RTD can affect the final PSD and also results in a distribution of polymer properties [126], [127]. Thus, the effect of RTD can be studied along with single particle models for a better understanding of the physio-chemical phenomena at the macroscale level. Control of the PSD is important as very fine particles (below about 80 µm) lead to fouling of the reactor and downstream processes whereas, large particles (over about 1000 µm) create melting problems in the barrel of extruders during processing.

The tanks-in-series (TIS) model [21], [27] and the segregation model [26], [128] of RTD have been used to study the effect of RTD on the PSD in slurry CSTRs. Soares and Romero [129] used Monte Carlo simulation to obtain the final PSD using an arbitrary RTD and initial catalyst PSD in a slurry reactor. Recently, Casalini et al. [26] employed the segregation model to obtain the PSD and final properties of the polymer from slurry CSTRs. The axial dispersion model has been employed to model the RTD in loop reactors [15].

The internal age distribution, $I(\theta)$, for N- ideal CSTRs in series using the TIS model is given by

$$I(\theta) = e^{-N\theta}\left[1 + N\theta + \frac{N^2}{2!}\theta^2 + \ldots\ldots + \frac{(N-1)^{N-1}}{(N-1)!}\theta^{N-1}\right] \qquad (2.29)$$

Here, θ is the dimensionless time, defined as $\theta = \dfrac{t}{\tau}$, and τ is the mean residence time of the reactor.

The exit age distribution, $E(\theta)$, for N ideal CSTRs in series using the TIS model is given by

$$E(\theta) = \frac{N^N}{(N-1)!}\theta^{N-1}\exp(-N\theta) \qquad (2.30)$$

The net rate of polymerization, R_{poly} (kg/h), in the reactor can be written as

$$R_{poly} = \tau I_c \int_{\theta=0}^{1} R_v(\theta)I(\theta)d\theta \qquad (2.31)$$

Here, R_v is the rate of polymer produced in kg polymer/(kg cat-h) and I_c is the catalyst feed rate in kg/h.

If the number average molecular weight and the weight average molecular weight of the jth macroparticle are $M_{n,j}$ and $M_{w,j}$, respectively, the average value of the

40

number average molecular weight, M_n, and the weight average molecular weight, M_w, of all the macroparticles can be obtained as

$$M_n = \frac{1}{\sum_{j=1}^{N_{mp}} \left(\frac{w_j}{w}\right) \Big/ M_{n,j}}$$

(2.32)

$$M_w = \sum_{j=1}^{N_{mp}} \left(\frac{w_j}{w}\right) M_{w,j}$$

(2.33)

Here, w_j and w are the mass of the jth macroparticle and the total mass of all the macroparticles, respectively. The total mass of all the macroparticles at the exit, w, can be obtained using the exit age distribution, $E(\theta)$, as

$$w = \int_0^\infty N_e E(\theta) \frac{4\pi}{3} \left[r_\theta^3 - r_{i,0}^3 \right] \rho_P d\theta$$

(2.34)

Here, N_e is the number of macroparticles exiting the reactor per unit time, r_θ is the radius of macroparticles having age between θ and $\theta + d\theta$ and $r_{i,0}$ is the radius of the catalyst particle in the feed. Thus, the values, M_n and M_w, are calculated as

$$M_n = \frac{\int_0^\infty E(\theta) \left[(r_\theta / r_{i,0})^3 - 1 \right] d\theta}{\int_0^\infty \frac{1}{M_n(\theta)} E(\theta) \left[(r_\theta / r_{i,0})^3 - 1 \right] d\theta}$$

(2.35)

$$M_w = \frac{\int_0^\infty E(\theta) \left[(r_\theta / r_{i,0})^3 - 1 \right] M_w(\theta) d\theta}{\int_0^\infty E(\theta) \left[(r_\theta / r_{i,0})^3 - 1 \right] d\theta}$$

(2.36)

The segregation model assumes that the macroparticle neither aggregates nor breaks inside the reactor. The PSD based on the mass of the macroparticle at the outlet, $f_m(r)$, in terms of the reactor RTD, $E(\theta)$, and the PSD of the catalyst at the inlet can be given as

41

$$f_m(r) = \frac{d}{dr} \int_{r_o=0}^{r_o=r} \int_0^\theta f_{m,0}(r_o) \frac{m(r_o,\theta)}{m(r_o,0)} E(\theta) d\theta dr_o \qquad (2.37)$$

The PSD based on the number of macroparticles, $f_n(r)$, can be obtained using the relation [128]

$$f_n(r) = \frac{f_n(r)/r^3}{\int_0^\infty \left[f_n(r)/r^3 \right] dr} \qquad (2.38)$$

Any generic property of the macroparticle, m $(r_o; r)$, with the initial size, r_o, to the final size, r, can be obtained using the age, θ^*, of the macroparticle. The fraction of particles with their initial size between r_o and $r_o + dr_o$ and the time spent between θ and $\theta + d\theta$ is given by

$$F(r_o,\theta) = f_n(r_o) E(\theta) \qquad (2.39)$$

Introducing the exit age distribution in terms of the final particle size, $H(r)$, such that

$$E(\theta)d\theta = H(r)dr \qquad (2.40)$$

$$H(r) = E(\theta) \frac{d\theta}{dr} \qquad (2.41)$$

Further, $H(r)$ can be expressed in terms of the microparticle growth factor, ϕ (= $R_{\mu p}/r_{cf}$), as

$$H(r) = \frac{E(\theta)}{r_o} \frac{d\theta}{d\phi} \qquad (2.42)$$

If, r_{min} and r_{max} are the minimum and maximum size of particles entering the reactor, then the fraction of particles of size range between r to $r + dr$ at the reactor outlet can be obtained as

$$f_n(r)dr = \int\limits_{r_o=r_{\min}}^{r_o=r_{\max}} f_n(r_o)E(\theta)\frac{d\theta}{d\phi}\bigg|_{\theta=\theta^*}\frac{dr_o}{r_o} \tag{2.43}$$

The final properties can be obtained using the average k^{th} order bulk moment, $\mu_k(r)$

$(=\lambda_k+\Lambda_k)$ as

$$\overline{\mu_k} = \frac{\int\limits_{r_o=r_{\min}}^{r_o=r_{\max}} f_n(r_o)\mu_k(r_o;r)E(\theta^*)m(r_o;r)\frac{d\theta}{d\phi}\bigg|_{\theta=\theta^*}\frac{dr_o}{r_o}}{\int\limits_{r_o=r_{\min}}^{r_o=r_{\max}} f_n(r_o)E(\theta^*)m(r_o;r)\frac{d\theta}{d\phi}\bigg|_{\theta=\theta^*}\frac{dr_o}{r_o}} \tag{2.44}$$

Finally, the overall moment can be obtained as

$$\mu_{k,overall} = \int\limits_{r=0}^{r=\infty} f_m(r)\overline{\mu_k}dr \tag{2.45}$$

Accordingly, the final properties can be calculated using the various overall bulk

moments as

$$M_n = \frac{\mu_{1,overall}}{\mu_{0,overall}}MW \tag{2.46}$$

$$M_w = \frac{\mu_{2,overall}}{\mu_{1,overall}}MW \tag{2.47}$$

$$PDI = \frac{M_w}{M_n} \tag{2.48}$$

The segregation model is simple and can be incorporated with simplified as well as complex mixing patterns in a reactor. Some workers [126], [130], [131] also used a population balance modeling (PBM) approach to characterize the final property of the macroparticles in gas phase reactors. The segregation model is reported to be computationally inexpensive [128] as compared to the PBM approach.

2.3.2 MASS AND HEAT BALANCE

The mass and heat balance equations for slurry phase ethylene polymerization in a CSTR (Figure 2.2) is given in Table 2.8. The equations are derived for the homo-polymerization of ethylene in a CSTR. The equations can be modified for the case of co-polymerization. The mass balance equations for the various components are based on the assumption that the liquid in the CSTR is well mixed. It is also assumed that the monomer is not present inside the macroparticles but solvent is present inside them corresponding to its equilibrium solubility in the polymer.
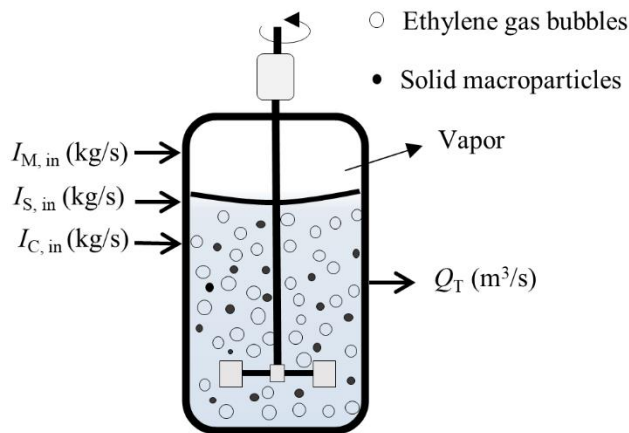

Fig. 2. 2 Schematic of slurry polymerization of ethylene in a CSTR; S: solvent, M: monomer, C: catalyst

Table 2. 8 Mass and heat balance equations at macroscale [55]

Mass balance equations

Components	Component balance equations

monomer

$$\frac{dI_M}{dt} = I_{M,in} \ - \ Q_T(1 - F)M_L(MW) \ - \ R_{poly}$$

catalyst

$$\frac{dI_C}{dt} = I_{C,in} \ - \ Q_T \, F \, f_c \, \rho_{s,avg}$$

polymer

$$\frac{dI_P}{dt} = - \, Q_T \, F \, (1 - f_c) \, \rho_{s,avg} \ + \ R_{poly}$$

solvent

$$\frac{dI_S}{dt} = I_{S,in} \ - \ Q_T(1 - F) \, \rho_S \left[1 - \frac{M_L(MW)}{\rho_M} \right] - Q_T F \left(1 - f_c \right) S_{He-PE} \rho_S$$

Interphase monomer transport equations

Gas to liquid $\quad R_{gl} = k_{gl} a_{gl} (v_G + v_L)(M^* - M_L)$

Liquid to solid $\quad R_{ls} = k_{ls} a_{ls} (v_L + v_S)(M_L - M_S)$

Inside the
macroparticle $\quad R_{diff} = D_{ef} \dfrac{\partial M}{\partial r} a_{ls} \left(v_L + v_s \right)$

Heat balance equation

Component, i $\quad \dfrac{d(\rho_i V_i C_{P,i} T)}{dt} = H_{in,i} - H_{out,i} + Q_{imp} - Q_{jacket} - Q_{ext}$

* The description of the symbols is given in the nomenclature

The mass transfer coefficients and the interfacial areas used in Table 2.8 can be estimated using several correlations of Calderbank and Moo-Young [132] and Ranz-Marshall [123]. The gas-liquid interfacial area is calculated from the values of the gas bubble diameter and the gas hold up using the correlations of [133] given in the literature. The correlations for the estimation of mass transfer coefficients in

the slurry polymerization process are given in Table 2.9. The correlations are also reviewed by [134].

Table 2. 9 Correlations for estimation of the mass transfer coefficients [55]

k_{gl} and a_{gl}	References
Sparged vessels	
$k_{gl} = 0.42 \left[\dfrac{\Delta \rho \, \mu_L \, g}{\rho_L^2} \right]^{1/3} Sc^{-1/2}$	[132]
$Sc = \dfrac{\mu_L}{\rho_L D_L}$, $\text{Re} = \dfrac{\rho_L N_s d_a^2}{\mu_L}$ and $N_F = \dfrac{(I_{M,in}/\rho_M)}{N_s d_a^3}$	
$P_s = N_P \, \rho_L N_s^3 d_a^5$	
$\dfrac{P_s}{P_d} = 1 - 12.2 \, N_F$ for $N_F < 0.037$	
$= 0.62 - 1.85 \, N_F$ for $0.037 < N_F < 0.15$	[135]
$\dfrac{\phi_g}{1-\phi_g} = 0.819 \, \dfrac{u_s^{2/3} \, N_s^{2/5} \, D_R^{4/15}}{g^{1/3}} \left(\dfrac{\rho_L}{\sigma_L} \right)^{1/5} \times \left(\dfrac{\rho_L}{\Delta\rho} \right) \left(\dfrac{\rho_L}{\rho_G} \right)^{-1/15} \left(\dfrac{\mu_L}{\mu_G} \right)^{-1/4}$	[133]
$d_b = 0.7 \, \dfrac{\sigma_L^{0.6}}{\left(P_d/v_L \right)^{0.4} \rho_L^{0.2}} \left(\dfrac{\mu_L}{\mu_G} \right)^{0.1}$	
$a_{gl} = \dfrac{6\phi_g}{d_b}$	[133]
Unsparged vessels	
$k_{gl} = 0.4 \left(\dfrac{P}{V} \dfrac{\mu_L}{\rho_L^2} \right)^{0.25} Sc^{-0.5}$	[136]
k_{ls} and a_{ls}	
$a_{ls} = \dfrac{\pi D_{mp}^2 N_E \, \theta}{v_L + v_s}$	
$Sh = \dfrac{k_{ls} d_{mp}}{D_L} = 2 + 0.6 \, Sc^{0.33} \, \text{Re}_s^{0.5}$	[123]
$\text{Re}_s = \dfrac{\rho_L v_t d_{mp}}{\mu_L}$	

* The description of the symbols is given in the nomenclature

2.4 AN OUTLOOK OF THE MULTI-SCALE MODELING

The multi-scale modeling in olefin polymerization processes is a complex amalgamation of chemical and physical interdependent effects. These effects are modeled at three different length scales. Thus, one of the main objectives of a multi-scale modeling study is to understand the interdependence of the chemical reactions and physical transports at the different length scales and their combined effects on the particle evolution, rate of polymerization and product quality.

An understanding of the intrinsic links among these effects at different length scales in slurry reactors is presented in Figure 2.3. The *microscale* modeling is mainly concerned with the chemical effects (i.e. kinetics, site heterogeneities, catalyst deactivation, etc.) at the catalyst active sites. The chemical effects control the microstructural and molecular properties (MWD, CCD, PSD, bulk density, etc.) of the final product at this scale. The product properties are not only affected by the chemical effects but also by the physical effects at the *mesoscale*. The liquid-solid hydrodynamics, sorption, swelling, interphase and intraparticle diffusional transport of mass and heat, etc., at the *mesoscale* level also play a role in determining the product quality and the reactor overall performance. The liquid-solid hydrodynamics in the slurry reactor affects the solid holdup, particle size distribution and reactor performance. Monomer sorption into the polymer affects the local monomer concentration. This affects the rate of polymerization [125]. The particle swelling and aggregation at the *mesoscale* can affect the local mass and heat transport and consequently affect the polymer properties, rate, yield and reactor dynamics. Interphase mass and heat transport can have a significant impact on the macroparticle temperature and monomer concentration [123]. This directly affects the rate of polymerization and the polymer yield. Intra-particle mass and heat transport result in a radial variation of both the monomer concentration and the temperature inside a particle. Mathematical models [24], [55], [134] have shown that the radial variation in the monomer concentration affects the MWD and PDI of the final product. This effect becomes more profound in the slurry reactors using

high activity catalysts as the intra-particle mass diffusion can become the rate-limiting step. The intra-particle temperature gradient can affect the rate constants and reaction kinetics and thus, affect the product quality. The reactor residence time distribution at the *macroscale* level can also affect the product particle size distribution and the in-homogeneities in the final product.
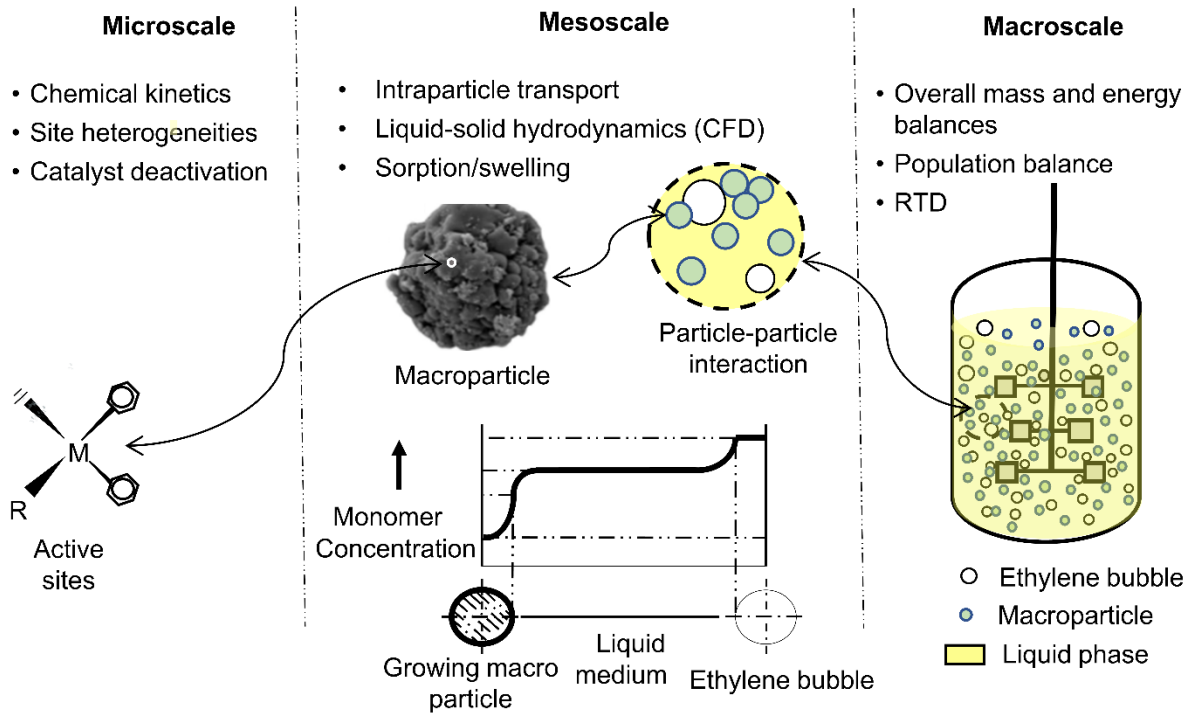

Fig. 2. 3 Schematic representation of the links between the chemical and physical effects at different length scales in the slurry phase ethylene polymerization processes

Thus, a complete model for slurry phase ethylene polymerization at the industrial scale should consider the physicochemical effects at all three scales. It is a big challenge to develop a *complete* model for an industrial-scale reactor due to the added complexity at each level, the availability of the information and the cost of computation. Thus, the level of complexity in modeling studies should depend on the use of the model.

48

2.5 COMPUTATIONAL TECHNIQUES FOR THE SIMULATION OF MATHEMATICAL MODELS

A *multi*scale reactor model may comprise of the kinetic model at the microscale, the diffusion model at the mesoscale and the RTD model equations, the overall balance equations, etc., at the macroscale. The kinetic model equations comprise a system of ODE-initial value problems (ODE-IVP) and contain only one independent variable, time, t. In contrast, the intraparticle balance equations (diffusion model) are partial differential equations (PDEs), which consist of more than one independent variable, generally, time, and the radius of the growing macroparticle. The intraparticle diffusion equations of the single-particle models are non-linear parabolic PDEs with Neumann boundary and initial conditions [137]. The overall balance equations for the steady-state and dynamic reactor models are generally a system of algebraic equations or a differential-algebraic system of equations (DAEs). A brief review of the multiscale modeling approach and the computational techniques used for olefin polymerization in slurry reactors is given in Table 2.10. The intraparticle diffusion and heat transfer equations (PDEs) can be reduced to a set of ODEs in time, t, using discretization methods. The finite difference method with unequal step size, finite element method, finite volume method, method of lines and the orthogonal collocation (OC) technique can be used to obtain the set of ODEs at the internal grid points [137]. Referring to Table 2.10, it can be seen that the finite difference method and the orthogonal collocation technique are the most widely used discretization methods for the PDEs in olefin polymerization processes.

Table 2. 10 A review on the modeling and simulation approaches

References	Modeling approach	Computational techniques (Simulation tools)
[93]	Kinetic model (micro)	Gear's method (DGEAR from the NAG lib.)
	PFM (meso)	Orthogonal collocation on finite-elements (DGEAR from the NAG lib.)
[24], [25]	Kinetic model (micro)	Gear's method (DGEAR from the NAG lib.)
	PMGM (meso)	Finite difference (DGEAR from the NAG lib.)
[27]	Kinetic model (micro)	Gear's method (LSODE from the NAG lib.)
	PMGM (meso)	Finite difference (LSODE from the NAG lib.)
	Overall mass balance (macro)	Modified Newton-Raphson and modified Levenberg-Marquardt method
	RTD, Tanks in series (macro)	Romberg/Gauss-Legendre quadrature
[138]	Kinetic model (micro)	differential-algebraic system equation solver (DDASSL)
	MGM (meso)	Finite difference (DDASL)
	Overall energy balance (macro)	DDASSL
[22]	Kinetic model (micro)	IVPAG from the IMSL lib.
	MGM (meso)	Finite difference (IVPAG from the IMSL lib.)
	Monomer gas liquid balance (macro)	Discretization and explicit method
[139]	PFM (meso)	Method of lines (a variable co-efficient ODE solver, VODE in FORTRAN)
[102]	MGM (meso)	Finite volume (Adam-Bashforth-Moulton solver of order 13, *ode* 113 solver in MATLAB)
[140]	PFM (meso)	Global collocation (DGEAR from the IMSL lib.)
[141]	PFM and MGM (meso)	Orthogonal collocation on finite-elements (gPROMS simulation software)

[5]	Dynamic model (macro)	Backward differentiation formula (implemented as MATLAB S-function in C-language)
[95], [140]	RPPFM (meso)	Global collocation method
[17]	Kinetic model (micro)	Orthogonal collocation
	MGM (meso)	Orthogonal collocation
	Overall mass and energy balance, component balance (macro)	Differential-algebraic system equation solver
[142]	Kinetic model (micro)	Gear's method (ode15s solver in MATLAB)
	PMGM and PMLM (meso) PMLM: Polymeric multilayer model	Finite difference (ode15s solver in MATLAB)
[143]	MGM (meso)	Finite dufference
	RTD, Tank in series (macro)	Relaxation type unsteady state approach with iteration
[144]	PMLM (meso)	Finite difference (PDEPE function in MATLAB)
[51]	Kinetic model (micro)	(ode15s solver in MATLAB)
	MGM (meso)	Finite difference techiques (ode15s solver in MATLAB)
[26]	Kinetic model (micro)	ode15s solver in MATLAB
	MGM (meso)	Finite difference (ode15s solver in MATLAB)
	RTD, segregated model (macro)	Numerical integration by the trapezoidal rule (*trapz* and *cumtrapz* algorithms in MATLAB)

The discretization using the finite difference method results in a large number of grid points which results in an accurate and stable solution. In contrast, discretization using orthogonal collocation results in much fewer grid points compared to that in the finite difference method. The intraparticle mass balance is

a typical reaction-diffusion problem, the Thiele modulus playing a very important role. When the diffusional rate is small compared to the reaction rate (a high value of the Thiele modulus), discretization using finite difference requires a very fine mesh compared to the orthogonal collocation method. In this case, the orthogonal collocation method will significantly reduce the number of ODEs and the simulation time. Fontes and Mendis [17] highlighted the advantages of orthogonal collocation over the finite difference method for the simulation of the MGM.

The ODEs in the olefin polymerization processes are generally *stiff*. Most of the ODE solvers become computationally expensive while solving stiff ODEs. Gear's method [137], [145], which is based on the multistep predictor and corrector equations, is probably the most widely used method for the simulation of stiff ODEs in slurry phase olefin polymerization processes. The Rosenbrock method is also used to solve stiff ODEs in gas phase olefin polymerization processes [146]. However, the performance of this method suffers when used to achieve high precision. Several computer packages include DDASSL, D02EJF (old variant, D02EBF) from the NAG subroutine, ODEPACK (old variant, LSODE and others), DGEAR (in IMSL), etc., have been used in previous studies. Other ODE solvers like ode15s, ode 23, ode 23s, ode 23t, ode 23tb, ode45, ode 113, etc., in MATLAB can also be used to solve the stiff ODEs. Among these, ode 15s in MATLAB is currently widely used for the simulation of stiff ODEs in olefin polymerization processes.

2.5 A GUIDELINE TO IMPLEMENT THE MATHEMATICAL MODEL AND SIMULATION

The slurry polymerization of olefins employs either CSTRs or loop reactors. A clear understanding of the important aspects of slurry polymerization processes is a pre-requisite to develop a model. Modeling approaches in CSTRs and loop reactors for slurry polymerization of olefins are almost the same at the micro and meso scales.

52

A general guideline to implement the mathematical model and its simulation at multi-scale is illustrated in Figure 2.4.

The kinetic model is an essential part of any modeling work as it directly predicts the properties of the final product. A simplified kinetic model proposed in Table 2.4 can be used to describe the microscale phenomena. The simplified kinetic model (Table 2.4) using two active sites each with distinct kinetic rate constants may be a good balance between the computational complexity and the accuracy. The intraparticle diffusion phenomena can be described using the single-particle models and the equilibrium monomer concentrations in various phases can be obtained using phase equilibrium considerations. A choice between the various single-particle models can be made by the user considering the advantages and disadvantages associated with the respective models as described in this article. The component balances and the overall material and energy balances describe the macro-level phenomena.

The intraparticle diffusion equations can be reduced to a set of ODEs using the finite difference or orthogonal collocation approach and solved using an ODE solver (e.g., ode15s in MATLAB). The material balances for the various live and dead chains give the set of ODEs using the method of moments. The solution of the moment equations using an ode solver gives the various moments of the live and dead chains to obtain the MWDs and the PDI. Data on a lab-scale, pilot plant, or industrial level can be used to estimate the kinetic parameters so that the model predictions match with experimental/industrial data. The overall material and energy balance equations are solved using an algebraic solver or a differential-algebraic solver depending on the nature of the equations.

Finally, the mathematical model can be solved to obtain the rate of polymerization, yield, and various properties of the final product. The model predictions can be validated using the available lab scale, pilot scale, or industrial data set.
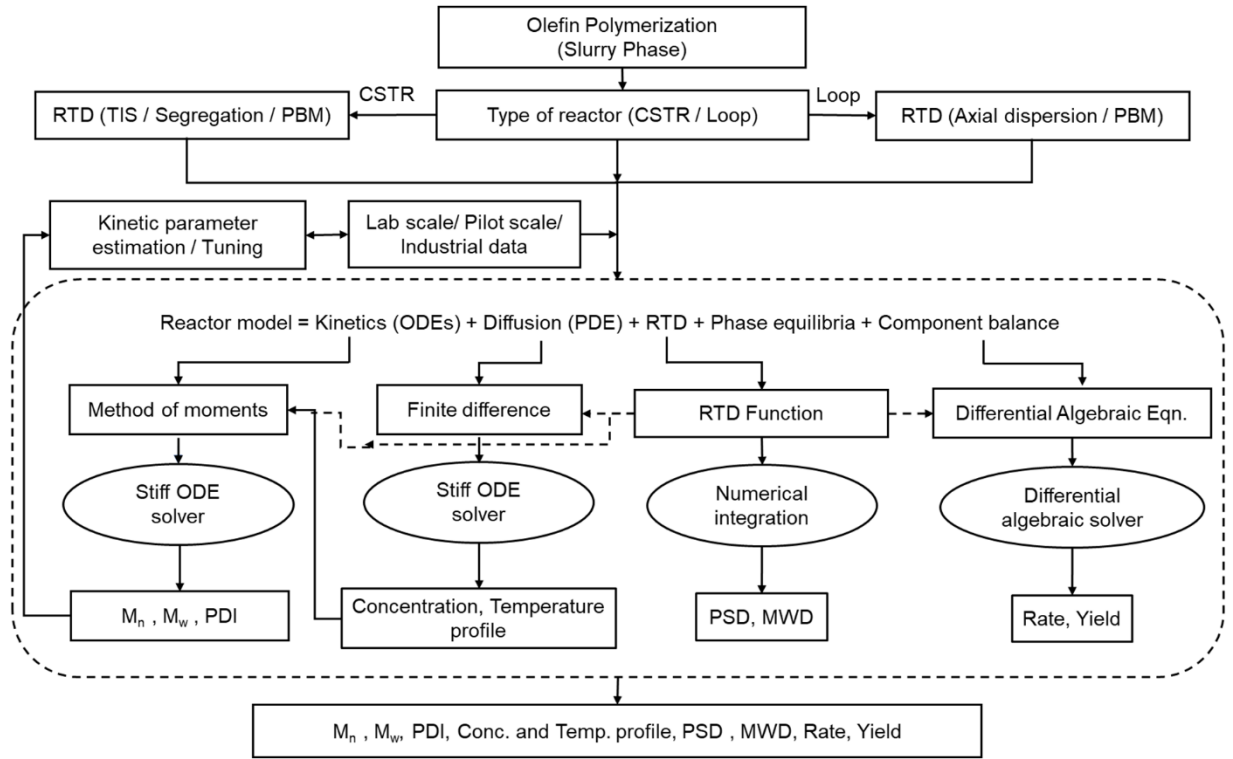
Fig. 2. 4 A general flow chart for the implementation of modeling at multi-scales and simulation

CHAPTER 3

MULTI-SCALE MODELING AND SIMULATION FOR AN INDUSTRIAL SLURRY PHASE HIGH DENSITY POLYETHYLENE REACTOR

Two models can be used to describe the production of polymers with broad MWDs. The first set of models [94], [147]–[150] suggests the presence of multiple active sites in the catalyst, with differences in their activities resulting in a polymer with broad MWDs. The second set of models [31], [90], [123], [138] considers the presence of transport resistances that affect the rate of monomer transport to the active sites of the catalyst. In the past several years, a significant number of studies have been reported in the open literature that focuses on the single-particle growth in heterogeneous Zeigler-Natta polymerizations of several monomers [49], [142]. Experimental observations [31] reveal that as the reaction starts, the original catalyst particles (macroparticles) fragment into several smaller-sized sub-particles. These sub-particles are called microparticles. As the reaction progresses polymer is formed and deposited around each microparticle. The monomer continuously reaches the active sites of the microparticles (through the layers of polymer already formed) and new layers are formed continuously. The new polymer layer surrounding the microparticles radially pushes the older layers and the macroparticle expands radially outward. This process continues till the macroparticle is present inside the reactor or the catalyst is completely deactivated. The incoming monomer experiences a higher diffusional resistance towards the catalyst, as the layer of polymer around the microparticle grows and the reaction progresses [123], [138].

Several physical models have been proposed in the literature for modeling particle growth in olefin polymerizations. Some of these include the solid core model, SCM [31], [151], the polymeric core model, PCM [92], [151], the polymeric flow model,

PFM [20], [85], [152], the multigrain model, MGM [26], [89]–[91], [153] and the polymeric multigrain model, PMGM [9], [24], [25].

The MGM presents a very detailed and clear picture of the particle morphology accounting for the fragmentation of the original catalyst particle and its expansion as the polymerization progresses. This model incorporates catalyst break-up into microparticles and the diffusion of monomer through the catalyst. The MGM can also include the heterogeneous nature of active sites. Several workers [27–30] have studied the polymerization phenomena and macroparticle expansion using this model. The high computational time is a major disadvantage with the MGM [24], [25].

Sarkar and Gupta [24], [25] developed a model combining the attributes of the polymeric flow model and the multigrain model. They referred to their model as the polymeric multigrain model (PMGM). They studied propylene polymerization in an isothermal slurry reactor using a single site, non-deactivating supported Z-N catalyst. Sarkar and Gupta [24] reported that higher PDIs can be predicted by using the PMGM with single-site non-deactivating catalysts. The PMGM was found to be much more computationally efficient compared to the MGM. Thus, the PMGM is modified and used in the present work.

The PMGM developed by Sarkar and Gupta [24] uses the average radius of the microparticles after disintegration and then calculates the size of the original catalyst. The modified PMGM uses the size of the original catalyst particle before disintegration and calculates the average radius of the microparticle after disintegration. The average size of the original catalyst particle is generally known whereas the size of the microparticle after disintegration is based on the visualization of catalyst disintegration in the model. The present model uses the known value of the diameter of the original catalyst particle to control the size of the microparticle (after disintegration). The analysis of the effect of the particle size

distribution (PSD) of the original catalyst on the PSD of the final product will be easier using the known value of the diameter of the original catalyst.

The tuning of the present model requires the size of the original catalyst particle as an input parameter. The tuned values of the model parameters depend on the size of the original catalyst. If the model starts with the known value of the diameter of microparticles then the variation in tuning parameter values will lead to different sizes of the original catalyst. Thus, it will complicate the tuning process of the developed model with industrial data.

The work reported [9], [20], [22], [49], [139] on the modeling of ethylene polymerization is limited to the micro and meso levels. Only a few studies [6], [26], [27] developed a *complete* model for olefin polymerization. Sarkar and Gupta [27] developed a model for polypropylene polymerization in CSTRs. However, their simulation was not validated against any experimental/industrial data. The model of Touloupides et al. [6] for a loop olefin reactor was also not validated against any experimental data. The model of Casalini et al. [26] for polyethylene polymerization in a series of CSTRs, indeed, was validated against a set of experimental data. This study used the MGM with multisite catalysts along with a segregated residence time distribution (RTD) model to describe the effect of RTD on the polymer properties. The MGM itself requires significantly high computational times than the PMGM for the simulation of an industrial reactor [24]. Considering the reactor residence time distribution in a model will significantly increase the simulation time. The computational time will further increase by incorporating a family of sites. The high computational times of such a model limit its use for optimization studies. Thus, there is a need to develop a computationally efficient reactor model which requires lower computational times for the simulation of *industrial* reactors, without losing much in terms of the accuracy in its prediction capability.

In this study, a *complete* and computationally efficient model for an isothermal slurry CSTR for high-density polyethylene is developed. The modified PMGM is used. The present model is tuned and validated with data available on an ***industrial*** isothermal slurry CSTR for high-density polyethylene. The sensitivity analysis of the tuned model is performed to understand the effects of tuning parameters on the polymer productivity, polymer yields, the bulk monomer concentration, required monomer to solvent ratio and the polydispersity index of the final product.

3.1 REACTOR MODELING

This study is on an isothermal, industrial slurry CSTR for high-density polyethylene. In this process, liquid n-hexane is used as a solvent. The volume of the industrial reactor is *approximately* 145 m^3 with an internal diameter of 5.6 m. It is a fully baffled reactor equipped with a turbine agitator which rotates at a constant rate of 90 RPM. Solid catalyst particles suspended in n-hexane, are introduced into the reactor at a rate that is sufficient to maintain the desired rate of polymerization. Ethylene (monomer) and hydrogen (chain transfer agent) are sparged into the reactor. These two components diffuse from the bubbles, through the solvent, to the catalyst surface where the polymerization takes place (inside the porous macroparticles).

The reactor usually operates at temperatures of about 77 - 85 $^\circ$C and pressures of about 7 - 8 bar [7]. The polymerization is highly exothermic and temperature control is critical. Most of the heat of polymerization is removed through the vaporization of large amounts of the solvent (n-hexane) in the slurry reactor. Indeed, good temperature control in the reactor requires maintaining a sufficient solvent-to-monomer ratio inside the reactor. It is observed from all the available data on the industrial reactors that the solvent-to-monomer ratio at the steady-state operation of the slurry phase ethylene polymerization in CSTRs is constant at around 1.6. This ratio is required for sufficient heat removal and to maintain the reactor at isothermal conditions. The reactor outlet is a slurry containing about 15
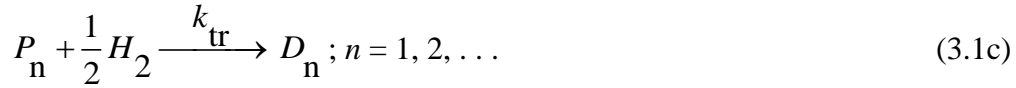
58

- 40 % solid [7] (polymer plus catalyst) and a small amount of unreacted ethylene and oligomers. This goes to downstream separation and drying sections, followed by mixing and pelletizing sections. The process has a very stable operation, good temperature control and a very high conversion (up to about 99 %) of ethylene.

A multi-scale mathematical model is developed herein to explain the polymerization of high-density polyethylene (HDPE) in an isothermal, industrial, continuous stirred tank slurry reactor (CSTR). The present reactor model is based on the following major assumptions

i. All the catalyst particles entering the reactor are spherical and are of the same average size

ii. The reactor is operating under isothermal conditions at steady state and a sufficient solvent-to-monomer ratio is maintained to ensure isothermal conditions. The intraparticle temperature gradient is reported to be negligible in the open literature [157] in slurry polymerizations. Therefore, the particle-energy-balance is not considerd in this work

iii. All the particles spend the same time (the mean residence time, θ) inside the reactor

iv. The liquid inside the CSTR is well mixed

v. A macroparticle leaving the reactor consists of catalyst and polymer. The monomer is not present *inside* a macroparticle coming out of the reactor (but unreacted monomer is present in the exit stream)

vi. The solvent is assumed to be present only in the liquid phase in the exit stream. The reported value of the hexane solubility in HDPE [158] shows that the solvent sorption in the polymer leaving the reactor is negligible (less than 2% of the solvent present in the liquid phase)

vii. Since a very small amount of hydrogen is fed to the reactor, it is not considered in the mass balance equation

3.1.1 KINETIC MODEL

A simplified kinetic model, as proposed in the literature [24], [25], is used in this study. The kinetic scheme includes a series of elementary reactions, namely, chain initiation, propagation and chain termination through hydrogen. This is given in Equations 1a – 1c. Here, P_0 represents the active catalyst (and its concentration), M represents the monomer (and its concentration), P_n and D_n represent an active site with a live polymer chain of length, n, and a dead polymer with chain length, n, respectively (and their concentrations):

$$P_0 + M \xrightarrow{k_P} P_1 \tag{3.1a}$$

$$P_n + M \xrightarrow{k_P} P_{n+1} \; ; n = 1, 2, \ldots \tag{3.1b}$$

$$P_n + \frac{1}{2} H_2 \xrightarrow{k_{tr}} D_n \; ; n = 1, 2, \ldots \tag{3.1c}$$

The corresponding moment equations of the live and dead polymer chains, λ_k and μ_k ($k = 0, 1, 2$), respectively, are defined as

$$\lambda_k = \sum_{n=1}^{\infty} n^k P_n \tag{3.2}$$

$$\mu_k = \sum_{n=2}^{\infty} n^k D_n \tag{3.3}$$

The moment equations are given in Table 3.1.

<div align="center">Table 3. 1 Moment Equations [24], [25]</div>

0th Moment (Live chain)	$\dfrac{d\lambda_0}{dt} = C_1 - C_2 \lambda_0$
1st Moment (Live chain)	$\dfrac{d\lambda_1}{dt} = C_1 - C_4 \lambda_1$
2nd Moment (Live chain)	$\dfrac{d\lambda_2}{dt} = C_1 + 2C_3 \lambda_1 - C_4 \lambda_2$
0th Moment (Dead chain)	$\dfrac{d\mu_0}{dt} = C_4 (\lambda_0 - P_1)$

1st Moment (Dead chain)	$\dfrac{d\mu_1}{dt} = C_4(\lambda_1 - P_1)$
2nd Moment (Dead chain)	$\dfrac{d\mu_2}{dt} = C_4(\lambda_2 - P_1)$
Mass Balance	$\dfrac{dP_1}{dt} = C_1 - C_3\lambda_0 - C_2 P_1$

where,

$$C_1 = k_p M \; C^*$$

$$C_2 = k_P M + k_{tr} H_2^{0.5}$$

$$C_3 = k_P M$$

$$C_4 = k_{tr} H_2^{0.5}$$

The moments, λ_k and μ_k ($k = 0, 1, 2$), can be used to give the number and weight average molecular weights, M_n and M_w, and the polydispersity index, *PDI*, of the polymer.

$$M_n = \left[\frac{\lambda_1 + \mu_1}{\lambda_0 + \mu_0}\right] \times MW \tag{3.4}$$

$$M_w = \left[\frac{\lambda_2 + \mu_2}{\lambda_1 + \mu_1}\right] \times MW \tag{3.5}$$

$$PDI = \frac{M_w}{M_n} \tag{3.6}$$

3.1.2 POLYMERIC MULTIGRAIN MODEL, PMGM

The polymeric multigrain model, PMGM [9], [24], [25], describes the diffusion of monomer inside the catalyst macroparticles and the (radially) outward movement of the polymer-coated microparticles as the reaction progresses. Experimental observation [31] reveals that very soon after the reaction starts, the original catalyst particles are fragmented into several smaller-sized sub-particles. This is modeled as follows. We assume that at $t = 0$, the catalyst sub-particles (all assumed spherical) are arranged in *close-packed* spherical shells. Also, it is *assumed* that at $t = 0$, all

the close-packed catalyst spheres in the ith shell have the same radius, $R_{c,i}$. The values of $R_{c,i}$ are random (and in a certain range) and are generated using a code, *Rand*, for random number generation. As the reaction progresses, polymer grows around each catalyst sub-particle as shown in Figure 3.1. The radius of the polymer coating is the same for all catalyst particles in any layer. It is also assumed that the number of catalyst sub-particles, N_i, in shell, i, remains constant throughout the polymerization. The number, N_i, of microparticles in the ith shell are calculated using mass balance (of the original catalyst particle before disintegration and the total mass of all the microparticles after disintegration), and is given by

$$N_i = \frac{(r_{i+1}^3 - r_i^3)(1-\varepsilon)}{R_{c,i}^3}$$ (3.7a)

Here, the ith shell extends between radii, r_i and r_{i+1} (r_i being measured from the origin, which is at the center of the first catalyst sub-particle) and ε is the void fraction associated with close-packed spheres. It is easy to see that

$$r_{i+1} = R_{c,1} + 2R_{c,2} + \ldots + 2R_{c,i}$$ (3.7b)

$$r_i = R_{c,1} + 2R_{c,2} + \ldots + 2R_{c,i-1}$$ (3.7c)

Here, $i = 1, 2, \ldots, P$.

The radius of microparticles in the ith shell are calculated using a random number generator, *Rand*, as reported in the literature [90]:

$$R_c = R_{c,av} + C(R_{c,max} - R_{c,av})\frac{1 - e^{\left(\frac{-(0.5 - Rand)^2}{2}\right)}}{(1 - e^{-0.125})}$$ (3.8)

$$0 < Rand < 1$$

$$Rand \leq 0.5; \qquad C = -1$$
$$Rand > 0.5; \qquad C = 1$$

$R_{c,max}$ and $R_{c,av}$ are the maximum and average radii of the microparticles after disintegration (these parameters are obtained as described later).

The number and weight average molecular weights of the polymer in the ith shell can be obtained as

$$M_{n,i} = \left[\frac{\lambda_1 + \mu_1}{\lambda_0 + \mu_0} \right]_i \times MW \tag{3.9}$$

$$M_{w,i} = \left[\frac{\lambda_2 + \mu_2}{\lambda_1 + \mu_1} \right]_i \times MW \tag{3.10}$$

The mean value of the number average ($\bar{M}_n$) molecular weight, the weight average ($\bar{M}_w$) molecular weight and the PDI ($\overline{PDI}$) of the entire macroparticle can be calculated by summing up over each shell as

$$\bar{M}_n = \frac{1}{\sum\limits_{i=1}^{P+1} \left(w_i \middle/ M_{n,i} \right)} \tag{3.11}$$

$$\bar{M}_w = \sum\limits_{i=1}^{P+1} \left(w_i M_{w,i} \right) \tag{3.12}$$

$$\overline{PDI} = \frac{\overline{M_w}}{\overline{M_n}} \tag{3.13}$$

Here, w_i is the mass fraction of the polymer of molecular weights, $M_{n,i}$ and $M_{w,i}$, in the ith shell.

The present model uses (tuned) values of the diameter of the original catalyst particle, D_{cat}, to determine the value of $R_{c,av}$ for a given (assumed) value of the number, P, of (computational) grid points shown in Figure 3.1. The exact details are described later. Since the present model differs slightly from the previous one (PMGM) we shall refer to it as the modified PMGM.
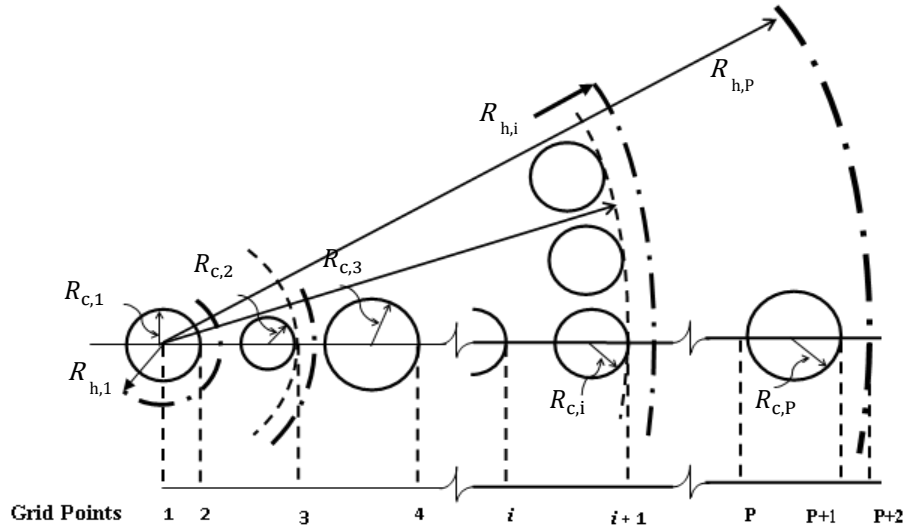
Fig. 3. 1 Catalyst sub-particles at time, t, with each catalyst microparticle being surrounded by a layer of polymer. $R_{c,i}$: radius of catalyst sub-particle in the ith shell, $R_{h,i}$: radius of macroparticle at the hypothetical grid point

The macroparticle growth at any time is described using the diffusion equation for a single macroparticle

$$\frac{\partial M}{\partial t} = D_{ef} \frac{1}{r^2} \frac{\partial}{\partial r}\left(r^2 \frac{\partial M}{\partial r}\right) - R_v \tag{3.14a}$$

$$BC\ 1:\ r = 0, \qquad \frac{\partial M}{\partial r} = 0 \tag{3.14b}$$

$$BC\ 2:\ r = R_{P+2}, \qquad D_{ef}\frac{\partial M}{\partial r} = k_{ls}\,(M_L - M_{P+2}) \tag{3.14c}$$

$$IC:\ t = 0, \qquad M = 0 \tag{3.14d}$$

In the above equation, M is the monomer concentration inside the macroparticle at any radial position, r, D_{ef} is the effective diffusivity of monomer inside the macroparticle, M_L is the monomer concentration in the *bulk* liquid phase (outside the macroparticle) and k_{ls} is the mass transfer coefficient at the liquid-solid interface. R_v is the rate of monomer consumption per unit macroscopic volume. It is assumed that the chain transfer agent, hydrogen, is uniformly distributed in the

macroparticle (due to it being a small molecule) during polymerization. The diffusion equation (PDE) for the single-particle (Equation 3.14) is converted into a set of ordinary differential equations (ODEs) at time, t. The finite-difference approximation with an unequal spacing of grid points [137] is used to obtain the set of ODEs at all the grid points. These ODEs are presented in Table 3.2. These ODEs are written at each of the computational grid points, i; $i = 1, 2, \ldots, P + 2$.

Table 3. 2 Diffusion Equations in the Macroparticle [24], [25]

Computational grid point	Diffusion Equation
$i = 1$	$$\frac{dM_1}{dt} = \frac{6\,D_{ef,1}\left(M_2 - M_1\right)}{\left(\Delta r_1\right)^2} - R_{v,1}$$
$i = 2$ to $P + 1$	$$\frac{dM_i}{dt} = \frac{2\,D_{ef,i}}{\Delta r_i + \Delta r_{i-1}}\left[M_{i+1}\left(\frac{1}{\Delta r_i} + \frac{1}{R_i}\right) - M_i\left(\frac{1}{\Delta r_i} + \frac{1}{\Delta r_{i-1}}\right) + M_{i-1}\left(\frac{1}{\Delta r_{i-1}} + \frac{1}{R_{i-1}}\right)\right]$$ $$- R_{v,i}$$
$i = P + 2$	$$\frac{dM_{P+2}}{dt} = -M_{P+2}\left[\frac{2k_{ls}}{\Delta r_{P+1}} + \frac{2D_{ef,P+2}}{\Delta r_{P+1}^2} + \frac{2k_{ls}}{R_{P+2}}\right] + M_{P+1}\left[\frac{2D_{ef,P+2}}{\Delta r_{P+1}^2}\right] + M_L\left[\frac{2k_{ls}}{\Delta r_{P+1}} + \frac{2k_{ls}}{R_{P+2}}\right]$$ $$- R_{v,P+2}$$

Here, $R_{v,1} = R_{v,P+2} = 0$

$$R_{v,i} = k_P\,C^*\,M(i)\left(N_{i-1}\frac{(4\pi/3)\,R_{c,i-1}^3}{(4\pi/3)\,(R_{h,i}^3 - R_{h,i-1}^3)}\right)$$

$$D_{ef,1} = D_{ef,P+2} = D_1$$

$$D_{ef,i+1} = D_1\frac{(V_i^h - V_i^{cat})}{V_i^h} \quad ;$$

$$V_i^h = \frac{4\pi}{3}(R_{h,i}^3 - R_{h,i-1}^3) \text{ and } V_i^{cat} = N_i\frac{4\pi}{3}R_{c,i}^3$$

The computational grid points:

$$R_1 = 0$$

$$R_2 = R_{c,i}$$

$$R_{i+1} = R_{c,i} + R_{h,\,i-1} + \frac{R_{h,\,i} - R_{h,\,i-1}}{2} \; ; \; i = 2, 3, \ldots, P$$

$$R_{P+2} = R_{h,P}$$

$$\Delta r_i = R_{i+1} - R_i \; ; \qquad i = 2, 3, \ldots, P+1$$

The rate of monomer consumption, R_{mp}, for each macroparticle is obtained by summing over all its computational shells:

$$R_{mp} = \frac{4\pi}{3} \, (MW) \, k_P C^* \, (\sum_{i=1}^{P} M_{i+1} \times N_i \times R_{c,i}^3) \tag{3.15}$$

In Equation 3.15, k_P is the propagation rate constant, C^* is the concentration of the catalyst active site, MW is the molecular weight of the monomer and M_{i+1} is the monomer concentration at the $(i + 1)^{th}$ computational grid point. The term, R_{mp}, represents the polymer production rate of each catalyst particle (kmol/cat. particle-s). Clearly, a higher value of R_{mp} is required to maximize the overall productivity of the polymerization process.

The *overall* rate of monomer consumption, R_{poly}, is calculated by summing over *all* the macroparticles staying inside the reactor for time, θ, the mean residence time:

$$R_{poly} = \left[\frac{4\pi}{3} \, (MW) \, k_P C^* \sum_{i=1}^{P} M_{i+1} \times N_i \times R_{c,i}^3 \right] \times N_E \theta = R_{mp} N_E \theta \tag{3.16}$$

Here, N_E is the total number of catalyst particles entering the CSTR per second (related to $I_{C,in}$). It is being assumed that each catalyst particle stays inside the CSTR for the *same* time, θ.

66

The polymer yield may be defined as the kg of polymer produced per kg of catalyst and may be expressed in terms of the diameter, D_{mp}, of the macroparticle (obtained from the model), the catalyst density, ρ_C, the polymer density, ρ_P, and the diameter, D_{cat}, of the original catalyst particle:

$$\text{Yield} = \frac{[(\pi/6) \times D_{mp}^3 \times \rho_P] \times N_E \theta}{[(\pi/6) \times D_{cat}^3 \times \rho_C] \times N_E \theta} = \frac{\rho_P}{\rho_C} \left(\frac{D_{mp}}{D_{cat}} \right)^3 \qquad (3.17)$$

From the above equation, it is clear that for a given value of ρ_P, ρ_C and D_{cat}, the polymer yield increases with an increase in D_{mp}. Hence, D_{mp} may be considered as a measure of the polymer yield (kg of polymer/kg-cat). It is to be emphasized that a higher value of the polymer yield (D_{mp}) is also desirable along with a higher value of the productivity (R_{mp}).

3.1.3 MASS TRANSFER ASPECTS

In our study, we have considered both the liquid phase as well as the gas-bubble phase. The gas-bubble phase contains monomer and hydrogen (in contrast to the vapor phase above the slurry, which contains n-hexane, unreacted monomer and hydrogen). Figure 3.3 shows, schematically, the variation of the monomer concentration inside the reactor at pseudo-steady-state conditions. R_{gl} is the gas-to-liquid mass transfer rate of the monomer. Similarly, R_{ls} is the liquid-to-macroparticle surface (solid) mass transfer rate of the monomer. R_{diff} is the rate of diffusion of the monomer to the inside of the macroparticle. At pseudo-steady state, $R_{gl} = R_{ls} = R_{diff}$. These are written as

$$R_{gl} = k_{gl} a_{gl} (v_G + v_L)(M^* - M_L) \qquad (3.18a)$$

$$R_{ls} = k_{ls} a_{ls} (v_L + v_S)(M_L - M_{P+2}) \qquad (3.18b)$$

$$R_{diff} = D_{ef} \frac{\partial M}{\partial r} a_{ls} \left(v_L + v_s \right) \qquad (3.18c)$$

In Equation 3.18, k_{gl} and k_{ls} are the gas-liquid and liquid-solid mass transfer coefficients, a_{gl} and a_{ls} are the gas-liquid and liquid-solid interfacial areas per unit volume, v_G, v_L and v_s are the total volumes of the gas, liquid and solid phases in the reactor volume and M_L and M^* are the liquid-phase monomer concentration and the equilibrium monomer concentration corresponding to the gas-liquid interface. At pseudo-steady state, the rates of mass transfer are all equal and are equal to the total rate of polymerization (in the macroparticle), R_{poly}.
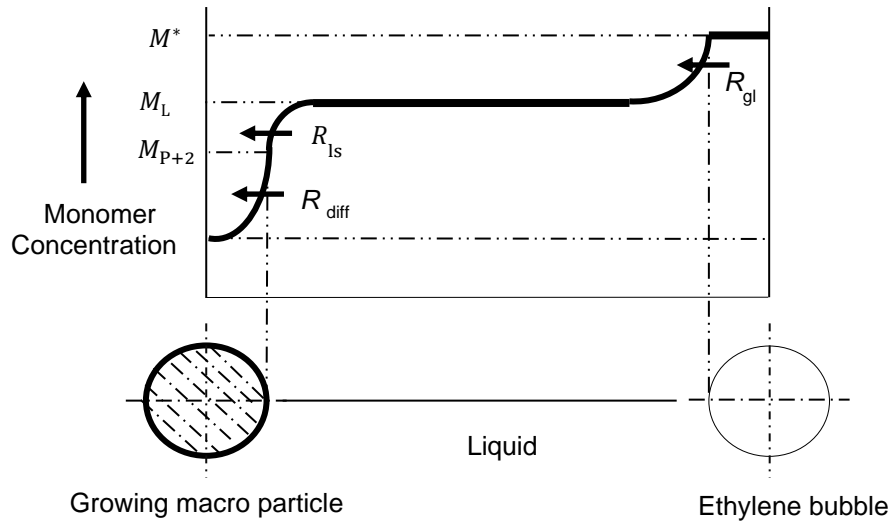
Fig. 3. 2 Variation of the monomer concentration inside the reactor with location, at any time. M^*: equilibrium monomer concentration at the gas-liquid interface, M_L: monomer concentration in bulk liquid, M_{P+2} : monomer concentration at the surface of the macroparticle

The mass transfer coefficients, k_{gl} and k_{ls}, and the interfacial areas, a_{gl} and a_{ls}, are estimated using the correlations summarized in Table 2.8. The value of k_{gl} is calculated using the correlation of Calderbank and Moo-Young [132] for mechanically agitated sparged reactors. The gas-liquid interfacial area, a_{gl}, is calculated from the values of the gas bubble diameter, d_b, and the gas hold up, ϕ_g, using the correlations [133], [135], [159] in Table 2.8. These above correlations

were also used in open literatures[160] [160]. The Ranz and Marshall correlation is used to calculate the values of k_{ls} and a_{ls}.

As the operating temperature in the reactor is much higher than the critical temperature of the monomer, we have used the concept of solubility of a gas in a liquid to estimate the equilibrium concentration, M^*, of the monomer in the liquid. The partial pressure of the monomer and hydrogen in the gas phase can be related to the equilibrium monomer concentration in the liquid phase using [124] Henry's law as

$$p_{et} = H_{et\text{-}hex} M^*$$
(3.19a)

$$p_{H_2} = H_{H_2\text{-}hex} M^*_{H_2}$$
(3.19b)

Here, $H_{et\text{-}hex}$ and $H_{H_2\text{-}hex}$ are Henry's law constants for ethylene in hexane and hydrogen in hexane, respectively.

3.1.4 OVERALL MASS BALANCE

To study the polymerization of ethylene in a CSTR, we need to write the set of linearly independent overall mass balance equations for the various components fed to the reactor. The steady-state mass balance equations for various components are written as

$$I_{M,in} - Q_T(1-F)M_L(MW) - R_{poly} = 0 \text{ (monomer)}$$
(3.20a)

$$I_{C,in} - Q_T F f_c \rho_{s,avg} = 0 \text{ (catalyst)}$$
(3.20b)

$$- Q_T F (1 - f_c) \rho_{s,avg} + R_{poly} = 0 \text{ (polymer)}$$
(3.20c)

$$I_{S,in} - Q_T(1 - F) \rho_S \left[1 - \frac{M_L(MW)}{\rho_M} \right] = 0 \text{ (solvent)}$$
(3.20d)

Here, $I_{M,in}$, $I_{S,in}$, and $I_{C,in}$ are the inlet mass flow rates of the monomer, solvent and the catalyst, respectively, Q_T is the volumetric flow rate of the slurry at the exit, F is the volume fraction of solids present in the slurry at the reactor outlet, f_c is the mass fraction of catalyst in the solids at the reactor outlet and $\rho_{s,avg}$ is the average density of the solid. The average density, $\rho_{s,avg}$, of the solid can be expressed assuming volume additivity (in terms of f_c, ρ_C and ρ_P) as

$$\frac{1}{\rho_{s,avg}} = \frac{f_c}{\rho_c} + \frac{1-f_c}{\rho_P} \tag{3.21}$$

Here, ρ_c and ρ_P are the densities of the catalyst and the polymer, respectively.

3.2 COMPUTATIONAL PROCEDURE

The flow chart used to solve the model equations is given in Figure 3.3. The *first* step is to read the kinetic parameters, k_P and k_{tr}, the parameters, D_{cat}, D_1, $I_{C,in}$, θ, p_{et}, N_E, ρ_P, ρ_M, ρ_C and ρ_S, the hydrogen concentration, H_2, and the number of grid points, P. The value of N_i and $R_{c,i}$ are generated using Equations 3.7 and 3.8, respectively. The mass transfer coefficients, k_{gl} and k_{ls}, etc., are estimated using Table 2.8. The single-particle diffusion equations (Equation 3.14) in their finite difference form (Table 3.2) are then solved from time 0 to θ using a *guess* value of M_L. The monomer profiles inside the macroparticle, M_i ($t = 0$ to θ), R_{mp} and subsequently, R_{poly}, are obtained at θ.

The value of R_{poly} obtained from the diffusion equations is used in the mass transfer equations. The value of R_{gl} is equated to R_{poly} at pseudo-steady-state conditions, as discussed earlier. An updated value of M_L is obtained from Equation 3.18 using the value of R_{gl}. Here, the equilibrium monomer concentration of the ethylene at the gas-liquid interface, M^*, is calculated using Henry's law and the partial pressure of the monomer in the vapor phase (read as input in Figure 3.2). The updated value of

M_L is used in the next iteration of solving the diffusion and the mass transfer equations. This process is repeated until a converged value of M_L is obtained. The monomer profile inside the macroparticle and the value of R_{poly} is also updated in each iteration to obtain the converged values. The overall mass balance equations (Equations 3.20) are then solved using the converged value of R_{poly} to obtain the values of the required monomer flow rate, $I_{M,in}$, the required solvent flow rate, $I_{S,in}$, $\rho_{s,avg}$ and f_c . The moment equations (Table 3.1) are then solved (after convergence of the monomer profile) to obtain the various moments of the live and dead polymer chains in each computational shell. These moments are used to find the number and weight average molecular weights, $M_{n,i}$ and $M_{w,i}$, for each shell. These are then used to obtain the number and weight average molecular weights, $\bar{M}_n$ and $\bar{M}_w$, for the entire macroparticle, followed by the $\overline{PDI}$. The system of ODEs in Tables 3.1 and 3.2 have been solved using the function, ode15s, of MATLAB®.

Read (industrial reactor data) $I_{C,\,in}$ and θ

Assume

k_P and D_1

Read (literature data) k_{tr}, D_{cat}, ρ_P, ρ_M, ρ_C, ρ_S, H_2, P

Read (industrial reactor data) p_{et}

Guess value $k = 1$

Generate $R_{c,i}$, N_i, k_{gl}, k_{ls}

M_L^k

Solve diffusion equations (Table 3.2)

R_{poly}

Mass transfer equations (Equation 3.18)

M_L^{k+1}

k = iteration no.

M_L^{k+1}

$M_L^{k+1} - M_L^k < \text{TOL}$

If No

Update all information M_i (t = 0 to θ), R_{poly}

If Yes

Overall mass balance (Equations 3.20)

Kinetic model (Table 3.1)

$I_{M,in}$, $I_{S,in}$, $\rho_{S,avg}$ and f_c

Tune k_P and D_1 (Equation 3.24)

M_n, M_w, $\bar{M}_n$, $\bar{M}_w$, $\overline{PDI}$

Fig. 3. 3 The algorithm used for solving the equations characterizing the reactor

3.3 TUNING OF DATA ON AN INDUSTRIAL REACTOR

The model is tuned using sets of available data for an *industrial* single-stage HDPE slurry CSTR. In the first step, the values of N_E are calculated for each of the data sets (using Equation 3.22a). Thereafter, an average value of D_{cat} is evaluated using Equation 12b and the N_{data} (= 7) sets of industrial reactor values of D_{mp}, $I_{M,in}$ and $I_{C,in}$:

$$\left(N_E\right)_i = \frac{1}{\rho_P} \frac{\left(I_{M,in}\right)_i}{\frac{\pi}{6}\left(D_{mp}\right)_i^3} \tag{3.22a}$$

$$D_{cat} = \frac{1}{N_{data}}\left(\frac{6}{\pi\rho_C}\right)^{1/3} \sum_{i=1}^{N_{data}} \frac{\left(I_{C,in}\right)_i^{1/3}}{\left(N_E\right)_i^{1/3}} \tag{3.22b}$$

In the second step, this value of D_{cat} is used to obtain the radii, $R_{c,i}$, of microparticles in each shell, after fragmentation, and the corresponding N_i. Sarkar and Gupta [24], [25] use an arbitrary value of $R_{c,av}$ and calculate the values of $R_{c,i}$, D_{cat} and N_i using Equations 2 and 3. In the present study, the mass balance given by Equation 13 is used along with Equations 2 and 3 to obtain the values of N_i and $R_{c,i}$, respectively:

$$\sum_{i=1}^{P}\left(N_i \frac{4\pi}{3} R_{c,i}^3\right) = \frac{\pi}{6} D_{cat}^3 \tag{3.23}$$

The value of $R_{c,max}$ is taken as 1.5 times the value of $R_{c,av}$, as suggested by some workers [24], [25], [90].

In the next step, the reactor model is simulated using the values of $I_{C,in}$ and θ of the industrial reactor as per the computational flow chart described in the previous section (and in Fig. 3.2). The values of k_P and D_1 are used as *tuning parameters*

(since, in the literature, a wide range of values of k_P are given) to predict the values of the required monomer mass flow rate, $I_{M,in}$, the required solvent mass flow rate, $I_{S,in}$, and the average diameter of the macroparticle, D_{mp}. The estimation of these two tuning parameters is performed using the minimization of the following objective function (sum-of-squares of the relative errors)

$$E = \left(\frac{I_{M,in} - I_{M,in}^{model}}{I_{M,in}} \right)^2 + \left(\frac{I_{S,in} - I_{S,in}^{model}}{I_{S,in}} \right)^2 + \left(f \times \frac{D_{mp} - D_{mp}^{model}}{D_{mp}} \right)^2 \qquad (3.24)$$

Here, $I_{M,in}$, $I_{S,in}$ and D_{mp} are values from the industrial reactor, while the values, $I_{M,in}^{model}$, $I_{S,in}^{model}$ and D_{mp}^{model}, are the model predictions. The factor, f, is the ratio of the minimum macroparticle diameter to the maximum macroparticle diameter, $D_{mp}^{min}/D_{mp}^{max}$, taken from the data set of the industrial reactor. Out of the seven data sets from the industrial reactor, three are used for model **tuning** and the remaining four are used for model **validation**.

The effect of various physico-chemical, and the kinetic parameters as well as the reactor operating conditions are studied using the tuned model. A set of reference values and ranges of operating conditions used in our analysis are given in Table 3.3.

Table 3. 3 Reference values of the parameters and ranges of the operating conditions used in the simulation

Parameter	Value	References
Diffusivity of monomer in n-hexane	1.25×10^{-8} m^2/s	[160], [161]
Density of catalyst	2600 kg/m^3	[143]
Density of n hexane	600.6 kg/m^3	[162]
Void fraction of close-packed spheres, ε	0.476	[24]
Termination rate constant, k_{tr}	$0.186 \times 10^{-1.5}$ m$^{1.5}$ kmol$^{-0.5}$ s^{-1}	[24]
Number of the computational shells, P	36	[24]
Hydrogen concentration, H_2	1×10^{-3} kmol/m^3	[24]
Concentration of active sites, C^*	1×10^{-2} kmol site/(m^3 of catalyst)	[157]
Henry's law constant of ethylene in n-hexane, $H_{et\text{-}hex}$	11.325×10^5 Pa-m^3/kmol	[160]
Reactor temperature, T	80-82 ^{o}C	plant data
Reactor pressure, P_t	7.5 - 8.2 bar	plant data
Ethylene partial pressure, p_{et}	0.60 - 0.75 bar	plant data
Catalyst volumetric flow rate (slurried in hexane)	115 – 245 l/hr	plant data
Reactor mean residence time, θ	1.3 - 1.9 hr	plant data
Ethylene mass flow rate, $I_{M,in}$	16.16 - 23.5 tons/hr	plant data

CHAPTER 4

MULTIOBJECTIVE OPTIMIZATION

Optimal operating conditions are required to obtain the maximum productivity of the polymer at a minimal cost. The optimum reactor operation should also ensure the operational safety of the reactor. Thus, a series of optimization problems starting with single objective optimization (SOO) problems to complex multi-objective optimization (MOO) problems have been formulated and solved. Multiobjective optimization using evolutionary algorithms are commonly used to obtain the set of optimal solutions for the objectives of conflicting nature. Genetic algorithms (GAs) are the widely used optimization technique to find the optimal solution for both SOO and MOO, constrained and unconstrained problems. This is a generic population-based computing technique influenced by the Darwinian concept of natural selection in biology. This technique emulates the idea of natural genetics to search the optimal solutions in the feasible domain using reproduction, crossover and mutation.

4.1. MOO FOR POLYOLEFINS POLYMERIZATION PROCESSES

Olefin polymerization processes often involve multiple objectives with conflicting nature. Several MOO studies on polyethylene reactors have been reported in the published literature with various objective functions, constraints and decision variables [163]–[165]. Yao et al. [163] employed a GA technique to maximize the productivity of LDPE in an industrial tubular reactor using the jacket temperature profile as the control function. The maximum reactor temperature and the range of jacket temperature were used as the constraints. Properties of the final product were not considered in this study. Agrawal et al. [164] optimized the operation of an industrial LDPE tubular reactor using binary-coded NSGA- II, and its jumping gene

adaptations. The two objective functions, maximization of monomer conversion and minimization of undesirable side product (with two constraints, the desired value of the number average molecular weight and maximum temperature inside the reactor) were used in this study. The reactor operating variables such as the inlet feed temperature, inlet pressures and feed flow rates of initiators, solvent, oxygen, were considered as the decision variables. The softer constrain was used to obtain the pareto-optimal solution rather than the hard (equality) end-point constrain. Furthermore, the NSGA-II-aJG and NSGA- II-JG performed better compared to the NSGA-II near the end-point constrain. Agrawal et al. [165] used three objectives (i) maximization of monomer conversion (ii) minimization of an undesirable side product, and (iii) minimization of compressor power input to optimize the design of an industrial LDPE tubular reactor. This study also used binary-coded NSGA- II and it's jumping gene adaptations. The results of design stage optimization and operation stage optimization were compared. The design stage optimization resulted in a significant improvement in the reactor performance compared to the operation stage optimization. The three objective optimizations produced a better solution compared to the two objective optimizations. Mogilicharla et al. [166] conducted the MOO of long-chain branched propylene polymerization using NSGA-II to obtain the pareto optimal set of solutions of the operating conditions. This study used the three conflicting objectives functions, maximization of the weight average molecular weight, maximization of the grafting density and minimization of total polymerization time. The two catalysts and one cocatalyst concentrations and the time gap between the catalyst injections were used as the decision variables. The optimal solutions led to the various competitive process possibilities and also showed improvement in the objective functions as compared to the literature data of Ye and Zhu [167] .

4.2 OPTIMIZATION STUDY OF THE HDPE SLURRY REACTOR

The optimization study is performed to obtain the optimal value of the set of decision variables corresponds to the maximization or minimization of one or more objectives. Appropriate constraints are often employed to maintain the safety and stability of the system. The main operating variables of the HDPE slurry reactor are shown in Figure 2.2. The monomer, ethylene, is the gas phase feed, the solvent (hexane) is liquid-phase feed while the solid catalyst is slurried with the solvent and continuously fed to the reactor.

4.2.1. CONSTRAINTS

The polymerization reaction is highly exothermic and temperature control is very important to avoid runaway reactions. All the heat of polymerization has to be removed through the solvent (n-hexane) in the slurry reactor. The solvent to monomer ratio, $I_{S,in}/I_{M,in}$, directly affects the temperature control of the reactor. It is observed from all the available data on the industrial reactors that the minimum value of this ratio at the steady-state operation of the slurry phase ethylene polymerization in CSTRs is 1.6. This ratio is required for sufficient heat removal and to maintain the reactor at isothermal conditions. Therefore, the constraint used in all the optimization problems is given by Eq. 4.1.

$$\frac{I_{S,in}}{I_{M,in}} > 1.6 \qquad\qquad (4.1)$$

4.2.2. DECISION VARIABLES

The volume of the reactor is constant and the mean residence time of the reactor mainly depends on the feed rates of monomer, $I_{M,in}$, and solvent, $I_{S,in}$, at a steady state. The productivity and the yield are the functions of the value of $I_{C,in}$ and θ as discussed in section 3.2. The rate of polymerization and the yield also depends on the equilibrium monomer (ethylene) concentration in the liquid phase. The equilibrium monomer concentration directly depends on the ethylene partial

78

pressure, p_{et}. Therefore, p_{et}, θ and $I_{C,in}$ are considered as the decision variables in the optimization study.

Bounds on the decision variables

$$0.8 < \theta \text{ (hr)} < 2$$
$$0.4 < p_{et} \text{ (bar)} < 0.9 \tag{4.2}$$
$$5 \times 10^{-4} < I_{C,in} (kg / s) < 15 \times 10^{-4}$$

4.2.3. OBJECTIVES

The main focus of the optimization study of the reactor is to find the optimal operating conditions to obtain the maximum productivity (R_{poly}) and yield (R_{mp}) at the minimal operating cost. The costs associated with the catalyst feed rate ($I_{C,in} = N_E \rho_C v_C$) and the mean residence time (θ) are considered as the major operating costs in this study. Therefore, the objectives of this study can be the maximization of both R_{poly} and yield R_{mp} and minimization of total catalyst present in the reactor at steady state ($N_E \theta$) or $I_{C,in}$.

4.2.4. FORMULATION OF THE OPTIMIZATION PROBLEMS

Problem 1 (SOO)

$$Max : I = R_{poly} \tag{4.3}$$

subject to

bounds

Equation (4.2)

constraint

Equation (4.1)

Problem 2 (SOO)

$$Max : I = R_{mp}$$ (4.4)

subject to

bounds

Equation (4.2)

constraint

Equation (4.1)

Problem 3 (MOO)

$$Max : I_1 = R_{poly}$$
$$Min : I_2 = N_E \theta$$ (4.5)

subject to

bounds

Equation (4.2)

constraint

Equation (4.1)

Problem 4 (MOO)

$$Max : I_1 = R_{poly}$$
$$Min : I_2 = I_{C,in}$$ (4.6)

Subject to

bounds

Equation (4.2)

constraint

Equation (4.1)

Problem 5 (MOO)

$$Max : I_1 = R_{poly}$$
$$Max : I_2 = R_{mp}$$ (4.7)

bounds

Equation (4.2)

constraint

Equation (4.1)

CHAPTER 5

RESULTS AND DISCUSSION

5.1 COMPARISON OF MODEL PREDICTIONS WITH DATA ON THE INDUSTRIAL REACTOR

The best-fit values of the tuning parameters obtained from the model tuning procedure given in Figure 3.3 are given in Table 5.1. The earlier reported values [22], [143] of these parameters are also given in Table 5.1. The other simulation parameters and operating conditions are at their reference values given in Table 3.3.

Table 5. 1 Best-fit values of the two tuning parameters

Parameter	Best-fit value (this study)	Soni and Bhagwat [143]	Bhagwat et al. [22]
$10^{-6} \times k_P$ (m^3/(kmol-s))	0.59	1.0	10
$10^{10} \times D_1$ (m^2/s)	1.14	1.0	1.0

One of the data sets of the industrial reactor is selected as a *reference* data set. Both the model-predicted values and the values from the industrial reactor data are normalized using the respective values of the reference data set (due to propriety reasons). In an industrial reactor operating at a steady-state, the *required value* of monomer flow rate, $I_{M,in}$, is decided by the value of the catalyst flow rate, $I_{C,in}$. An increase in $I_{M,in}$ from this *required value* at a given $I_{C,in}$ leads to a continuous accumulation of the monomer in the vapor space. This will lead to a continuous increase in both the partial pressure of the monomer and the total pressure of the reactor. This will make the operation unstable. The present model also considers $I_{C,in}$ as an input condition and predicts the required value of $I_{M,in}$ for a set of the assumed value of model tuning parameters. In the industrial reactor, the inlet flow rate of solvent, $I_{S,in}$ and the value of $I_{M,in}$ decide the residence time of the reactor,

θ. Whereas, the simulation of the present model considers the values of θ along with $I_{C,in}$ as input conditions and predicts the required values of $I_{S,in}$ and $I_{M,in}$. A comparison of the tuned model-predicted values of $I_{M,in}$ and $I_{S,in}$ with the corresponding values of the industrial reactor data set (plant-data) at different values of θ are shown in Figures 5.1a and 5.1b, respectively. The productivity and yield control the average size of macroparticle, D_{mp}, at given values of $I_{M,in}$, $I_{C,in}$ and θ. The present model also predicts the values of D_{mp} at different values of $I_{C,in}$ and θ. A comparison of the tuned model-predicted values of D_{mp} with the corresponding values of the industrial reactor data set (plant-data) at different values of θ is shown in Figures 5.1c.

The values of $I_{C,in}$, $I_{M,in}$ and $I_{S,in}$ from the plant data are controlled by the operator at the inlet of the reactor. This is why, Figure 5.1a and Figure 5.1b show a smooth variation for the plant data values of $I_{M,in}$ and $I_{S,in}$. Whereas, a small error in the model predictions makes the variation in the model-predicted values of $I_{M,in}$ and $I_{S,in}$ not so smooth in Figure 5.1a and Figure 5.1b. However, the agreement between the plant data and the model predicted values of $I_{M,in}$ and $I_{S,in}$ is observed to be quite good. A similar agreement is observed in Figure 5.1c between the plant data values with the model prediction for D_{mp}. It is to be noted here that the value of D_{mp} is also obtained as an output from the tuned model and is also not controlled by the operator. This is why there is no smooth variation for both the values in Figure 5.1c.
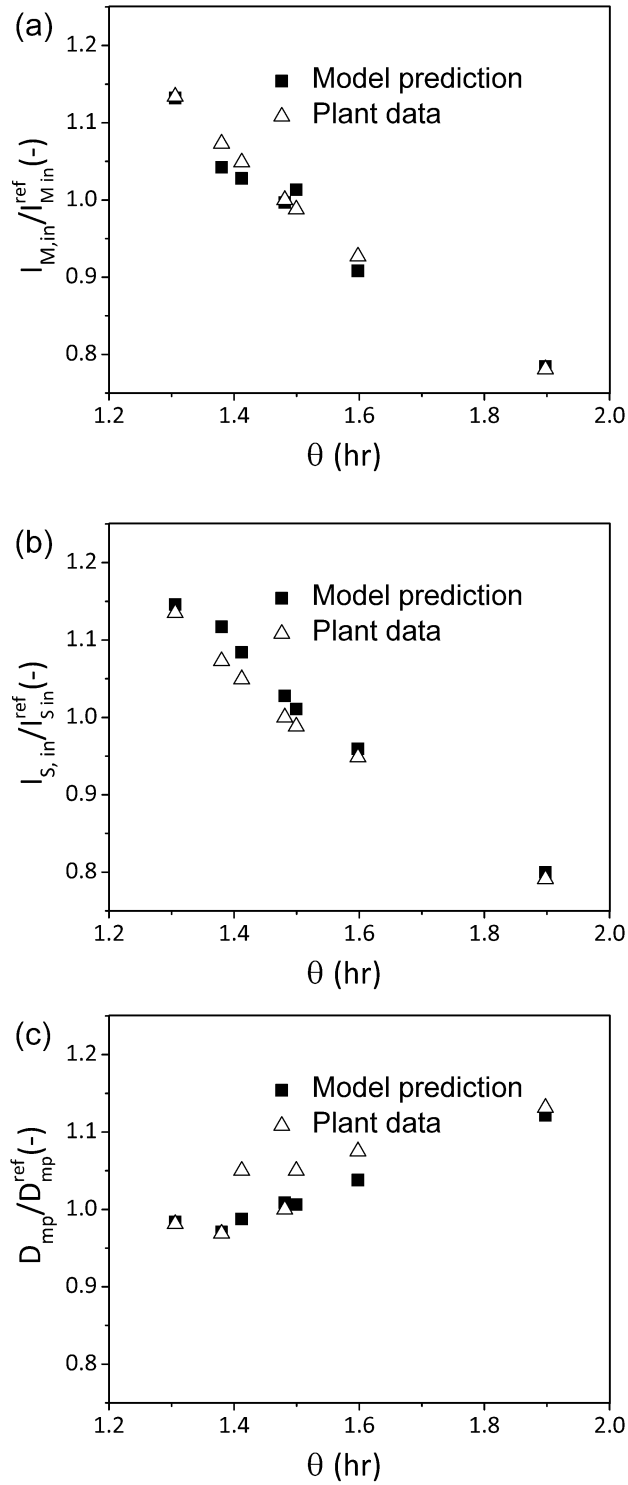
Fig. 5. 1 Comparison of tuned model-predictions with the industrial reactor data
(a) $I_{M,in}$ *vs.* θ, (b) $I_{S,in}$ *vs.* θ and (c) D_{mp} *vs.* θ

5.2 SENSITIVITY TO MODEL PARAMETERS

Having compared the tuned model-predictions with the industrial reactor data, we now focus on the study of the effect of the two main tuning parameters, D_1 and k_P (parametric study). Figure 5.2 shows the effect of D_1 on R_{mp}, M_L, D_{mp}, the solvent to monomer ratio, $I_{S,in}/I_{M,in}$ and the $\overline{PDI}$. As D_1 increases, more monomer diffuses inside the macroparticle, thus increasing the monomer concentration, M_i, inside the macroparticle, and so, R_{mp}. Similarly, increasing D_1 leads to a reduction in M_L, the monomer concentration in the bulk liquid. These effects are shown in Figure 5.2a. Since R_{mp} increases with an increase in D_1, the macroparticle diameter, D_{mp}, increases (note that θ and $I_{C,in}$ are both constant). An increase in D_1 leads to an increase in $I_{M,in}$ and a decrease in the ratio, $I_{S,in}/I_{M,in}$ (shown in Figure 5.2b). An increase in the value of D_1 leads to a decrease in $\overline{PDI}$. This is because an increase in D_1 leads to a *flatter* monomer profile inside the macroparticle, thus reducing the $\overline{PDI}$. Our tuned model predicts a value of $\overline{PDI}$ between 4 - 5 (for the reference values of the other simulation parameters given in Table 3.3).
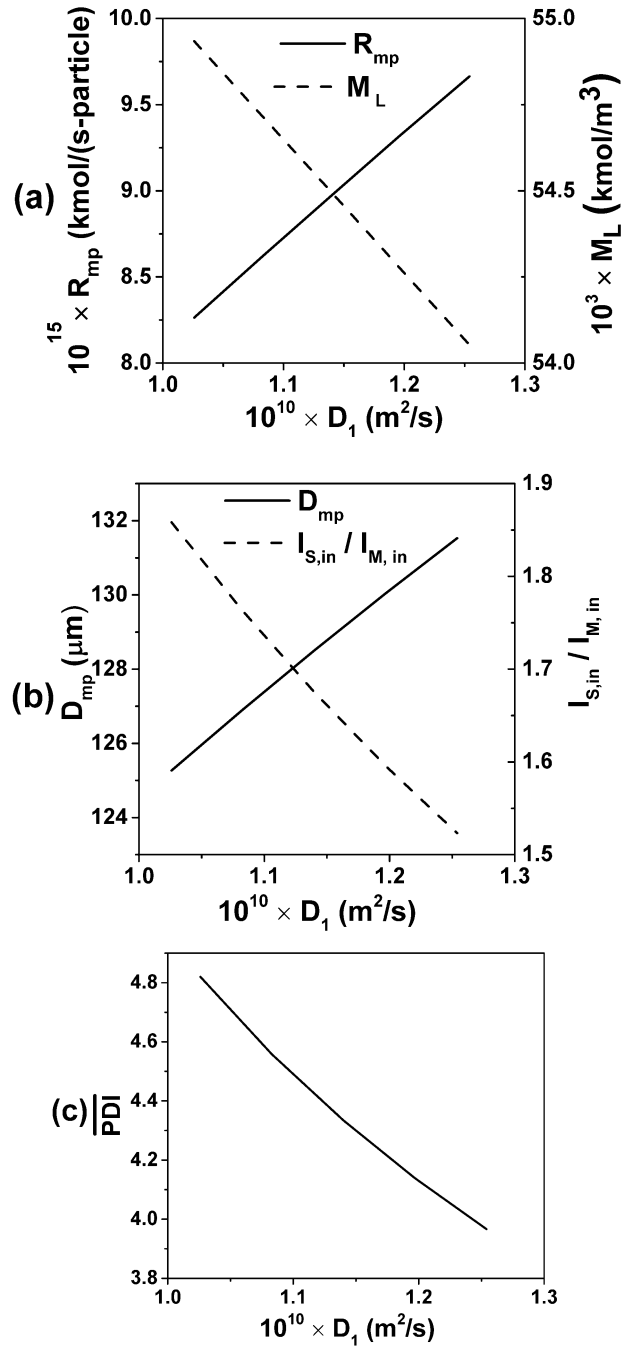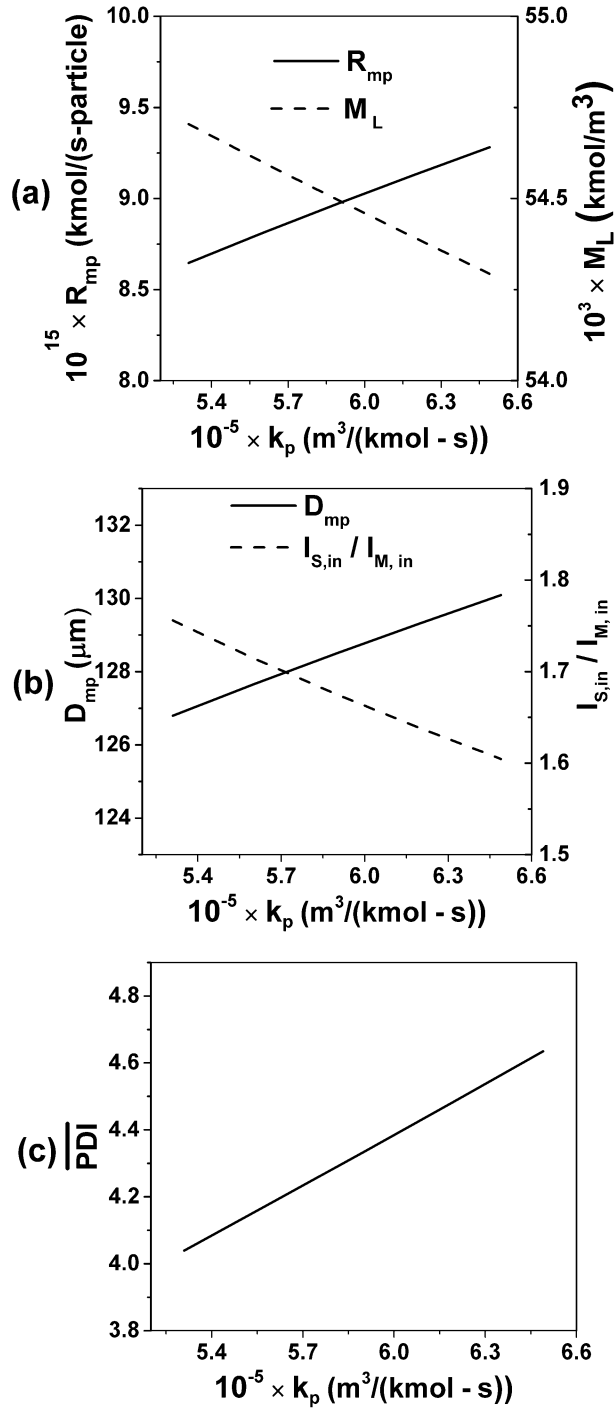
Fig. 5. 2 Influence of D_1 on (a) R_{mp} and M_L, (b) D_{mp} and $I_{S,in}/I_{M,in}$ and (c) $\overline{PDI}$

The influence of varying the propagation rate constant, k_P, is shown in Figure 5.3. As seen in Figure 5.3a an increase in the value of k_P leads to an increase in the value of R_mp and decrease in the value of M_L. This is because an increase in the value of k_P leads to an increase in the value of $k_\mathrm{P}C^*M_\mathrm{i}$, despite a decrease in the value M_i (clearly, the effect of k_P dominates), thus increasing R_mp (Figure 5.3a). As k_P increases, M_i decreases, leading to a decrease in the value of M_L (in Figure 5.3a). An increase in the value of R_mp with an increase in k_P leads to an increase in D_mp and the required rate of monomer input, $I_\mathrm{M,in}$ and, consequently, the ratio, $I_\mathrm{S,in}/I_\mathrm{M,in}$ decreases (Figure 5.3b). As k_P increases, M_i falls more sharply with the radial location inside the macroparticle and leads to an increase in the value of $\overline{PDI}$ (Figure 5.3c).

Fig. 5. 3 Influence of k_p on (a) R_{mp} and M_L, (b) D_{mp} and $I_{S,in}/I_{M,in}$ and (c) $\overline{PDI}$

5.3 EFFECT OF REACTOR OPERATING VARIABLES

5.3.1 EFFECT OF REACTOR RESIDENCE TIME AND CATALYST FEED RATE

The effect of the two *operating* variables, θ and $I_{C,in}$, of the reactor on R_{poly}, R_{mp}, D_{mp} and $I_{S,in}/I_{M,in}$ are shown in Figure 5.4. The value of R_{mp} represents the polymer production rate of each catalyst particle whereas the value of R_{poly} represents the overall polymer production rate. Increase in either θ or $I_{C,in}$ ($I_{C,in} = N_E \rho_C v_C$) leads to an increase in the value of the total number of macroparticles present in the reactor, $N_E \theta$. Thus, the range of $N_E \theta$ is kept the same so as to carry out a comparative study of the effect of θ and $I_{C,in}$ on various reactor performance parameters. The rate of monomer consumption per particle, R_{mp}, is multiplied with the number of macroparticles present in the reactor, $N_E \theta$, to give the total rate of monomer consumption, R_{poly}. The simulation results show this trend of increasing R_{poly} with an increase in both θ and $I_{C,in}$ (Figures 5.4a and 5.4b). The comparison shows that at lower values of $N_E \theta$, R_{mp} is higher (Figure 5.4b), while at higher values of $N_E \theta$, R_{mp} is higher (Figure 5.4a). This is because at lower values of $N_E \theta$, the value of θ is higher in Figure 5.4b, while at higher values of $N_E \theta$, the value of θ is higher in Figure 5.4a. As discussed above, the value of $N_E \theta$ can be increased either by increasing θ or $I_{C,in}$. The value of R_{mp} will be higher if $N_E \theta$ is increased by increasing θ than by increasing $I_{C,in}$. In both cases, the increase in R_{poly} also increases R_{gl}, as discussed before. The increase in R_{gl} leads to a decrease in M_L according to Equation 3.18a. The decrease in M_L leads to a decrease in M_i and consequently, R_{mp}. Thus, an increase in either θ or $I_{C,in}$ should decrease R_{mp}. However, the simulation results show this trend only for an increase in $I_{C,in}$ (Figure 5.4b). The simulation results shown in Figure 5.4a indicate that the value of R_{mp} increases with an increase in θ upto a certain value, θ^{opti}. Thereafter, it decreases
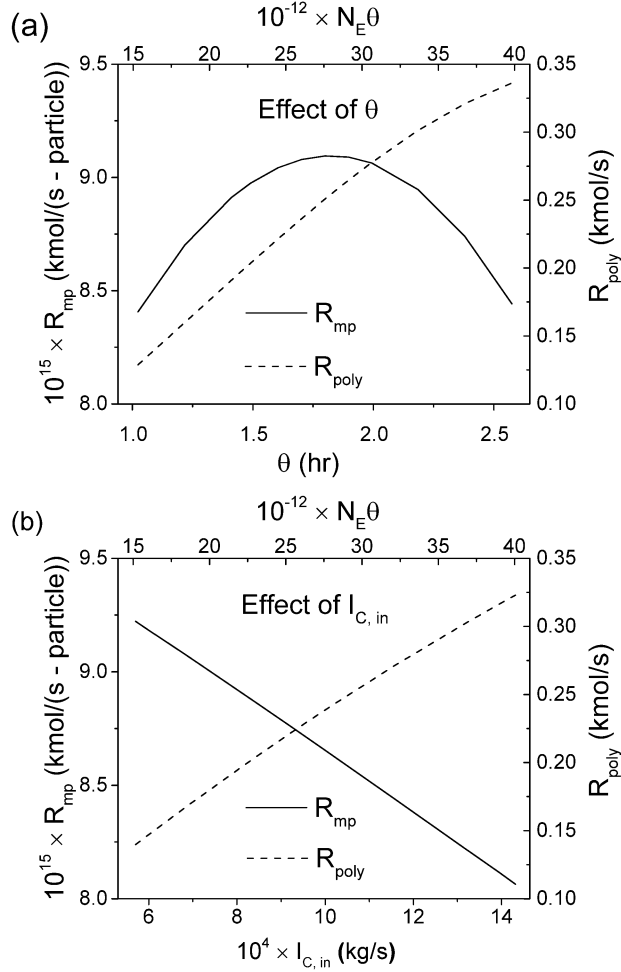
89

Fig. 5. 4 Effect of variation of (a) θ on R_{mp} and R_{poly} at constant $I_{C,in}$, (b) $I_{C,in}$ on R_{mp} and R_{poly} at constant θ

with further increases in θ. This is because the profile of monomer concentration becomes flatter with increase in θ as shown in Figure 5.5. This leads to an increase in M_i at lower values of P (inside the macroparticle) as shown in the inset of Figure 5.5. However, decrease in M_L (with an increase in θ) decreases the values of M_i at higher values of P (near the surface, inside the macroparticle). The increase in M_i at lower values of P dominates at values of θ below θ^{opti} and this leads to the increase in R_{mp} with increase in θ. The decrease in M_i at higher values of P starts

dominating as the value of θ goes beyond θ^{opti} and this leads to a decrease in R_{mp} with an increase in θ.
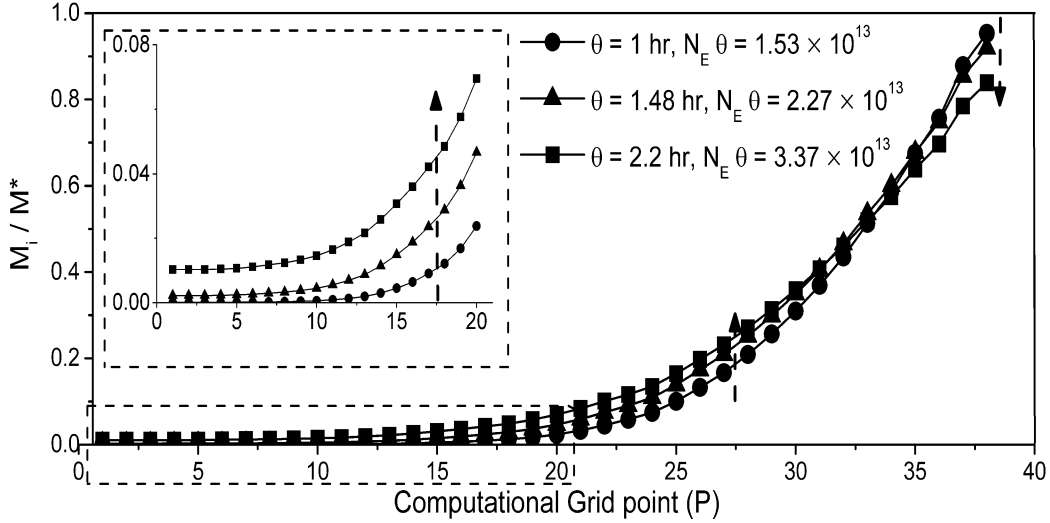
Fig. 5. 5 Normalized monomer profile (M_i / M^*) *vs.* *P* at various θ. The monomer profile is shown in the inset at lower values of *P*

The effects of θ and $I_{\text{C,in}}$ on D_{mp} and $I_{S,in}/I_{\text{M,in}}$ obtained from the reactor model are shown in Figures 5.6 a and 5.6 b. The values of D_{mp} represents the polymer yield as discussed before. It is important to note that the ratio, $I_{S,in}/I_{\text{M,in}}$, affects the temperature control of the reactor. The polymerization reaction is highly exothermic and temperature control is very critical. All the heat of polymerization has to be removed through the solvent (n-hexane) in the slurry reactor. Thus, higher values of $I_{S,in}/I_{\text{M,in}}$ are required for operational safety. The value of $I_{\text{M,in}}$ is directly proportional to the value of R_{poly}. Whereas, the value of $I_{\text{S,in}}$ depends on the value of $I_{\text{M,in}}$ and the value of θ.
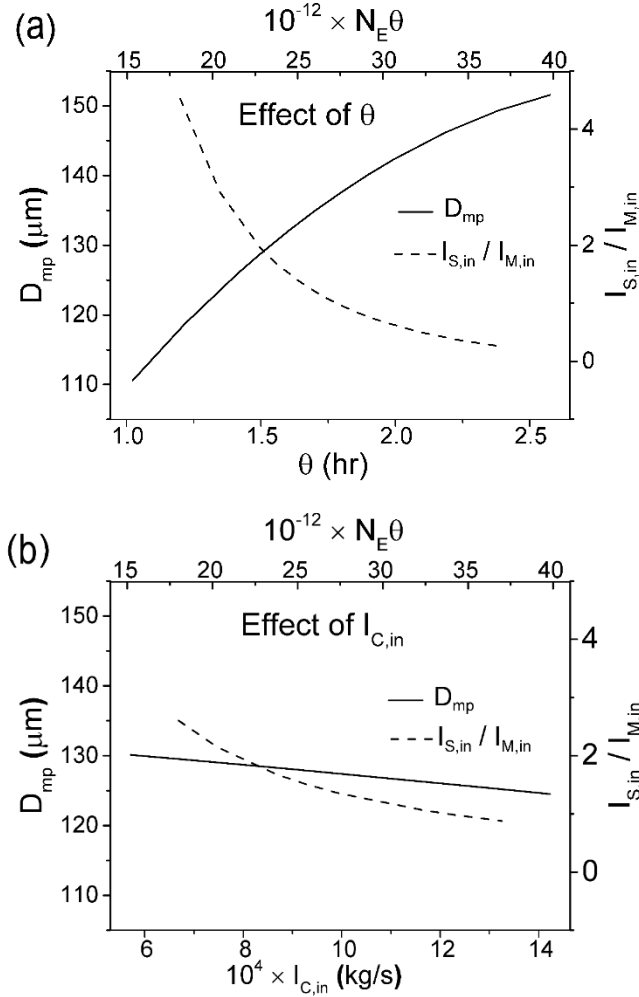
Fig. 5. 6 Effect of variation of (a) θ on D_{mp} and $I_{S,in}/I_{M,in}$ at constant $I_{C,in}$ and (b) $I_{C,in}$ on D_{mp} and $I_{S,in}/I_{M,in}$ at constant θ

It is observed from Figure 5.6 a that the value of D_{mp} (polymer yield) increases if the value of $N_E\theta$ is increased by increasing θ. Figure 5.6 b shows that the value of D_{mp} decreases slightly if the value of $N_E\theta$ is increased by increasing $I_{C,in}$. The observation from Figure 5.6 a can be attributed to the fact that the macroparticles stay for a longer time inside the reactor (due to increasing θ) and therefore, the value of D_{mp} will be higher. In Figure 5.6 b, θ remains constant, while $N_E\theta$ is increased by increasing $I_{C,in}$. The increase in $I_{C,in}$ leads to a decrease in R_{mp} as

92

discussed in Figure 5.4b. This is why in Figure 5.6 b, the value of D_{mp} decreases by increasing $I_{C,in}$.

It is observed that the values of $I_{S,in}/I_{M,in}$ worsen with the increase in $N_E\theta$ either by increasing θ or by increasing $I_{C,in}$ (Figures 5.6 a and 5.6 b). At a constant θ, an increase in $I_{C,in}$ increases the value of R_{poly} as discussed before (Figure 4.4b). This leads to an increase in $I_{M,in}$ and a decrease in $I_{S,in}$ as θ is kept constant. Therefore, the ratio $I_{S,in}/I_{M,in}$ decreases with an increase in $I_{C,in}$ in Figure 5.6 b. The decrease in $I_{S,in}/I_{M,in}$ is observed to be steeper in Figure 5.6 a than in Figure 5.6 b. This is because the increase in θ also leads to a decrease in the sum of $I_{S,in}$ and $I_{M,in}$. Thus, the model gives an insight that if $N_E\theta$ is increased by increasing θ then the polymer yield, D_{mp}, improves at the cost of compromising the operational *safety* ($I_{S,in}/I_{M,in}$) of the reactor [operational safety is reflected by low values of ($I_{S,in}/I_{M,in}$) since low values of this ratio lead to difficult temperature control in the reactor, and, indeed, there is a possibility of runaway reaction occurring]. Whereas, if $N_E\theta$ is increased by increasing $I_{C,in}$, the cost of operational safety ($I_{S,in}/I_{M,in}$) is less but the yield slightly worsens.

The effect of the *operating* variables, θ and $I_{C,in}$ on $\overline{PDI}$ is shown in Figure 5.7. It is observed that the value of $\overline{PDI}$ decreases if the value of $N_E\theta$ is increased by increasing θ, while it increases if it is increased by increasing $I_{C,in}$. This is due to the fact that as θ increases, the monomer profile becomes flatter as discussed above (Figure 5.5). This leads to a decrease in the diffusional resistance inside the macroparticle. The decrease in diffusional resistance decreases the value of $\overline{PDI}$ with increase in θ (Figure 5.7 a). It is also observed that an increase in the value of $I_{C,in}$ for a constant θ leads to a slightly steeper monomer profile and consequently the value of $\overline{PDI}$ increases slightly (Figure 5.7 b).
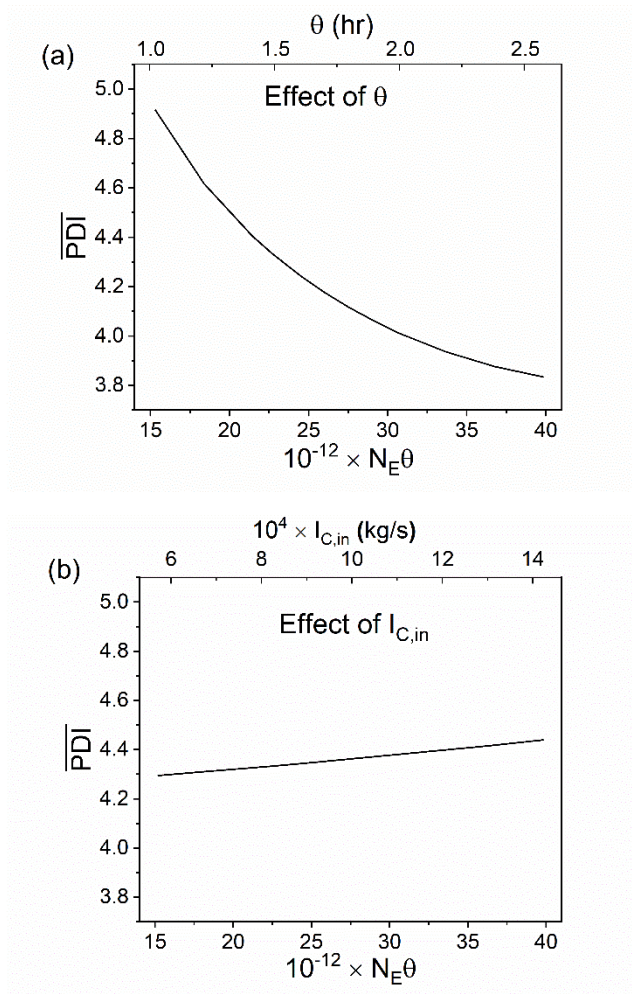
Fig. 5. 7 Effect of variation of (a) θ on $\overline{PDI}$ at constant $I_{C,in}$, (b) $I_{C,in}$ on $\overline{PDI}$ at constant θ

The combined effect of θ and $I_{C,in}$ on R_{mp} is shown in Figure 5.8. The variation of R_{mp} with θ at different values of $I_{C,in}$ shows that as the value of $I_{C,in}$ is increased the maximum in R_{mp} shifts towards lower values of θ. The value of R_{mp} starts decreasing with increase in θ (beyond θ^{opti}) because of the decrease in the value of M_L as discussed before. An increase in either θ or $I_{C,in}$ leads to a decrease in the

value of M_L. Thus, the decrease in the value of M_L with increase in θ will be faster at higher values of $I_{C,in}$ in comparison to that at lower values of $I_{C,in}$. Therefore, the maxima in R_{mp} occurs at lower values of θ when $I_{C,in}$ is increased. Thus, the model gives insight that an increase in $I_{C,in}$ leads to a decrease in the polymer production rate per catalyst particle (R_{mp}). The maxima in R_{mp} is achieved at lower values of θ if the value of $I_{C,in}$ is increased.
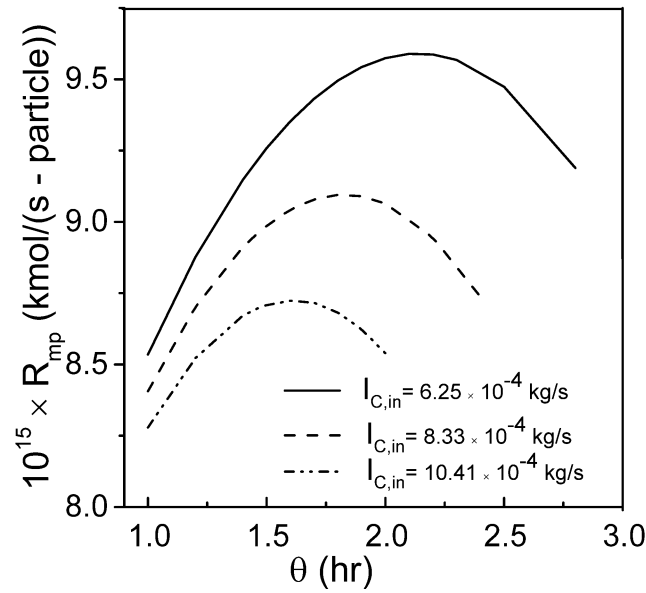
Fig. 5. 8 Variation of R_{mp} *vs.* θ at various $I_{C,in}$

5.3.2 EFFECT OF HYDROGEN CONCENTRATION

The effect of hydrogen concentration on the rate of polymerization is reported in the open literature [23], [143], [168]. Ha et al. [23] and Soni and Bhagwat [32] in their study on the ethylene polymerization in a slurry reactor observed a negligible impact of hydrogen on the rate of polymerization. A recent study [50] on slurry phase olefin polymerization also considered no effect of hydrogen on the rate of polymerization. It is worth mentioning that the present work considers the

initiation, chain propagation and chain transfer by hydrogen, similar to the kinetic model used by Ha et al. [23]and Soni and Bhagwat [21]. Therefore, this model also suggests no effect of hydrogen on the rate of polymerization as evident in the rate expression in Equation 3.16.

The effect of hydrogen on the number average molecular weight, M_n, and the weight average molecular weight, M_w, are shown in Figure 5.9. It is observed that, both M_n and M_w decrease with the increase in hydrogen concentration. This is because hydrogen is simply a chain transfer agent and it controls the molecular weights. It is also observed in the figure that both M_n and M_w vary inversely with the square root of the hydrogen concentration. This is because, the average molecular weights are proportional to the ratio of rate of propagation and rate of chain transfer whereas, the rate of the chain transfer reaction is proportional to the square root of the hydrogen concentration. Thus, the variation of the average molecular weights with hydrogen concentration is per the kinetic model used in this study.

The PDI is the ratio of M_w and M_n. It is observed in Figure 5.9 that both M_w and M_n show similar variations (slope ≈ 0.5) with respect to the hydrogen concentration. This suggests the negligible effect of the hydrogen concentration on the PDI. A similar observation is also reported in the open literature [23], [143], [168] for the effect of hydrogen concentration on the PDI.
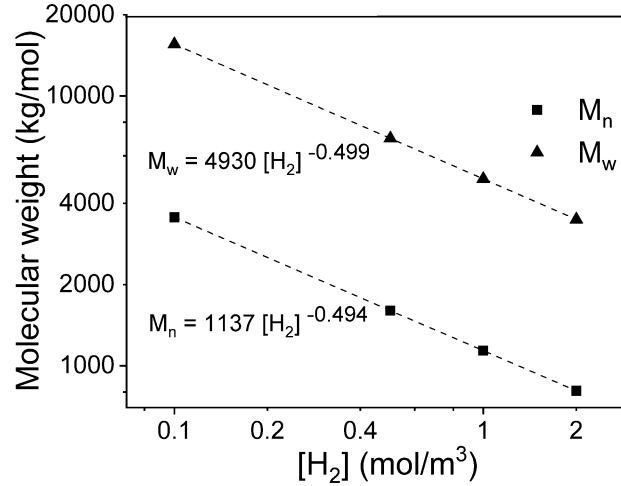
Fig. 5. 9 Effect of hydrogen concentration on the number average molecular weight and the weight average molecular weight

5.4 OPTIMIZATION RESULTS

The single objective optimization (SOO) and multiobjective optimization problems are solved using the genetic algorithm (GA). The Pareto optimal solution is obtained using NSGA-II algorithm. The optimization toolbox of MATLAB^{TM} is used to obtain the Pareto optimal solution for the SOO and MOO problems. The computational parameters used to solve the SOO and MOO problems are given in Table 5.2.

Table 5. 2 The computational parameters used in the optimization studies

Parameter	Value
Population size	80
Number of generations	200
Cross over probability	0.9
Mutation probability	1/number of variables

The converged Pareto set of SOO and MOO problems, Equations (4.3)-(4.7), are shown in Figure 5.10.
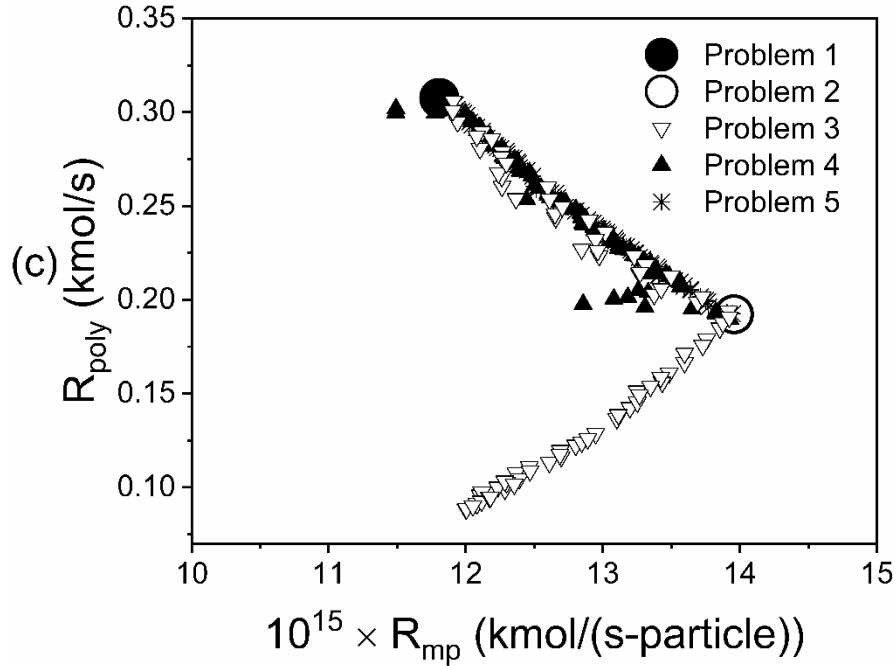
(a)

(b)
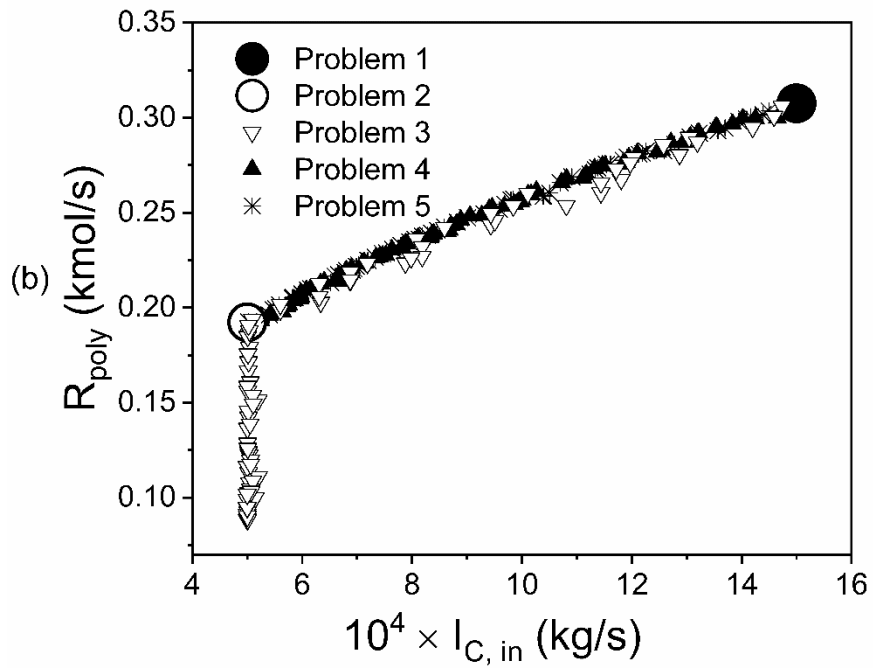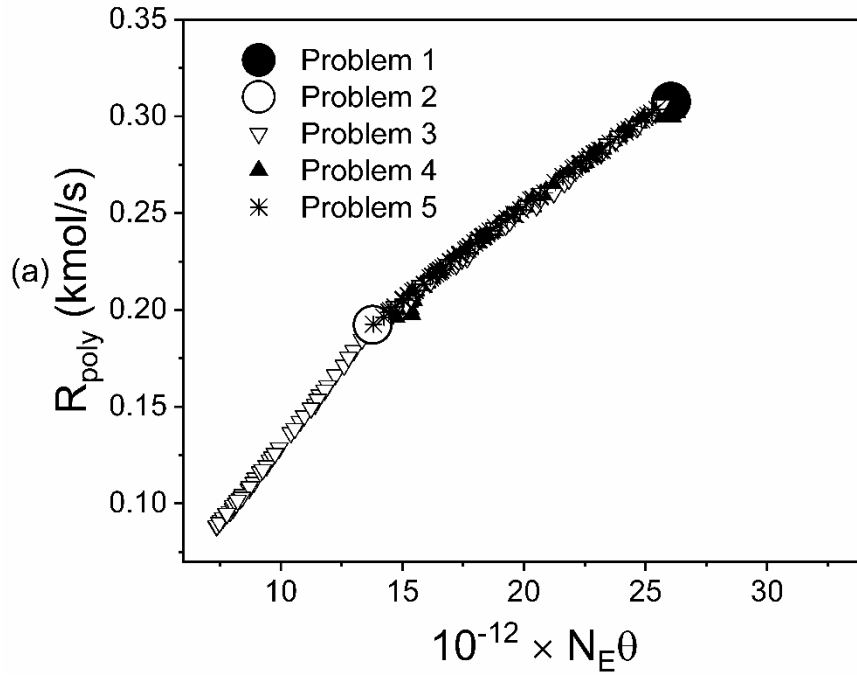
Fig. 5. 10 The converged Pareto set of SOO and MOO problems, equations (4.3)-(4.7)

The operating cost of the HDPE slurry polymerization processes can be linked to the values of $I_{C,in}$ and θ. An increase in either θ or $I_{C,in}$ ($I_{C,in} = N_E \rho_C v_C$) leads to an increase in the value of the total number of macroparticles present in the reactor, $N_E\theta$. A higher value of $N_E\theta$ corresponds to a higher operating cost and vice versa. It is understood that the maximum values of rate and yield are desired at the minimum operating cost at the commercial scale. The SOO problems 1 and 2 are the maximization of R_{poly} (productivity) and R_{mp} (yield) subjected to the bounds on the decision variables (Equation 4.2) and a constraint on the operational safety (Equation 4.1). It is observed in Figure 5.10a from the solution of the SOO problem 1 (Equation 4.3) that the maximum value of productivity is obtained at the maximum value of $I_{C,in}$ (upper bound) and the maximum value of $N_E\theta$ and the corresponding value of θ is 0.945 hr. At this value of $N_E\theta$, the value of polymer yield is observed to be minimum (Figure 5.10c). Thus, the maximum productivity is obtained at the maximum operating cost and the corresponding value of polymer yield is at the minimum value. It is also observed in Figure 5.10 (a-c) that, the

maximum value of the polymer yield (problem 2, Equation 4.4) is obtained at the minimum value of $I_{C,in}$ (lower bound), and the corresponding values of θ is 1.50 hr. At this value of $N_E\theta$, the value of productivity is observed to be minimum (Figure 5.10 (a-c), problem 2). Thus, the solution of SOO problems gives only one set of the optimal solution. To obtain the optimal values of productivity and polymer yield at various operating costs, we need to solve the MOO problems. Therefore, the MOO is performed on conflicting objectives to obtain the whole range of the set of optimal solutions. This is to be noted that in all the problems (problem 1 to 5) the corresponding optimal value of p_{et} is observed at its upper bound (0.9 bar).

The MOO problems (problems 3-5) comprise of two conflicting objectives. Three different sets of converged optimal solutions are obtained from the three different objective formulations (problems 3-5). These three sets of optimal solutions are plotted in terms of objective functions of problem 3 in Figure 5.10(a), problem 4 in Figure 5.10(b) and problem 5 in Figure 5.10(c). The optimal solutions obtained from problem 3 show a distinct behavior in Figures 5.10(b) and 5.10(c). This is because the second objective (minimize $N_E\theta$) can be controlled by either $I_{C,in}$ or θ as discussed above. Figure 5.10(b) clearly shows that the solutions of problem 3 can be divided into two sets. First, when R$_{poly}$ increases due to an increase in the value of θ at constant $I_{C,in}$ (lower bound). Second, when R$_{poly}$ increases due to increase in $I_{C,in}$. The optimal solutions of problem 3 in Figure 5.10(c) further shows that the increase in θ values at constant $I_{C,in}$ (lower bound) leads to an increase in R_{mp}. After maximum R_{mp} value is achieved at this value of $I_{C,in}$ (lower bound), the value of R_{poly} can not be increased by further increasing θ. In other words, the catalyst particles are completely utilized at this maximum θ. After this, the value of R_{poly} will increase only by increasing the value of $I_{C,in}$. The second set of the solutions of problem 3 and the entire solution set of problem 4 and problem 5

100

belongs to this category. The corresponding plots of the decision variables of these three problems are shown in 5.11 (a-e). These figures also verify the above observation of the two different sets of optimal solutions of problem 3. Since the first set of solutions of problem 3 represent the under-utilized catalyst particles, the second set of solutions of problem 3 (and the solutions of problem 4 and 5) are useful results for practical purposes.
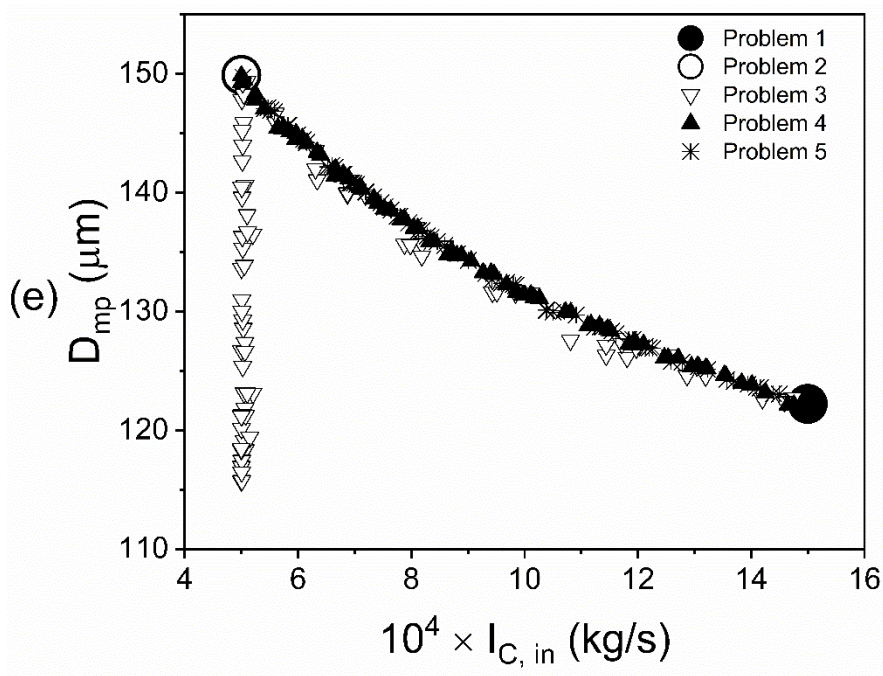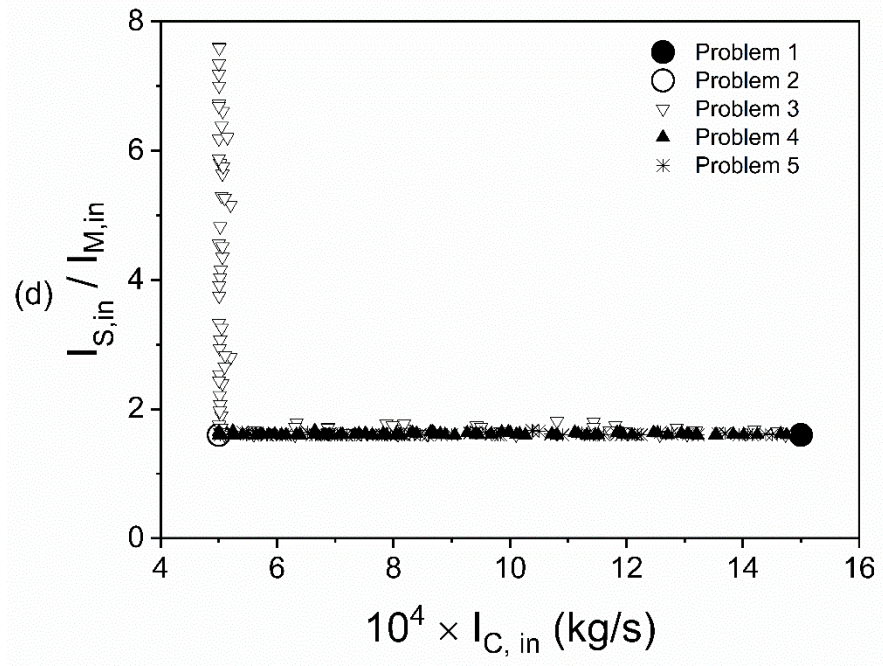
(b)

(c)
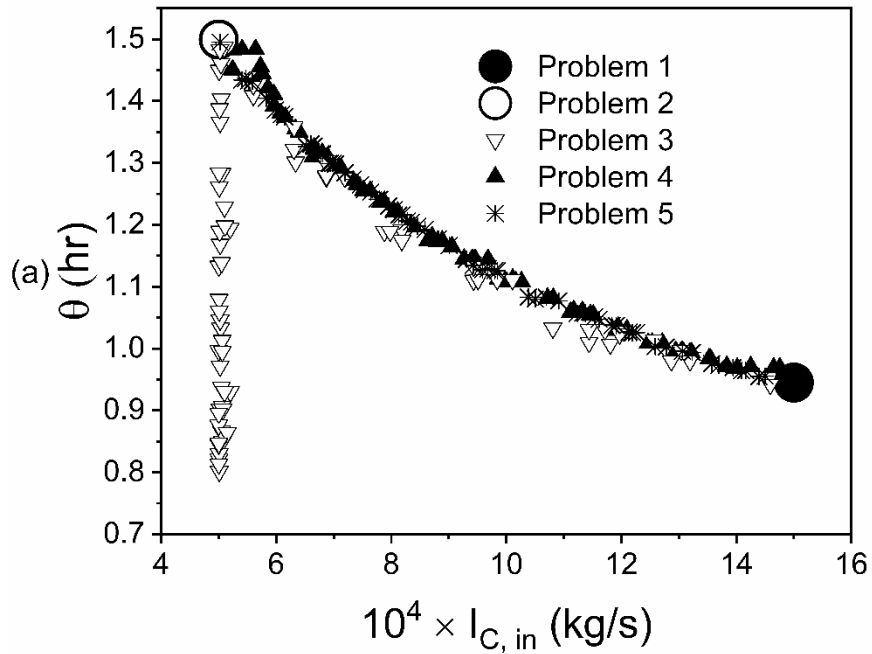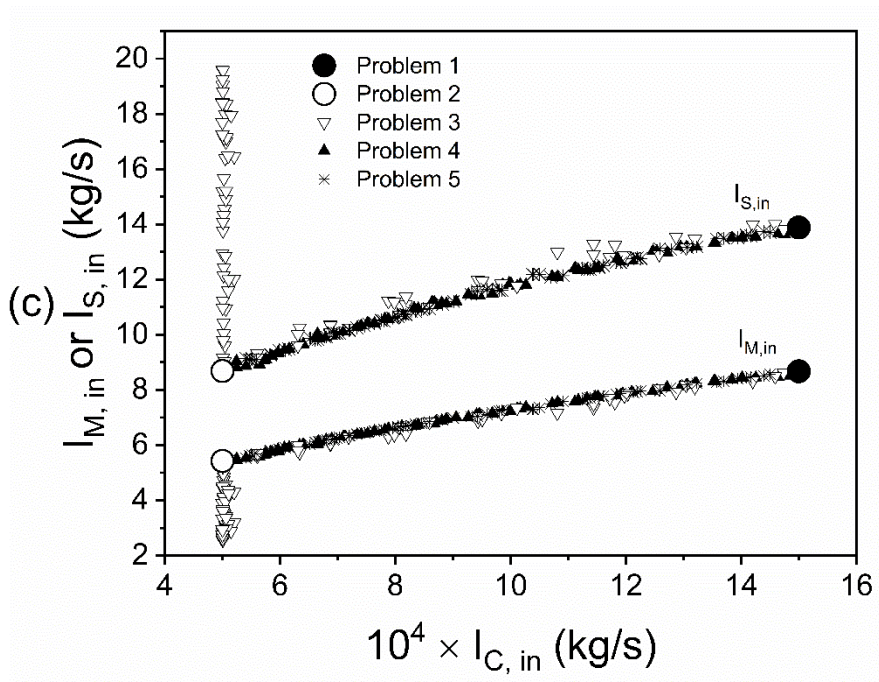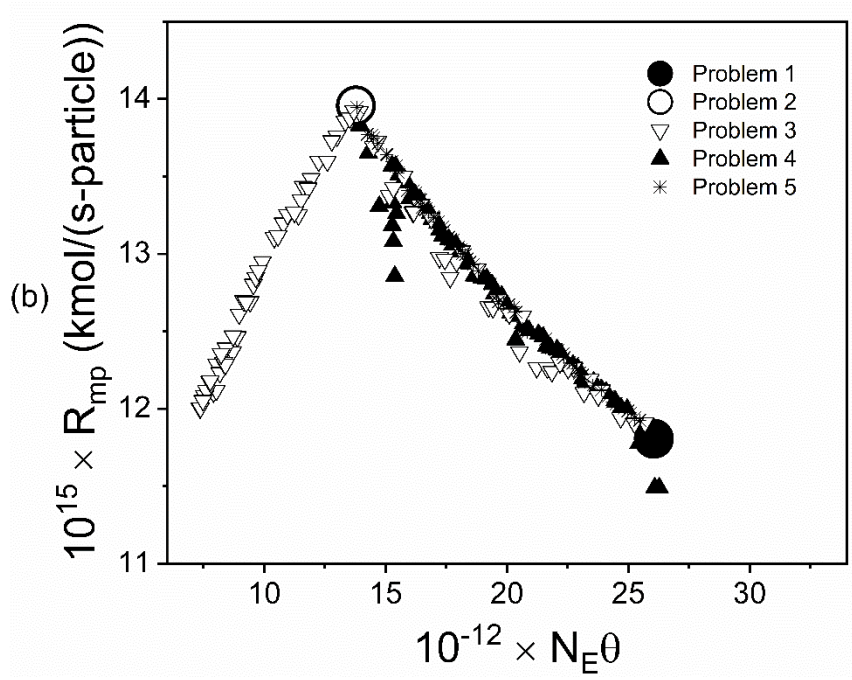
Fig. 5. 11 The converged optimal solutions of problems 1 to 5 (a) θ vs $I_{C,in}$ (b) R_{mp} vs $N_E \theta$ (c) $I_{M,in}$, $I_{S,in}$ vs $I_{C,in}$ (d) $I_{S,in} / I_{M,in}$ vs $I_{C,in}$ (e) D_{mp} vs $I_{C,in}$

103

It is observed in Figure 5.10 (a) that the optimal value of R_{poly} increases with an increase in the value of $N_E\theta$. Whereas, the optimal value of R_{mp} first increases with an increase in the value $N_E\theta$ reaches maxima and then decreases with an increase in the value of $N_E\theta$ (Figure 5.11 b). This is because the increase in the value of R_{mp} is due to an increase in the value of θ at the constant value of $I_{C,in}$ (controlled by its lower bound) (Figure 5.11 a). The corresponding optimal values of $\theta, I_{M,in}$, $I_{S,in}$, $I_{S,in}/I_{M,in}$, D_{mp} and $I_{C,in}$ are shown in Figures 5.11 (a-e). The available data on the industrial HDPE slurry reactor indicates that for a given value of $I_{C,in}$ the reactor is not operated below a particular value of θ. The HDPE slurry reactor is also not operated at a very high value of the ratio, $I_{S,in}/I_{M,in}$. A very high value of this ratio leads to a low monomer concentration in the liquid phase which affects the overall rate and yield. This is also evident from the unrealistic optimal solutions of $I_{M,in}$, $I_{S,in}$ and the ratio, $I_{S,in}/I_{M,in}$, for problem 3 in Figures 5.11(c) and 5.11(d), respectively. This indicates that the minimization of $N_E\theta$ as objective in problem 3 leads to the infeasible optimal operating conditions for the lower values of $N_E\theta$. Therefore, the minimization of $I_{C,in}$ and maximization of R_{mp} are considered as the conflicting objectives to the maximization of R_{poly} in problem 4 and problem 5, respectively.

It is observed in Figures 5.10 and 5.11 that the solution of MOO problems 4 and 5 results in similar optimal solutions of objectives and decision variables. It is also observed that some optimal solutions of problem 4 (Figures 5.10 (c) and 5.11 (b)) are not consistent with the trend observed in other problems. Thus, problem 5 is the most appropriate choice of conflicting objectives out of the three MOO problems and provides a whole range of the set of optimal solutions.

5.4.1 EFFECT OF ETHYLENE PARTIAL PRESSURE

To understand the effect of variation of ethylene partial pressure, p_{et}, on objectives and decision variables the upper bound of the p_{et} is varied. As discussed above, the optimal value of p_{et} is obtained at its upper bound (0.9 bar) for problems 1 to 5. Figure 5.12 shows the effect of variation of p_{et} on the optimal set of solutions of problem 5. It is observed in Figure 5.12 (a) that, a decrease in the value of p_{et} results in the decrease in the optimal value of R_{poly} for a given value of $I_{C,in}$. This is because a low value of p_{et} corresponds to a low value of the monomer concentration in the liquid phase and inside the macroparticles. A low value of monomer concentration inside the macroparticle lowers the optimal value of R_{poly}.

The corresponding optimal values of θ are also shown in figure 5.12 (b). A decrease in the value of p_{et} leads to the decrease in the monomer concentration inside the macroparticle and therefore, the particle has to stay for a longer time inside the reactor to obtain the maximum rate of polymerization, R_{poly}, for a given value of $I_{C,in}$.
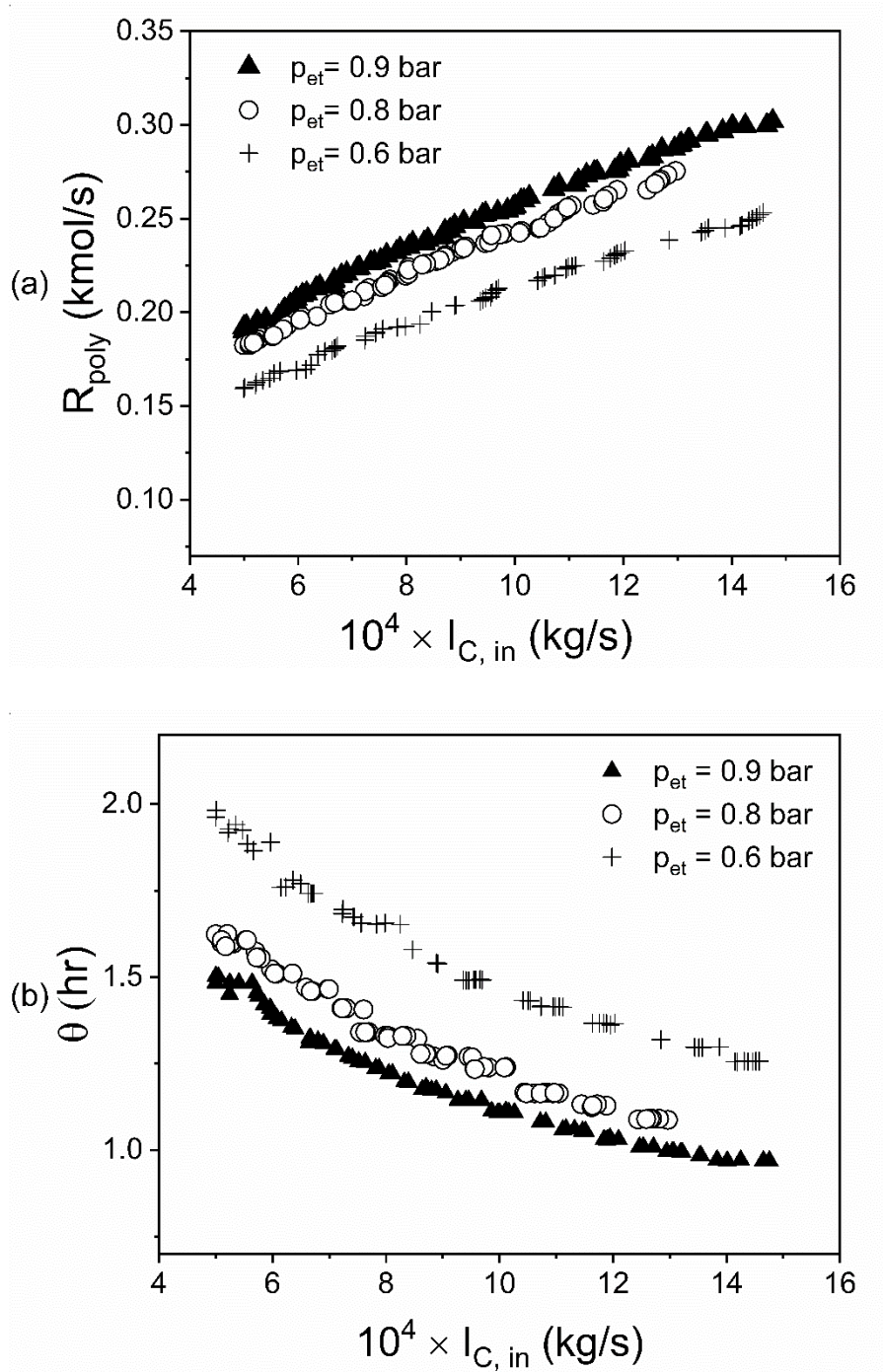
Fig. 5. 12 Effect of p_{et} on (a) R_{poly} vs $I_{C,in}$ (b) θ vs $I_{C,in}$

106

CHAPTER 6

CONCLUSIONS

Polyethylene is an important polymeric material due to its increasing presence in day-to-day life and industrial use. Slurry processes are most widely used for the production of polyethylene due to their several advantages over other processes. In this thesis, we have discussed the slurry phase ethylene polymerization processes and reviewed the mathematical modeling and simulation approaches at multi-scale levels. These are discussed to provide a foundation and framework to develop new models or to improve existing ones.

It has been shown that several advances have been made in modeling at specific scales, but the development of a complete and computationally efficient multiscale mathematical model is still an open challenge. The kinetic model at the microscale level is the most essential component of any modeling work on catalytic olefin polymerization. A framework of kinetic modeling including *all* essential elementary steps has been presented. The level of complexity in a kinetic model is linked to the required computational effort to estimate a large number of kinetic parameters. The lumped active site model can reduce the number of kinetic parameters to some extent. A simplified kinetic model is proposed which can be used to implement the mathematical model at the multiscale level. The single-particle models at the mesoscale level are used to obtain the rate of polymerization, polymer yield, polymer properties, and intraparticle concentration and temperature gradients. Although the existing models are quite successful in predicting the conditions of industrial interest, their strengths and shortcomings must be clearly understood during their implementation.

It is a big challenge to develop and implement a multiscale model which requires lower amounts of time for the simulation of industrial reactors without

compromising much with the accuracy in its prediction capability. The computational time for the simulation of industrial reactors using a multiscale model can be reduced by supplying only the required information at every scale during its simulation. Considerable effort is required to develop efficient algorithms for the simulation of industrial reactors using existing mathematical models.

A mathematical model can also be used as an effective tool for process optimization studies. Performing multi-objective optimization (MOO) using a state-of-art algorithm is a computationally rigorous activity. Thus, the time consumed in simulation is extremely crucial for solving MOO problems. To build such a model which can be used for MOO studies, one has to make a trade-off between the computational complexity and the accuracy.

A computationally efficient model has been developed for an isothermal *industrial* HDPE CSTR using a simplified kinetic model, diffusion, interphase mass transfer aspects and an overall mass balance. The PMGM is modified to be used for a given particle size of catalyst instead of using an average radius of microparticle after disintegration. This is used to model the phenomena of catalyst disintegration, monomer diffusion and macroparticle growth. The tuned reactor model using a 'training' set of the data from an industrial reactor shows a good agreement on the 'validation' set. The tuned reactor-model shows that it is more sensitive to variations in the diffusivity, D_1, compared to the kinetic parameter, k_P. Although the present model has been developed for catalytic polymerization in a single, isothermal, slurry CSTR, it can be extended to slurry-phase series of CSTRs and loop reactors for olefin polymerization with minor modifications. The advantage of a low computation time to solve this model can be exploited for further studies in process optimization.

The analysis of the tuned reactor model gives an insight to a plant-operator that the overall rate of production (R_{poly}) can be increased by increasing either θ or $I_{C,in}$. However, both the polymer production rate per catalyst particle (R_{mp}) and the polymer yield (D_{mp}) decrease with an increase in $I_{C,in}$ at a constant value of θ. The

polymer yield could be improved by increasing the reactor residence time but at the cost of compromising the operational safety as well as the value of $\overline{PDI}$. The present model also suggests that a maximum value of the polymer production rate per catalyst particle is obtained by maintaining a certain residence time. This residence time can be reduced by increasing the catalyst flow rate. Simulation results show that both the number average molecular weight and the weight average molecular weight are inversely proportional to the square root of the hydrogen concentration.

The SOO studies indicate that the maximum value of the overall rate of polymerization and yield is obtained at the maximum and minimum values of the catalyst feed rate, respectively. The MOO problems consist of conflicting objectives, maximization of the overall rate of polymerization, yield, and minimization of the catalyst feed rate. The minimization of the catalyst feed rate and the maximization of yields are observed to be the same objectives and give similar optimal solutions. The solution of MOO problems indicates the optimal value of R_{poly} increases with an increase in the value of $N_E\theta$ or $I_{C,in}$. Whereas, the optimal value of R_{mp} decreases with an increase in the value of $N_E\theta$ or $I_{C,in}$ in the feasible region of reactor operation.

6.1 FUTURE WORK

To reduce the computational time, this work employed a simplified kinetic model with a single-site non-deactivating catalyst. The reactor model developed in this study was mainly focused on the prediction of the rate of polymerization and at the industrial scale. The prediction of broad MWD requires the use of multiple active sites in the kinetic model. This study needs to be extended to devise a more efficient simulation algorithm that requires less computational time for the use of multiple active sites in the kinetic model. This will also help in the consideration of the MWD or PDI of the final product as an objective in the MOO study. The model

can be further extended to series of CSTRs to predict the rate of polymerization, yield, and MWD at the industrial scale.

REFERENCES

1. Global Polyolefin Market (2020) Trends, share, size, analysis 2018-2026. https://www.inkwoodresearch.com/reports/polyolefin-market/#report-summary. (Accessed 18 Mar 2020).

2. Polyolefins Market (20202). Size, share, outlook, forecast & industry report 2023. https://www.marketresearchfuture.com/reports/polyolefins-market-2949. (Accessed 18 Mar 2020).

3. Chum, P.S. and Swogger, K.W. (2008) Olefin polymer technologies-history and recent progress at the Dow Chemical Company. Prog. Polym. Sci., vol. 33, no. 8, pp. 797–819.

4. Xie, T., McAuley, K.B., Hsu J.C.C. and Bacon, D.W. (1994) Gas phase ethylene polymerization: production processes, polymer properties, and reactor modeling. Ind. Eng. Chem. Res., vol. 33, no. 3, pp. 449–479.

5. Reginato, A.S., Zacca. J.J. and Secchi, A.R. (2003) Modeling and simulation of propylene polymerization in nonideal loop reactors. AIChE J., vol. 49, no. 10, pp. 2642–2654.

6. Touloupides, V., Kanellopoulos, V., Pladis, P., Kiparissides, C., Mignon, D. and Van-Grambezen, P. (2010) Modeling and simulation of an industrial slurry-phase catalytic olefin polymerization reactor series. Chem. Eng. Sci., vol. 65, no. 10, pp. 3208–3222.

7. Dengfei ,W., Guoxing, Y., Feng, G., Guo, F., Wang, J. and Jiang, Y. (2018) Progress in technology and catalysts for continuous stirred tank reactor type slurry phase polyethylene processes. Pet. Chem., vol. 58, no. 3, pp. 264–273.

8. Zhou, Y., Zhang, R., Ren, H., He, X., Liu, B., Zhao, N. and Liu B. (2020)

Ethylene polymerization over novel organic magnesium based V/Ti bimetallic Ziegler-Natta catalysts. J. Organomet. Chem., vol. 908, p. 121066.

9.   Sau, M. and Gupta, S.K. (1993) Modelling of a semibatch polypropylene slurry reactor. Polymer, vol. 34, no. 21, pp. 4417–4426.

10.   Smith, M. (2005) Chevron Phillips slurry-loop-reactor process for polymerizing linear polyethylene. In: Meyers, R.A. (Ed.) Handbook of petrochemicals production processes. Mc-Graw Hill Education.

11.   McKenna, T.F. and Soares, J.B.P. (2001) Single particle modelling for olefin polymerization on supported catalysts: a review and proposals for future developments. Chem. Eng. Sci., vol. 56, no. 13, pp. 3931–3949.

12.   Daftaribesheli, M. (2009) Comparison of catalytic ethylene polymerization in slurry and gas phase, Ph.D. thesis, The Netherlands, University of Twente.

13.   Chen, X., Shao, Z., Gu, X., Feng, L. and Beigler L.T. (2019) Process intensification of polymerization processes with embedded molecular weight distributions models: an advanced optimization approach. Ind. Eng. Chem. Res., vol. 58, no. 15, pp. 6133–6145.

14.   Burdett, I.D. and Eisinger, R.S. (2017) Ethylene polymerization processes and manufacturing of polyethylene. In: Spalding, M.A. and Chatterjee, A.M. (Ed.). Handbook of industrial polyethylene and technology, definitive guide to manufacturing, properties, processing, applications and markets. Wiley, Scrivener Publishing, pp. 62–94.

15.   Zacca, J.J. and Ray, W.H. (1993) Modelling of the liquid phase polymerization of olefins in loop reactors. Chem. Eng. Sci., vol. 48, no. 22, pp. 3743–3765.

16.   Pontes, K.V., Cavalcanti, M., Filho, R.M. and Embiruçu, M. (2010) Modeling and simulation of ethylene and 1-butene copolymerization in solution with a ziegler-natta catalyst. Int. J. Chem. React. Eng., vol. 8, no. 1.

17. Fontes, C.H. and Mendes, M.J. (2005) Analysis of an industrial continuous slurry reactor for ethylene-butene copolymerization. Polymer, vol. 46, no. 9, pp. 2922–2932.

18. Ray, W.H. (1991) Modelling of addition polymerization processes — free radical, ionic, group transfer, and Ziegler–Natta kinetics. Can. J. Chem. Eng., vol. 69, no. 3, pp. 626–629, 1991.

19. Kiparissides, C. (1996) Polymerization reactor modeling: A review of recent developments and future directions. Chem. Eng. Sci., vol. 51, no. 10, pp. 1637–1659.

20. Kulkarni, S., Mishra, V. and Bontu, N.M. (2019) A comprehensive model for the micro and meso-scale level olefin polymerization: framework and predictions. Iran. Polym. J., vol. 28, no. 7, pp. 597–609.

21. Soni, N.J. and Bhagwat, S.S. (2008) Simulation of slurry polymerization of ethylene. Int. J. Chem. React. Eng., vol. 6, no. 1, A107.

22. Bhagwat, M.S., Bhagwat, S. S., and Sharma, M. M. (1994) Mathematical modeling of the slurry polymerization of ethylene: gas-liquid mass transfer limitations. Ind. Eng. Chem. Res., vol. 33, no. 10, pp. 2322–2330.

23. Ha, K., Yoo, K. and Rhee, H. (2001) Modeling and analysis of a slurry reactor system for heterogeneous olefin polymerization : the effects of hydrogen concentration and initial catalyst size. J. Appl. Polym. Sci., vol. 79, no. 13, pp. 2480–2493.

24. Sarkar, P. and Gupta, S. K. (1991) Modelling of propylene polymerization in an isothermal slurry reactor. Polymer, vol. 32, no. 15, pp. 2842–2852.

25. P. Sarkar and S. K. Gupta, (1992) Simulation of propylene polymerization: an efficient algorithm. Polymer, vol. 33, no. 7, pp. 1477–1485.

26. Casalini, T., Visscher, F., Tamaddoni, M., Friederichs, N., Bertola, F., Storti, G. and Morbidelli, M. (2018) The effect of residence time distribution on the

slurry-phase catalytic ethylene polymerization: an experimental and computational study. Macromol. React. Eng., vol. 12, no. 3, p. 1700058.

27.   Sarkar, P. and Gupta, S.K. (1992) Steady state simulation of continuous-flow stirred-tank slurry propylene polymerization reactors. Polym. Eng. Sci., vol. 32, no. 11, pp. 732–742.

28.   Soares, J.B.P. and McKenna T.F.L. (2012) Polyolefin reaction engineering. Wiley, Weinheim.

29.   Alizadeh, A. and McKenna T.F.L. (2017) Particle growth during the polymerization of olefins on supported catalysts. part 2: current experimental understanding and modeling progresses on particle fragmentation, growth, and morphology development. Macromol. React. Eng., vol. 12, no. 1, p. 1700027.

30.   Hock, C. W. (1966) How ticl3 catalysts control the texture of as-polymerized polypropylene. J. Polym. Sci. Part A-1 Polym. Chem., vol. 4, no. 12, pp. 3055–3064.

31.   Buls, V.W. and Higgins, T.L. (1970) A particle growth theory for heterogeneous Ziegler polymerization. J. Polym. Sci. Part A-1 Polym. Chem., vol. 8, no. 5, pp. 1037–1053.

32.   Boor, J.J. (1979) Ziegler–Natta catalysts polymerizations. Academic, New york, 1979.

33.   Wilchinsky, Z.W., Looney, R.W. and Tornqvist, E.G.M. (1973) Dependence of polymerization activity on particle and crystallite dimensions in ball milled TiCl3 and TiCl3 · 0.33AlCl3 catalyst components. J. Catal., vol. 28, no. 3, pp. 351–367.

34.   Noristi, L., Marchetti, E., Baruzzi, G. and Sgarzi, P. (1994) Investigation on the particle growth mechanism in propylene polymerization with MgCl2-supported Ziegler–Natta catalysts. J. Polym. Sci. Part A Polym. Chem., vol.

32, no. 16, pp. 3047–3059.

35. McDaniel, M.P. (1981) Fracturing silica-based catalysts during ethylene polymerization. J. Polym. J. Polym. Sci. Polym. Chem. Ed., vol. 19, no. 8, pp. 1967–1976.

36. Weist, E.L., Ali, A.H., Naik, B.G. and Conner, W.C. (1989). Morphological study of supported chromium polymerization catalysts. 2. initial stages of polymerization. Macromolecules, vol. 22, no. 8, pp. 3244–3250.

37. Neto A. G. M, and Pinto, J. C. (2001) Steady-state modeling of slurry and bulk propylene polymerizations. Chem. Eng. Sci., vol. 56, no. 13, pp. 4043–4057.

38. Khare, N.P., Seavey, K.C., Liu, Y.A., Ramanathan, S., Lingard, S. and Chen, C.C. (2002) Steady-state and dynamic modeling of commercial slurry high-density polyethylene (HDPE) processes. Ind. Eng. Chem. Res., vol. 41, no. 23, pp. 5601–5618.

39. Krallis, A., Kanellopoulos, V. and Ali M.A.H. (2015) Comprehensive study of reactants depletion in catalytic olefin polymerization industrial loop reactors. Ind. Eng. Chem. Res., vol. 54, no. 33, pp. 8247–8254.

40. Kissin, Y.V., Mink, R.I., Nowlin, T.E. and Brandolini, A.J. (1999) Kinetics and mechanism of ethylene homopolymerization and copolymerization reactions with heterogeneous Ti-based Ziegler–Natta catalysts. Top. Catal., vol. 7, no. 1/4, pp. 69–88.

41. Kissin, Y.V. (2001) Main kinetic features of ethylene polymerization reactions with heterogeneous Ziegler-Natta catalysts in the light of a multicenter reaction mechanism. J. Polym. Sci. Part A Polym. Chem., vol. 39, no. 10, pp. 1681–1695.

42. Pladis, P., Baltsas, A., Meimaroglou, D. and Kiparissides, C. (2018) A dynamic simulator for slurry-phase catalytic olefin copolymerization in a

series of cstrs: prediction of distributed molecular and rheological properties. Macromol. React. Eng., vol. 12, no. 4, p. 1800017.

43.   Neto, A.G.M., Freitas, M.F., Nele M. and Pinto, J.C. (2005) Modeling ethylene/1-butene copolymerizations in industrial slurry reactors. Ind. Eng. Chem. Res., vol. 44, no. 8, pp. 2697–2715.

44.   Wu, L., Bu, N. and Wanke, S.E. (2005) Kinetic behavior of ethylene/1-hexene copolymerization in slurry and solution reactors. J. Polym. Sci. Part A Polym. Chem., vol. 43, no. 11, pp. 2248–2257.

45.   Weijuan, M., Jianwei, L.I., Biaohua, C. and Hongbo, L.I. (2013) Modeling and simulation of ethylene polymerization in industrial slurry reactor series. Chinese J. Chem. Eng. vol. 21, no. 8, pp. 850–859.

46.   Chakravarti, S. and Ray, W.H. (2001). Kinetic study of olefin polymerization with a supported metallocene catalyst. II. Ethylene/1-hexene copolymerization in gas phase. J. Appl. Polym. Sci., vol. 80, no. 8, pp. 1096–1119.

47.   Thompson, D.E., McAuley, K.B. and McLellan, P.J. (2007) A simplified model for prediction of molecular weight distributions in ethylene-hexene copolymerization using Ziegler-Natta catalysts. Macromol. React. Eng., vol. 1, no. 5, pp. 523–536.

48.   McAuley, K.B., MacGregor, J. F., and Hamielec, A. E. (1990) A kinetic model for industrial gas-phase ethylene copolymerization," AIChE J., vol. 36, no. 6, pp. 837–850.

49.   Touloupides, V., Kanellopoulos, V., Krallis, A., Prokopis, P.P. and Kiparissides, C. (2010) Modeling and simulation of particle size distribution in slurry-phase olefin catalytic polymerization industrial loop reactors. Comput. Aided. Chem. Eng. vol. 28, no. C, pp. 43–48.

50.   Soares, J.B.P. and Romero, J. (2017) A Monte Carlo method to quantify the

116

effect of reactor residence time distribution on polyolefins made with heterogeneous catalysts: part i-catalyst/polymer particle size distribution effects. Macromol. React. Eng. vol. 12, no. 1., 1700031

51.   Casalini, T., Visscher, F., Janssen, E., Bertola, F., Storti, G. and Morbidelli, M. (2016) Modeling of polyolefin polymerization in semibatch slurry reactors: experiments and simulations. Macromol. React. Eng. vol. 11, no. 1, pp. 1–19.

52.   Zakharov, V., Matsko, M., Echevskaya, L. and Mikenas, T. (2007) Ethylene polymerization over supported titanium-magnesium catalysts: heterogeneity of active centers and effect of catalyst composition on the molecular mass distribution of polymer. Macromol. Symp. vol. 260, no. 1, pp. 184–188.

53.   Wang, Q., Murayama, N., Liu, B. and Terano, M. (2005) Effects of electron donors on active sites distribution of MgCl2-supported Ziegler-Natta catalysts investigated by multiple active sites model. Macromol. Chem. Phys.   vol. 206, no. 9, pp. 961–966.

54.   Gemoets, F., Zhang, M., Karjala, T.W. and Kolthammer, B.W.S. (2010) Kinetic study of ethylene homopolymerization in slurry using a Ziegler-Natta catalyst. Macromol. React. Eng. vol. 4, no. 2, pp. 109–122, 2010, doi: 10.1002/mren.200900055.

55.   Thakur, A.K., Gupta, S.K. and Chaudhari, P. (2020) Modeling and simulation of an industrial slurry phase ethylene polymerization reactor: effect of reactor operating variables. Iran. Polym. J. vol. 29, no. 9, pp. 811–825.

56.   Chaudhari, P. and Gupta S.K. (2012) Multiobjective optimization of a fixed bed maleic anhydride reactor using an improved biomimetic adaptation of NSGA-II. Ind. Eng. Chem. Res. vol. 51, no. 8, pp. 3279–3294.

57.   Chaudhari, P. and Garg, S. (2019) Multi-objective optimization of maleic anhydride circulating fluidized bed (CFB) reactors. Chem. Eng. Res. Des.

vol. 141, pp. 115–132, Jan. 2019, doi: 10.1016/j.cherd.2018.10.020.

58.   Chen, C. (2018) Designing catalysts for olefin polymerization and copolymerization: beyond electronic and steric tuning. Nat. Rev. Chem. vol. 2, no. 5, pp. 6–14.

59.   Touloupidis, V. (2014) Catalytic olefin polymerization process modeling: Multi-scale approach and modeling guidelines for micro-scale/kinetic modeling. Macromol. React. Eng. vol. 8, no. 7, pp. 508–527.

60.   Jäntschi, L., Bálint, D. and Bolboaca, S.D. (2016) Multiple linear regressions by maximizing the likelihood under assumption of generalized gauss-laplace distribution of the error. Comput. Math. Methods. Med. 8578156.

61.   Sirohi, A. and Choi, K.Y. (1996) On-line parameter estimation in a continuous polymerization process. Ind. Eng. Chem. Res. vol. 35, no. 4, pp. 1332–1343.

62.   Kemeny, S., Manczinger, J., Skjold-Jørgensen, S. and Toth, K. (1982) Reduction of thermodynamic data by means of the multiresponse maximum likelihood principle. AIChE J., vol. 28, no. 1, pp. 20–30.

63.   Ramteke, M. and Gupta, S.K. (2011) Kinetic modeling and reactor simulation and optimization of industrially important polymerization processes: a perspective. Int. J. Chem. React. Eng. vol. 9, no. 1.

64.   Choi, K.Y., Tang, S. and Sirohi, A. (1997) Estimation of kinetic parameters in transition-metal-catalyzed gas-phase olefin copolymerization processes. Ind. Eng. Chem. Res. vol. 36, no. 4, pp. 1095–1102.

65.   Matos, V., Moreira, M., Neto, A.G.M., Nele, M., Melo, P.A. and Pinto J.C. (2007) Method for quantitative evaluation of kinetic constants in olefin polymerizations, 3 kinetic study of the hipp synthesis. Macromol. React. Eng. vol. 1, no. 1, pp. 137–159.

66.   Khare, N.P., Lucas, B., Seavey, K.C., Liu, Y. A., Sirohi, A., Ramanathan,

S., Lingard, S., Song, Y. and Chen, C.C. (2004) Steady-state and dynamic modeling of gas-phase polypropylene processes using stirred-bed reactors. Ind. Eng. Chem. Res. vol. 43, no. 4, pp. 884–900.

67. Embiruçu, M., Prata, D.M., Lima, E.L. and Pinto, J.C. (2008) Continuous soluble Ziegler-Natta ethylene polymerizations in reactor trains, 2 - estimation of kinetic parameters from industrial data. Macromol. React. Eng. vol. 2, no. 2, pp. 142–160.

68. Nanthapoolsub, U., Anantawaraskul, S. and Saengkhamkhom, K. (2013) Simultaneous deconvolution of mwd and ccd of ethylene/1-olefin copolymers using genetic algorithm. Macromol. Symp. vol. 330, no. 1, pp. 142–149.

69. Salas, S.D., Brandão, A.L.T., Soares, J.B.P. and Romagnoli, J.A. (2019) Data-driven estimation of significant kinetic parameters applied to the synthesis of polyolefins. Processes vol. 7, no. 5, p. 309.

70. Touloupidis, V., Albrecht, A. and Soares, J.B.P. (2018) A methodology for estimating kinetic parameters and reactivity ratios of multi-site type catalysts using polymerization, fractionation, and spectroscopic techniques. Macromol. React. Eng. vol. 12, no. 2, p. 1700056.

71. Ray, W.H. (1972) On the mathematical modeling of polymerization reactors. J. Macromol. Sci. Part C, vol. 8, no. 1, pp. 1–56.

72. Hamielec, A.E., MacGregor, J.F. and Penlidis, A. (1987) Multicomponent free-radical polymerization in batch, semi- batch and continuous reactors. Makromol. Chemie. Macromol. Symp. vol. 10–11, no. 1, pp. 521–570.

73. Dubé, M.A., Soares, J.B.P., Penlidis, A. and Hamielec, A.E. (1997) Mathematical modeling of multicomponent chain-growth polymerizations in batch, semibatch, and continuous reactors: a review. Ind. Eng. Chem. Res. vol. 36, pp. 966–1015.

74. Mantzaris, N.V., Kelley, A.S., Daoutidis, P. and Srienc, F. (2002) A population balance model describing the dynamics of molecular weight distributions and the structure of PHA copolymer chains. Chem. Eng. Sci. vol. 57, no. 21, pp. 4643–4663.

75. Soares, J.B.P. (2001) Mathematical modelling of the microstructure of polyolefins made by coordination polymerization: A review. Chem. Eng. Sci. vol. 56, no. 13, pp. 4131–4153.

76. Flory, P.J. (1953) Principles of polymer chemistry. Cornell University Press, Ithaca, NY.

77. Laurence, R.L. and Chiovetta, M.G. (1983) Heat and mass transfer during olefin polymerization from the gas phase. In: Reichert, K.H. and Geisler, W. (Ed.), Polymer reaction engineering: infuence of reaction engineering on polymer properties. Munich: Hanser, pp. 74–111.

78. Chiovetta, M.G. (1983) Heat and mass transfer during the polymerization of alpha-olefins from the gas phase. University of Massachusetts at Amhurst.

79. Ferrero, M.A. and Chiovetta, M.G. (1987) Catalyst fragmentation during propylene polymerization: part ii. microparticle diffusion and reaction effects. Polym. Eng. Sci. vol. 27, no. 19, pp. 1448–1460.

80. Ferrero, M.A. and Chiovetta, M.G. (1987) Catalyst fragmentation during propylene polymerization: part i. the effects of grain size and structure. Polym. Eng. Sci. vol. 27, no. 19, pp. 1436–1447.

81. Estenoz, D.A. and Chiovetta, M.G. (1996) A structural model for the catalytic polymerization of ethylene using chromium catalysts. part i: description and solution. Polym. Eng. Sci. vol. 36, no. 17, pp. 2208–2228.

82. Estenoz, D.A. and Chiovetta, M.G. (1996) A structural model for the catalytic polymerization of ethylene using chromium catalysts. part ii: thermal effects. Polym. Eng. Sci. vol. 36, no. 17, pp. 2229–2240.

83. Grof, Z., Kosek, J., Marek, M. and Adler, P.M. (2003) Modeling of morphogenesis of polyolefin particles: catalyst fragmentation. AIChE. J. vol. 49, no. 4, pp. 1002–1013.

84. Horáčková, B., Grof, Z. and Kosek, J. (2007) Dynamics of fragmentation of catalyst carriers in catalytic polymerization of olefins. Chem. Eng. Sci. vol. 62, no. 18–20, pp. 5264–5270.

85. Najafi, M., Parvazinia M. and Ghoreishy, M.H.R. (2014) Modelling the catalyst fragmentation pattern in relation to molecular properties and particle overheating in olefin polymerization. Polyolefins Journals. vol. 1, no. 2, pp. 77–91.

86. Najafi, M., Parvazinia, M. (2015) Computational modeling of particle fragmentation in the heterogeneous olefin polymerization. Macromol. Theory Simulations. vol. 24, no. 1, pp. 28–40.

87. Soares, J.B.P. and Hamielec, A.E. (1995) Metallocene/Aluminoxane catalysts for olefin polymerization. a review. Polym. React. Eng. vol. 3, no. 2, pp. 131–200.

88. Soares, J.B.P. and Hamielec, A.E. (1995) General dynamic mathematical modelling of heterogeneous Ziegler-Natta and metallocene catalyzed copolymerization with multiple site types and mass and heat transfer resistances. Polym. React. Eng. vol. 3, no. 3, pp. 261–324.

89. Crabtree, J.R., Grimsby, F.N., Nummelin, A.J. and Sketchley, J.M. (1973) The role of diffusion in the Ziegler polymerization of ethylene. J. Appl. Polym. Sci. vol. 17, pp. 959–976.

90. Nagel, E.J., Kirillov, V.A. and Ray, W.H. (1980) Prediction of molecular weight distributions for high-density polyolefins. Ind. Eng. Chem. Prod. Res. Dev. vol. 19, no. 3, pp. 372–379.

91. Varshney, P., Kunzru, D. and Gupta, S.K. (2015) Modelling of the riser

reactor in a resid fluidised-bed catalytic cracking unit using a multigrain model for an active matrix-zeolite catalyst. Indian. Chem. Eng. vol. 57, no. 2, pp. 115–135.

92. Singh, D. and Merrill, R.P. (1971) Molecular weight distribution of polyethylene produced by Ziegler-Natta catalysts. Macromolecules vol. 4, no. 5, pp. 599–604.

93. Galvan, R. and Tirrell, M. (1986) Orthogonal collocation applied to analysis of heterogeneous Ziegler-Natta polymerization. Comput. Chem. Eng. vol. 10, no. 1, pp. 77–85.

94. Galvan, R. and Tirrell, M. (1986) Molecular weight distribution predictions for heterogeneous Ziegler-Natta polymerization using a two-site model. Chem. Eng. Sci. vol. 41, no. 9, pp. 2385–2393.

95. Kanellopoulos, V., Dompazis, G., Gustafsson, B. and Kiparissides, C. (2004) Comprehensive analysis of single-particle growth in heterogeneous olefin polymerization: the random-pore polymeric flow model. Ind. Eng. Chem. Res. vol. 43, no. 17, pp. 5166–5180.

96. Buls, V.W. and Higgins, T.L. (1970) A particle growth theory for heterogeneous Ziegler polymerization. J. Polym. Sci. Part A-1 Polym. Chem. vol. 8, pp. 1025–1035.

97. Weist, E.L., Ali, A.H., Naik, B.G. and Conner, W.C. (1989) Morphological study of supported chromium polymerization catalysts. 2. initial stages of polymerization. Macromolecules. vol. 22, no. 8, pp. 3244–3250.

98. Michaels, A.S. and Parker, R.B. (1959) Sorption and flow of gases in polyethylene. J. Polym. Sci. vol. 41, no. 138, pp. 53–71.

99. Michaels, A.S. and Bixler, H.J. (1961) Flow of gases through polyethylene. J. Polym. Sci.   vol. 50, no. 154, pp. 413–439.

100. Michaels, A.S. and Bixler, H.J. (1961) Solubility of gases in polyethylene.

J. Polym. Sci. vol. 50, no. 154, pp. 393–412.

101. Wakao, N. and Smith, J.M. (1964) Diffusion and reaction in porous catalysts. Ind. Eng. Chem. Fundam vol. 3, no. 2, pp. 123–127.

102. Kittilsen, P., McKenna T.F., Svendsen, H., Jakobsen, H.A. and Fredriksen, S.B. (2001) The interaction between mass transfer effects and morphology in heterogeneous olefin polymerization. Chem. Eng. Sci. vol. 56, no. 13, pp. 4015–4028.

103. Shi, D. P., Luo, Z. H. and Zheng, Z. W. (2010) Numerical simulation of liquid-solid two-phase flow in a tubular loop polymerization reactor. Powder Technol. vol. 198, no. 1, pp. 135–143.

104. Liu, P., Liu, W., Wang, W.J., Li, B.G. and Zhu, S. (2016) A comprehensive review on controlled synthesis of long-chain branched polyolefins: Part 1, Single catalyst systems. Macromol. React. Eng. vol. 10, no. 3, pp. 156–179.

105. Zhou, R., Chen J., Yang N., Jinghai, Li J., Fernandez, A. and Ricoux P. (2018) Modeling of complex liquid-solid flow of particle swelling in slurry loop reactors. Chem. Eng. Sci. vol. 176, pp. 476–490.

106. Gao, X., Shi, D.P., Chen, X.Z. and Luo, Z.H. (2010) Three-dimensional CFD model of the temperature field for a pilot-plant tubular loop polymerization reactor. Powder Technol. vol. 203, no. 3, pp. 574–590.

107. Alobaid, F., Ströhle, J. and Epple, B. (2013) Extended CFD/DEM model for the simulation of circulating fluidized bed. Adv. Powder Technol. vol. 24, no. 1, pp. 403–415.

108. Gidaspow, D. (2019) High production circulating fluidized bed polymerization reactors," Powder Technol., vol. 357, pp. 108–116.

109. Hui, P., Yuan-Xing, L. and Zheng-Hong, L. (2019) Computational fluid dynamics simulation of gas–liquid–solid polyethylene fluidized bed reactors incorporating with a dynamic polymerization kinetic model. Asia-Pac. J.

Chem. Eng. vol. 14, no. 1, p. e2265,

110. Schneiderbauer, S., Puttinger, S., Pirker, S., Aguayo, P. and Kanellopoulos, V. (2015) CFD modeling and simulation of industrial scale olefin polymerization fluidized bed reactors. Chem. Eng. J. vol. 264, pp. 99–112.

111. Khan, M.J.H., Hussain, M.A., Mansourpour, Z., Mostoufi, N., Ghasem, N.M. and Abdullah, E.C. (2014) CFD simulation of fluidized bed reactors for polyolefin production - a review. J. Ind. Eng. Chem. pp. 3919–3946.

112. Li, Y., Ma Y., Reddy R.K., Vijay S., Elovainio E., Wurnitsch C. and Nandakumar, K. (2015) CFD investigations of particle segregation and dispersion mechanisms inside a polyolefin 8-leg loop reactor of industrial scale. Powder Technol. vol. 284, pp. 95–111.

113. Li, Y., Yu, J., Reddy, R. K., Vijay, S., Elovainio, E., Wurnisch, C. and Nandakumar, K. (2017) Computational study on the effect of slug dynamics on the operation of a polyolefin 8-leg loop reactor of industrial scale. Powder Technol. vol. 319, pp. 452–462.

114. Wen, C. Y. and Yu, Y. H. (1966) Mechanics of fluidization. Chemical Engineering Progress, Symposium Series. vol. 62, no. 1, pp. 100–111.

115. Beetstra, R., Van Der Hoef, M. A. and Kuipers, J. A. M. (2007) Drag force of intermediate reynolds number flow past mono- and bidisperse arrays of spheres. AIChE J. vol. 53, no. 2, pp. 489–501.

116. Singh, P. P., Cushman, J. H. and Maier, D. E. (2003) Three scale thermomechanical theory for swelling biopolymeric systems. Chem. Eng. Sci. vol. 58, no. 17, pp. 4017–4035.

117. Lettieri, P., Renzo Di Felice, D.R., Pacciani, R. and Owoyemi O. (2006) CFD modelling of liquid fluidized beds in slugging mode. Powder Technol. vol. 167, no. 2, pp. 94–103.

118. Cornelissen, J. T., Fariborz, T., Escudiéa, R., Naoko, E. and John R. Grace

J.R. (2007) CFD modelling of a liquid-solid fluidized bed. Chem. Eng. Sci. vol. 62, no. 22, pp. 6334–6348.

119. Huang, X. (2011) CFD modeling of liquid-solid fluidization: effect of drag correlation and added mass force. Particuology, vol. 9, no. 4, pp. 441–445.

120. Yan, W. C., Luo, Z. H. and Guo, A. Y. (2011) Coupling of CFD with PBM for a pilot-plant tubular loop polymerization reactor. Chem. Eng. Sci. vol. 66, no. 21, pp. 5148–5163

121. Lu, R., Zhang, L., Philippe, Ricoux P. and Wang, L. (2019) Experiments and CFD-DEM simulations of cohesive particles sedimentation in stilled fluid. Powder Technol. vol. 356, pp. 222–230.

122. Kong, J. J., Eason, J. P., Chen, X. and Biegler, L.T. (2020) Operational optimization of polymerization reactors with computational fluid dynamics and embedded molecular weight distribution using the iterative surrogate model method. Ind. Eng. Chem. Res. vol. 59, no. 19, pp. 9165–9179.

123. Floyd, S., Hutchinson, R.A. and Ray, W.H. (1986) Polymerization of olefins through heterogeneous catalysis v. gas-liquid mass transfer limitations in liquid slurry reactors. J. Appl. Polym. Sci. vol. 32, pp. 5451–5479, 1986.

124. Naderpour, N., Vasheghani-farahani, E., Famili, M.H.N. and Vatankhah, M. (2010) Kinetics of slurry and gas phase polymerizations of ethylene using a novel heterogeneous Ziegler-Natta catalyst of specific morphology. Iran. Polym. J. vol. 19, no. 11, pp. 895–906.

125. Hutchinson, R.A. and Ray, W.H. (1990) Polymerization of olefins through heterogeneous catalysis. viii. monomer sorption effects. J. Appl. Polym. Sci. vol. 41, no. 1–2, pp. 51–81.

126. Zacca, J. J., Debling, J. A. and Ray, W. H. (1997) Reactor residence-time distribution effects on the multistage polymerization of olefins - II. Polymer properties: Bimodal polypropylene and linear low-density polyethylene.

Chem. Eng. Sci. vol. 52, no. 12, pp. 1941–1967.

127. Zacca, J. J., Debling, J. A. and Ray, W. H. (1996) Reactor residence time distribution effects on the multistage polymerization of olefins - I. Basic principles and illustrative examples, polypropylene," Chem. Eng. Sci., vol. 51, no. 21, pp. 4859–4886.

128. McCoy, J.T., Rawatlal, R. (2012) A more efficient simulator of particle size distribution in slurry phase polyolefin systems. Comput. Chem. Eng. vol. 36, no. 1, pp. 68–78.

129. Liu, B., Romero, J., Liu, B. and Soares, J. B. P. (2018) A monte carlo method to quantify the effect of reactor residence time distribution on polyolefins made with heterogeneous catalysts: part iii—particle composition distribution effects. Macromol. React. Eng., vol. 12, no. 6.

130. Luo, Z. H., Su, P. L., You, X. Z., Shi, D. P. and Wu, J. C. (2009) Steady-state particle size distribution modeling of polypropylene produced in tubular loop reactors. Chem. Eng. J., vol. 146, no. 3, pp. 466–476.

131. Che, Y., Tian, Z., Liu, Z., Zhang, R., Gao, Y., Zhou, E., Wang, S. and Liu, B. (2015) A CFD-PBM model considering ethylene polymerization for the flow behaviors and particle size distribution of polyethylene in a pilot-plant fluidized bed reactor. Powder Technol., vol. 286, pp. 107–123.

132. Calderbank, P. H. and Moo-Young, M. B. (1961) The continuous phase heat and mass-transfer properties of dispersions. Chem. Eng. Sci., vol. 16, no. 1–2, pp. 39–54.

133. Kawase, Y. and Hashiguchi, N. (1996) Gas-liquid mass transfer in external-loop airlift columns with newtonian and non-newtonian fluids. Chem. Eng. J. Biochem. Eng. J. vol. 62, no. 1, pp. 35–42.

134. Floyd, S., Choi, K.Y., Taylor, T.W. and Ray, W.H. (1986) Polymerization of olefins through heterogeneous catalysis iv. modeling of heat and mass

transfer resistance in the polymer particle boundary layer. J. Appl. Polym. Sci. vol. 31, pp. 2231–2265, 1986.

135. Treybal, R.E. (1980) Mass transfer operations. New York, McGraw-Hill.

136. Lamont, J.C. and Scott, D.S. (1970) An eddy cell model of mass transfer into the surface of a turbulent liquid. AIChE J. vol. 16, no. 4, pp. 513–519.

137. Gupta, S.K. (2019) Numerical methods for engineers, 4th ed. New Age International publishers.

138. Hutchinson, R.A., Chen, C.M. and Ray, W.H. (1992) Polymerization of olefins through heterogeneous catalysis x: modeling of particle growth and morphology. J. Appl. Polym. Sci. vol. 44, pp. 1389–1414.

139. Hoel, E.L., Cozewith, C. and Byrne, G.D. (1994) Effect of diffusion on heterogeneous ethylene propylene copolymerization. AIChE J. vol. 40, no. 10, pp. 1669–1684.

140. Yiagopoulos, A., Yiannoulakis, H., Dimos, V., Kiparissides, C. (2001) Heat and mass transfer phenomena during the early growth of a catalyst particle in gas-phase olefin polymerization: the effect of prepolymerization temperature and time. Chem. Eng. Sci. vol. 56, no. 13, pp. 3979–3995.

141. Veera, U.P., Weickert, G, and Agarwal, U.S. (2002) Modeling monomer transport by convection during olefin polymerization. AIChE J. vol. 48, no. 5, pp. 1062–1070.

142. Ali, D. and Ahmad, R. (2008) Modeling and simulation of olefin polymerization at microstructure level. Iran. J. Chem. Chem. Eng. vol. 27, no. 2, pp. 13–22.

143. Soni, N.J. and Bhagwat, S.S. (2008) Simulation of slurry polymerization of ethylene. Int. J. Chem. React. Eng. vol. 6, p. A107, 2008.

144. Luo, Z.H., Wen, S.H. and Zheng Z.W. (2009) Modeling the effect of

polymerization rate on the intraparticle mass and heat transfer during propylene polymerization in a loop reactor. J. Chem. Eng. Japan. vol. 42, no. 8, pp. 576–580.

145. Ray, A. K. and Gupta, S. K. (2003) Mathematical methods in chemical & environmental engineering. Thomson Learning.

146. Shamiri, A., Hussain, M.A., Mjalli, F.S., Mostoufi, N. and Shafeeyan, M.S. (2011) Dynamic modeling of gas phase propylene homopolymerization in fluidized bed reactors. Chem. Eng. Sci.vol. 66, no. 6, pp. 1189–1199.

147. Bohm, L. L., Goebel, P. and P. R. Schoneborn, P. R. (1990) Detailed reaction engineering as a basis of modern slurry technology for PE-HD-production. Die Angew. Makromol. Chemie, vol. 3310, no. 174, pp. 3291–3310.

148. Ahmadi, M., Nekoomanesh, M. and Arabi, H. (2010) A simplified comprehensive kinetic scheme for modeling of ethylene/1-butene copolymerization using ziegler-natta catalysts. Macromol. React. Eng. vol. 4, no. 2, pp. 135–144.

149. Nassiri, H., Arabi, H. and Hakim, S. (2012) Kinetic modeling of slurry propylene polymerization using a heterogeneous multi-site type Ziegler-Natta catalyst. React. Kinet. Mech. Catal. vol. 105, no. 2, pp. 345–359.

150. Abbasi, M.R., Shamiri, A. and Hussain, M.A. (2016) Dynamic modeling and Molecular Weight Distribution of ethylene copolymerization in an industrial gas-phase Fluidized-Bed Reactor. Adv. Powder Technol., vol. 27, no. 4, pp. 1526–1538.

151. Schmeal W. R. and Street, J. R. (1971) Polymerization in Expanding Catalyst Particles. AIChE J. vol. 17, no. 5, pp. 1188–1197.

152. Nouri, M., Parvazinia, M. and Arabi, H. (2015) Effect of fragment size distribution on reaction rate and molecular weight distribution in heterogeneous olefin polymerization. Iran. Polym. J. vol. 24, no. 6, pp. 437–

448.

153. Choi, K.Y. and Ray, W.H. (1985) Polymerization of olefins through heterogeneous catalysis. ii. kinetics of gas phase propylene polymerization with ziegler-natta cata1ysts. J. Appl. Polym. Sci. vol. 30, pp. 1065–1081.

154. Taylor, T. W., Choi, K. Y., Yuan, H., and Ray, W. H. (1981) Physicochemical kinetics of liquid phase propylene polymerization," in Transition metal catalyzed polymerizations : alkenes and dienes : Eleventh Macromolecular Meeting held at Midland, Michigan, August 17-21, 1981, pp. 191–223.

155. Debling, J.A. and Ray, W. H. (1995) Heat and mass transfer effects in multistage polymerization processes: impact polypropylene. Ind. Eng. Chem. Res. vol. 34, no. 10, pp. 3466–3480.

156. Han-Adebekun, G.C., Hamba, M. and W. H. Ray, W. H. (1997) Kinetic study of gas phase olefin polymerization with a TiCl4/MgCl2 catalyst I. Effect of polymerization conditions," J. Polym. Sci. Part A Polym. Chem., vol. 35, no. 10, pp. 2063–2074.

157. Floyd, S., Heiskanen, T., Taylor, T. W., Mann, G. E. and Ray, W. H. (1987) Polymerization of olefins through heterogeneous catalysis. VI. Effect of particle heat and mass transfer on polymerization behavior and polymer properties. J. Appl. Polym. Sci., vol. 33, no. 4, pp. 1021–1065.

158. Krajakova, L, Laskova, M., Chmelar, J. Jindrova, K. and Kosek, J. (2019) Sorption of liquid diluents in polyethylene: comprehensive experimental data for slurry polymerization. Ind. Eng. Chem. Res. vol. 58, no. 17, pp. 7037–7043.

159. Bhavaraju, S. M., Russell, T. W. F., and Blanch, H. W. (1978) The design of gas sparged devices for viscous liquid systems. AIChE J. vol. 24, no. 3, pp. 454–466.

160. Li, J., Tekie, Z., Mizan, T. I., Morsi, B. I., Maier, E. E. and Singh, C. P. P. (1996) Gas-liquid mass transfer in a slurry reactor operating under olefinic polymerization process conditions. Chem. Eng. Sci. vol. 51, no. 4, pp. 549–559.

161. Wilke, C. R. and Chang, P. (1955) Correlation of diffusion coefficients in dilute solutions. AIChE J. vol. 1, no. 2, pp. 264–270.

162. Rumble, J. R., Lide, D. R. and Bruno, T. J. (2019) CRC handbook of chemistry and physics, 100th ed. Taylor & Francis.

163. Yao, F. Z., Lohi, A., Upret, S. R. and Dhib, R. (2004) Modeling, simulation and optimal control of ethylene polymerization in non-isothermal, high-pressure tubular reactors. Int. J. Chem. React. Eng., vol. 2, A16.

164. Agrawal, N., Rangaiah, G. P., Ray, A. K. and Gupta, S. K. (2006) Multi-objective optimization of the operation of an industrial low-density polyethylene tubular reactor using genetic algorithm and its jumping gene adaptations. Ind. Eng. Chem. Res. vol. 60, no. 7, pp. 3182–3199.

165. Agrawal, N., Rangaiah, G. P., Ray, A. K. and Gupta, S. K. (2007) Design stage optimization of an industrial low-density polyethylene tubular reactor for multiple objectives using NSGA-II and its jumping gene adaptations. Chem. Eng. Sci., vol. 62, no. 9, pp. 2346–2365.

166. Mogilicharla, A., Majumdar, S. and Mitra, K. (2014) Modeling and optimization of propylene polymerization with branching. IFAC Proceedings. Vol. 47, no. 3, pp. 3992-3997.

167. Ye, Z. and Zhu, S. (2003) Synthesis of branched polypropylene with isotactic backbone and atactic side chains by binary iron and zirconium single-site catalysts. J. Polym. Sci. Part A Polym. Chem. vol. 41, no. 8, pp. 1152–1159.

168. Keii, T., Suzuki, E., Tamura, M. and Doi, Y. (1981) Transition metal

catayzed polymerization. in MMI Int. Symp. on transition metal catalyzed polymerization: unsolved problems, p. 37.

PUBLICATIONS FROM THIS THESIS

➢ Amit K. Thakur, Santosh K. Gupta, Pranava Chaudhari., Slurry-phase ethylene polymerization processes: a review on multiscale modeling and simulations, *Rev. Chem Eng.* **(2020)**. *(IF: 5.315)*.

➢ Amit K. Thakur, Santosh K. Gupta, P Chaudhari., Modeling and simulation of an industrial slurry phase ethylene polymerization reactor: effect of reactor operating variables, *Iran. Polm. J.* **(2020)**; 9: 811-825 *(IF: 1.707)*.

PLAGIARISM CERTIFICATE

1. We _____Dr. Pranava Chaudhari_____ (Internal Guide), Dr. Santosh K. Gupta (Co Guide/ ~~External Guide~~) certify that the Thesis titled

    Modeling and Multi Objective Optimization of an Industrial High Density Polyethylene Slurry Reactor

    _____

    submitted by Scholar Mr/ ~~Ms~~_____Amit Kumar Thakur_____having SAP ID

    __500042449_____has been run through a Plagiarism Check Software and the Plagiarism Percentage is reported to be _____01_%.

2. Plagiarism Report generated by the Plagiarism Software is attached .

_____

Signature of the Internal Guide

Dr. Pranava Chaudhari

_____

Signature of ~~External Guide~~/ Co Guide

Dr. Santosh K. Gupta

_____ 24/05/2021

Signature of the Scholar

Amit Kumar Thakur

Curiginal

Document Information

Analyzed document	Thesis _Revision_23 May 2021.pdf (D106093541)
Submitted	5/23/2021 10:44:00 AM
Submitted by	Amit
Submitter email	akthakur@ddn.upes.ac.in
Similarity	1%
Analysis address	akthakur.upes@analysis.urkund.com

Sources included in the report

W   URL: https://www.researchgate.net/profile/Doufnoune_Rachida2/post/How_to_computationall ...
Fetched: 2/28/2021 5:58:25 AM   ⊞   1

W   URL: https://www.researchgate.net/publication/229395106_Modeling_and_simulation_of_an_i ...
Fetched: 2/13/2021 6:53:20 PM   ⊞   2

SA   **PhD Thesis_Nikhil Prakash_2005PHXF401.pdf**
Document PhD Thesis_Nikhil Prakash_2005PHXF401.pdf (D24265672)   ⊞   3

W   URL: https://sciencedocbox.com/Chemistry/71176203-Polymer-reaction-engineering.html
Fetched: 9/27/2019 4:33:57 PM   ⊞   2

W   URL: https://www.mdpi.com/2227-9717/7/2/67/htm
Fetched: 12/19/2019 10:14:55 AM   ⊞   2

SA   **University Of Petroleum And Energy Studies / Group 15 end review major project final .pdf**
Document Group 15 end review major project final .pdf (D103300768)
Submitted by: akthakur@ddn.upes.ac.in
Receiver: akthakur.upes@analysis.urkund.com   ⊞   1